Karl-Franzens-Universität
Graz
Institut für Physik

SYSTEMATIC COMPARISON BETWEEN NON-PERTURBATIVE FUNCTIONAL METHODS IN LOW-ENERGY QCD MODELS

Dissertation

zur Erlangung des akademischen Grades eines

Doktor der Naturwissenschaften

an der

Karl-Franzens-Universität Graz

vorgelegt von

JORDI PARÍS-LÓPEZ

Betreut durch Univ.-Prof. Dr. Reinhard Alkofer

Graz, Winter 2019

Abstract

The non-perturbative behaviour of Quantum Chromodynamics requires the use of sophisticated tools to extract properties of hadrons. In recent years, the non-perturbative approach called Functional Methods has been greatly developed theoretically and numerically, successfully describing properties of low-energy QCD. This approach, which is defined in the continuum, has besides others two different kinds of equivalent formulations: the Dyson-Schwinger and Bethe-Salpeter equations formalism, and the Functional Renormalisation Group.

We analyse the Functional Renormalisation Group approach as a method to extract properties of bound states of quarks in low-energy QCD models. The flexibility of this method allows us to approach the system in different approximations and truncations, that are analysed and compared.

The validity of the Functional Renormalisation Group approach in contrast to the Dyson-Schwinger equations formalism is compared in the theoretical, practical and computational levels. We analyse how results and approximations are comparable in different low-energy QCD systems and which features of the theory are limited to one of the approaches.

Kurzfassung

Die nicht-störende theoretischen Aspekte der Quantenchromodynamik erfordern für die Untersuchung der Eigenschaften von Hadronen entsprechende Werkzeuge. In den letzten Jahren wurden hierzu Funktionale Methoden sowohl theoretisch wie auch numerisch weiterentwikelt und zur erfolgreichen Beschreibung der Quantenchromodynamik in Niederenergisektor benutzt. Dieser im Kontinuum definierte Zugang besitzt neben weiteren Formulierungen zwei oft benutzte Methoden: den Dyson-Schwinger–Bethe-Salpeter-Formalismus und die Funktionale Renormierungsgruppe.

Wir benutzen die Funktionale Renormierungsgruppe, um Eigenschaften von gebundenen Systemen von Quarks in Niederenergie-Quantenchromodynamik-Modellen zu extrahieren. Die Flexibilität dieser Methode ermöglicht es uns, das System in verschiedenen Näherungen und Verkürzungen zu betrachten, die analysiert und verglichen werden.

Die Gültigkeit des Ansatzes der funktionalen Renormalisierungsgruppe im Vergleich zum Formalismus der Dyson-Schwinger-Gleichungen wird auf theoretischer, praktischer und rechnerischer Ebene verglichen. Wir analysieren, wie Ergebnisse und Näherungen in verschiedenen Niedrigenergie-QCD-Systemen vergleichbar sind und welche Merkmale der Theorie auf einen der Ansätze beschränkt sind.

to Cristina

Contents

Chapter 1

Introduction

Hadrons constitute the macroscopic degrees of freedom of Quantum Chromodynamics (QCD) as bound states of quarks and gluons. Empirical trace of colourless hadrons has been detected in research facilities in the form of baryons and mesons - as predicted by the quark model [1] - as well as other excited bound states found experimentally. A great amount of experimental data has been obtained in many hadron colliders such as the Large Hadron Collider (LHC), the Relativistic Heavy ION Collider (RHIC) and Tevatron, among many others, by observing resonances in hadron cross-sections or scattering experiments. Every detected resonance is tabulated by the Particle Data Group [2], taking part in a great classification list of the particle spectrum that grows continually. A wider knowledge of the hadron spectrum and its properties should lead us to a deeper understanding of subatomic interactions in the most fundamental level. Nonetheless, there is a vast quantity of elementary properties of subatomic physics that are still not well understood. The confinement of the microscopic degrees of freedom of QCD -quarks and gluons- into hadrons, the generation of masses understood as a dynamical breaking of chiral symmetry or missing expected resonances in the physical spectrum are some of the unknowns yet to be comprehended. In order to approach these problems, phenomenology needs to be complemented with theoretical descriptions.

The great success of Quantum Field Theory (QFT) as a description of Particle Physics is unquestionable. The feats achieved in Quantum Electrodynamics (QED) [3], as well as in perturbative QCD, suggest that QFT is the most indicated theory to approach Particle Physics. Furthermore, the predictions of QCD suggest that it is the correct theory to describe strong interactions. Accordingly, the mastery of QCD and QCD-like quantum field theories is required to relate theoretical features involving hadrons with phenomenology. However, the non-perturbative behaviour of QCD at low energy scales forbids the use of the methods so successful in QED, and requires sophisticated non-perturbative tools or Effective Field Theory (EFT) approaches. For instance, constituent quark models [4, 5] describe hadrons using effective quarks that contain, in addition to a large mass value, the dynamical effects of the interactions within hadrons. Another approach is Chiral Perturbation Theory [6,7] where Green's functions are expanded in powers of the external momenta and quark masses. Another great candidate to describe low-energy strongly-interacting theories is Lattice QCD [8–10]. Using a discretisation of the space-time and the path integral formulation, Lattice QCD provides successful predictions of low-energy QCD using Monte-Carlo simulations that are commonly interpreted as data from *theoretical experiments*. Its successes and

constant development have made Lattice QCD a branch of Physics on its own. Nevertheless, there exist some drawbacks in Lattice QCD. Simulations are performed in finite grids due to discretisation of the space-time. Real-time calculations are a major challenge due to the interpretation of the Euclidean action in its exponential form as a probability amplitude, and great computational power is required.

Last, but not least, the tools that are also used to deal with the non-perturbative effects of continuum QCD are the two widely employed Functional Methods: the Dyson-Schwinger equations (DSEs) [11, 12] and the Functional Renormalisation Group (FRG) [13]. These approaches are derived from the properties of the path integral and can be treated in a wide range of scales. They have proven to provide an accurate description of the infrared behaviour of QCD, as well as predictions of properties of bound states, further studies of the hadron spectrum and numerical calculations of, e.g., nucleon form factors. The methods are, nevertheless, not infallible. The DSEs can be interpreted as the quantum equations of motion and encode, in the form of an infinite tower of coupled non-linear integral equations, the complete information of the Green's functions of a QFT. The set of equations cannot be solved exactly in general and requires truncations or approximations that allow a self-consistent solution. Not only does this approach require a careful treatment of the entities involved after the implementation of the truncation, but also has proven to require great computational power. For further details and reviews of the DSEs, see e.g. references [14–21]. On the other hand, the formulation of the FRG is based on the usual Renormalisation Group [22,23]. The scale parameter is introduced as an additional variable which, through a convenient treatment of the properties of the path integral, yields an infinite tower of coupled differential equations that, in order to be solved self-consistently, requires also a truncation, for further details, see [24–28] . The equivalence between both functional approaches is long known [29]. Nevertheless, practical cases involve different types of truncations in every method as well as distinct numerical challenges and interpretations. Depending on the system, the use of one of the functional methods may be more convenient than the other due to their intrinsic properties. Hence, a systematic study between the different methods in different systems is needed, in order to optimise future functional approaches.

The aim of this thesis is to analyse the viability of the different continuum methods and to provide the mathematical tools to use them in every situation. In particular, the FRG is used in low-energy effective models with different approximations, and we show how properties of bound states are obtained from the computed results. In Chapter 2, basics concepts of QFT and QCD are reviewed. The formal derivation and properties of the main functional approaches is included in this chapter as well. Chapter 3 provides a detailed use of the FRG in order to solve the Quark-Meson (QM) model, a low-energy QCD effective model made of quark and mesonic degrees of freedom. In Chapter 4 we perform a direct comparison between the continuum methods in different systems, analysing which features are gained or lost in each of the methods, as well as what new concepts can be learned. We discuss also the viability of the methods. In Chapter 5 we summarise and announce our conclusions.

The appendices provide further information involving details of the calculations and derivations. In Appendix A the notation and diagrammatic conventions used throughout the thesis are shown. Appendix B describes every mathematical technique used during the calculations in detail. In Appendix C the explicit functional equations of every system are shown both in the FRG and in DSE, and finally in Appendix D we mention which computational tools are used in every case.

Chapter 2

Theoretical Framework

In this chapter we discuss the importance of the Green's functions, their relation with the generating functional and their connected and 1PI counterparts. We show how they relate to bound state equations and which symmetries they must preserve.

Afterwards, QCD and its most relevant features are reviewed, including its formulation in the path integral as a gauge theory. Afterwards, the basics of the DSE-BSE methods are described, together with their derivation and a practical case in the Rainbow-Ladder truncation.

Finally, the FRG is introduced as a functional method and Wetterich's flow equation [13] is derived. Important methodical features of the FRG and technical details are explicitly shown, together with the general formulation of the dynamical hadronisation technique.

Further details on the functional methods can be found in reviews related to the DSE [14–21] and FRG [24–28] approaches.

2.1 Functionals and Green's Functions

The dynamical content of any quantum field theory, and in particular QCD, is encoded within its Lagrangian or, equivalently, its action. Despite knowing the explicit classical form of such functionals, acquiring the physical content of QCD is a challenging task due to its non-perturbative behaviour at low energies. Furthermore, bound states are inherently non-perturbative, therefore the techniques so successfully implemented in QED can no longer be used within the theory of strong interactions.

The main objects of interest within Quantum Field Theory are the Green's or correlation functions. These entities are known to properly describe the behaviour of a propagating particle, as well as its interactions. As it will be shown in this chapter, Green's functions are the elements of a bound state equation capable of describing properties of such states. Hence, an adequate starting point for any non-perturbative method is the generating functional in its path integral form, since its properties allow an easy extraction of Green's functions that, afterwards, act as inputs to derive properties of bound states.

The generating functional or partition function $Z[\mathcal{J}]$ defines a quantum field theory within a path integral formulation. In Euclidean space-time, it reads

$$Z[\mathcal{J}] \equiv \int \mathcal{D}\Phi \exp\left\{-S[\Phi] + \int_x \mathcal{J}^{\boldsymbol{a}}\,\Phi^{\boldsymbol{a}}\right\} = G_{i_1\ldots i_n}\mathcal{J}_{i_1}\ldots\mathcal{J}_{i_n}\ , \tag{2.1}$$

where Φ represents a superfield of n fundamental fields, $S[\Phi]$ is the bare action of the system and $\mathcal{J}^a$ encodes every source term associated with the superfield. The index $\boldsymbol{a}$ is summed over every possible index, includes the appropriate sign according to the bosonic or fermionic nature of every field and incorporates space-time dependence, see Appendix A for further details. Correlation functions $G_{i_1\ldots i_n} = \langle\Phi_{i_1}\ldots\Phi_{i_n}\rangle$ are obtained through the application of derivatives with respect to the sources $\mathcal{J}$ and averaging over every field configuration as expressed in equation (2.2):

$$\langle\Phi_{\boldsymbol{a_1}}(x_1)\ldots\Phi_{\boldsymbol{a_n}}(x_n)\rangle = \frac{1}{Z[\mathcal{J}=0]}\left(-\frac{\delta}{\delta\mathcal{J}_{\boldsymbol{a_1}}(x_1)}\right)\ldots\left(-\frac{\delta}{\delta\mathcal{J}_{\boldsymbol{a_n}}(x_n)}\right)Z[\mathcal{J}]\Big|_{\mathcal{J}=0}. \tag{2.2}$$

2.1.1 Irreducibility

The attainable information derived from the partition function $Z[\mathcal{J}]$ certainly describes the full quantum field theory but, due to the way it is formulated, redundant contributions in the Green's functions arise, making $Z[\mathcal{J}]$ not the most efficient functional to work with. A more effective and compact approach to derive correlators is to use related, yet different generating functionals. These are the Euclidean *generating functional of connected correlated functions* or Schwinger functional $W[J]$ and the Euclidean *Effective Action* $\Gamma[\varphi]$. They are directly related to $Z[\mathcal{J}]$:

$$W[\mathcal{J}] = \log Z[\mathcal{J}] \qquad , \qquad \Gamma[\varphi] = \sup_{\mathcal{J}}\left(\int_y \mathcal{J}_{\boldsymbol{a}}\varphi_{\boldsymbol{a}} - W[\mathcal{J}]\right). \tag{2.3}$$

The parameter $\varphi_{\boldsymbol{a}}$ is the averaged value of the superfield Φ_a under presence of a source. Shall Φ_a include composite fields, the effective action will encode the information differently. Throughout this work, $\Phi_{\boldsymbol{a}}$ will contain only single fields and, consequently, the source terms will read the usual notation $\mathcal{J}_{\boldsymbol{a}} = J_{\boldsymbol{a}}$. Under this consideration, the parameters $\varphi_{\boldsymbol{a}}$ and $J_{\boldsymbol{a}}$ are related through functional derivatives:

$$\frac{\delta W[J]}{\delta J_i(x)} = \frac{1}{Z[J]}\frac{\delta Z[J]}{\delta J_i(x)} = \langle\Phi_i(x)\rangle_J \equiv \varphi_i(x), \tag{2.4}$$

$$\frac{\delta\Gamma[\varphi]}{\delta\varphi_i(x)} = \int_y J_i^{sup}(y)\delta(x-y) = J_i^{\text{sup}}(x) \equiv J_i(x). \tag{2.5}$$

Notice that in the last step we defined $J_i^{\text{sup}} \equiv J_i$. From the definition of the effective action, $\Gamma[\varphi]$ only makes sense once $\int J\varphi - W[J]$ reaches its supremum. Furthermore, one can show the following relation from the definition of the effective action in expression (2.3) that:

$$\frac{\delta^2 W[J]}{\delta J_{\boldsymbol{a}} \delta J_{\boldsymbol{b}}} = \left(\frac{\delta^2 \Gamma[\varphi]}{\delta \varphi_{\boldsymbol{a}} \delta \varphi_{\boldsymbol{b}}} \right)^{-1}, \tag{2.6}$$

which also establishes a relation between the connected correlators obtained by $W[J]$ with the ones derived by the effective action. It can be proven that $W[J]$ and $\Gamma[\varphi]$ are defined, topologically in terms of Feynman diagrams, by connected and 1-particle-irreducible (1PI) diagrams respectively. The connected and 1PI Green's functions associated are obtained through functional derivatives:

$$\frac{\delta^n W[J]}{\delta J_{\boldsymbol{a_1}} \ldots \delta J_{\boldsymbol{a_n}}} = \langle \Phi_{\boldsymbol{a_1}} \ldots \Phi_{\boldsymbol{a_n}} \rangle_{\text{conn}}, \tag{2.7}$$

$$\frac{\delta^n \Gamma[\varphi]}{\delta \varphi_{\boldsymbol{a_1}} \ldots \delta \varphi_{\boldsymbol{n}}} = \langle \Phi_{\boldsymbol{a_1}} \ldots \Phi_{\boldsymbol{a_n}} \rangle_{\text{1PI}}. \tag{2.8}$$

Due to its simplicity and its properties (which will become clear in the following sections), the main object we will use is the 1PI effective action $\Gamma[\varphi]$. In analogy to (2.1) and using the properties of (2.5), the path integral expression of the effective action is

$$e^{-\Gamma[\varphi]} = \int \mathcal{D}\Phi \exp\left\{ -S[\Phi + \varphi] + \int_x \frac{\delta \Gamma[\varphi]}{\delta \varphi_{\boldsymbol{a}}} \Phi_{\boldsymbol{a}} \right\}, \tag{2.9}$$

where a field shift has been performed on the right hand side for convenience. Equation (2.9) is an Euclidean integro-differential equation but, in general, a solution for $\Gamma[\varphi]$ cannot be exactly provided. A first functional technique is the one called *vertex expansion*, where the effective action is expressed as an infinite sum of 1PI vertex functions:

$$\Gamma[\varphi] = \sum_{n=0}^{\infty} \frac{1}{n!} \int_{x_1} \ldots \int_{x_n} \varphi_{i_1}(x_1) \ldots \varphi_{i_n}(x_n) \Gamma^{(n)}_{i_1,\ldots,i_n}(x_1, \ldots, x_n). \tag{2.10}$$

By plugging this expansion in both sides of (2.9), an infinite set of coupled equations for every n-point vertex function $\Gamma^{(n)}_{i_1,\ldots,i_n}$ is obtained. These coupled equations are called Dyson-Schwinger equations (DSE) and correspond to the quantum equations of motion. The derivation of such equations and the approach in which they are solved constitute one of the functional methods and has become a matter of research for the last decades, see [15–21, 30–34].

2.1.2 Bound state equations

Bound states appear in quantum field theory as intermediate states of many-body systems. In particular in QCD, mesons and baryons shall appear in a particle exchange of four and six fermionic interaction respectively. The T-matrix of such systems encodes the information of the bound states and is constructed from the amputated, dressed and connected n-point Green's function $G^{(n)}$ following the expression:

$$G^{(n)} = G_0^{(n)} + G_0^{(n)} T^{(n)} G_0^{(n)}, \tag{2.11}$$

where $n = 4, 6$ for mesons and baryons respectively, $T^{(n)}$ is the T-matrix of the n-body system and $G_0^{(n)}$ is the dressed, disconnected n-point Green's function. The compact notation of the expression includes index contraction and integration over all momenta. The Green's functions $G^{(n)}$ and the T-matrix satisfy also Dyson's equations [11]:

$$G^{(n)} = G_0^{(n)} + G_0^{(n)} K^{(n)} G^{(n)}, \tag{2.12}$$

$$\Updownarrow$$

$$T^{(n)} = K^{(n)} + K^{(n)} G_0^{(n)} T^{(n)}, \tag{2.13}$$

being $K^{(n)}$ the interaction kernel that contains all possible 2PI diagrams. The proof that both equations are equivalent is easily found, by inserting (2.12) and (2.13) in the Green's function expression (2.11). In this work uniquely mesons will be treated, therefore the $G^{(n)}$ are understood as 4-point fermionic Green's functions. They conceal all the information of intermediate mesons manifested as poles. Choosing a complete set of eigenstates, the matrix elements $G^{(n)}$ and $T^{(n)}$ are rewritten according to the basis expansion:

$$G^{(n)} \sim \sum_\lambda \frac{\Psi^{(\lambda)} \bar{\Psi}^{(\lambda)}}{P^2 + M_\lambda^2} \quad , \quad T^{(n)} \sim \sum_\lambda \frac{\Gamma^{(\lambda)} \bar{\Gamma}^{(\lambda)}}{P^2 + M_\lambda^2} \, , \tag{2.14}$$

where the sum of the index λ is performed over all the possible meson exchanges. The eigenstates $\Psi^{(\lambda)}$ are the Bethe-Salpeter amplitudes (BSA) and $\Gamma^{(\lambda)}$ are the amputated BSAs. They both contain the information of every possible bound state, including momentum dependence and tensor structures, which depend on the system. For simplicity, the bound states in this expression are considered non-degenerate. The expression (2.14) is introduced in Dyson's equation (2.13) and the first order residues around the pole $P^2 = -M_\lambda^2$ are compared. The resulting expression leads, in a compact form with indices omitted, to the homogeneous Bethe-Salpeter equation [35]:

$$\Psi = G_0 K \Psi \tag{2.15}$$

$$\Gamma = K G_0 \Gamma \tag{2.16}$$

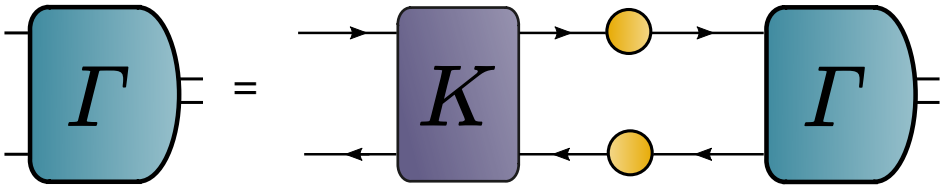

Figure 2.1: Pictorial representation of the Bethe-Salpeter equation for the amputated amplitudes Γ for a mesonic system.

The Bethe-Salpeter equation can be expressed diagrammatically as shown in Figure 2.1. The solution of the BSE yields the Bethe-Salpeter amplitude, which is the wave function of the bound states. As the equations suggest, the disconnected 4-point Green's function in form of two fermionic propagators needs to be previously known, as well as a full knowledge of the interaction kernel K. In general, the latter is not small and requires a parametrisation according to the symmetries of the theory and, in most cases, a reasonable truncation, see [36–40].

2.1.3 Symmetries and Ward-Takahashi identities

Symmetries play a key role in Nature : they define how models and theories are built according to the properties of a system and, when the symmetries are continuous, lead to conservation laws and invariance of equations of motion. During the development of quantum mechanics, symmetries gained a much greater importance when they allowed the qualification of bosonic and fermionic particles, in addition to their distinction via quantum numbers [41]. Quantum Field Theory included special relativity in its formulation, as well as its symmetries ruled by translation, rotation and boost transformations given by the Poincaré group. Under this group, elementary particles are totally classified according to their massive or massless nature, spin and quantum numbers given by discrete symmetries like parity and electrical charge.

General quantum field theories allow further symmetries in their formulation. Certainly, the Abelian and non-Abelian local gauge symmetries were the ones that implicated greater changes in the vision of modern Physics, since they successfully describe the strong, weak and electromagnetic interactions in a fundamental level [42–44]. They introduced the concept of gauge bosons and gauge transformations and established the basis of the Standard Model in the form of $SU(3) \times SU(2) \times U(1)$ gauge symmetry.

The symmetries described in a quantum field theory are not always satisfied by Nature, even though many physical properties can be understood from them. The symmetries are in some cases broken. There exist different cases of symmetry breaking:

- *Explicit symmetry breaking*: The dynamics of the system are only approximately symmetric and the contribution of the symmetry breaking is considered a small correction, leading to only approximated conservation laws. This is the case of chiral symmetry in non-Abelian gauge theories, where axial current is only preserved when fermions are massless.

- *Spontaneous symmetry breaking*: The dynamics of the system is completely symmetric, but the normally infinitely-degenerated ground state of the system is set to be unique [45, 46]. The explicit expression of the system is modified according to this ground state, apparently breaking this symmetry which is now only hidden.

Such symmetry considerations are of great importance in the Standard Model and, in particular, as will be seen in the next subsections, in QCD. The behaviour of the symmetries of the system needs to be reflected in the Green's functions and, by extension, within the path integral. Under this assumption, relations between correlators and conservation rules appear naturally from the properties of the path integral.

First of all, it is convenient to explicitly know how the path integral transforms under field transformations. Let the path integral Z be transformed as $Z \to Z' = Z + \delta Z$ under the infinitesimal field transformation $\Phi' \to \Phi + \delta\Phi$. Defining $\tilde{S}$ as the sum of the bare action and source terms $\tilde{S} = S_{bare} + S_{ST}$, the generating functional transforms as:

$$Z' = \int \mathcal{D}\Phi' \exp\left(-\tilde{S}[\Phi']\right) = \int \mathcal{D}\Phi(1 + \delta\mathcal{D}\Phi - \delta\tilde{S}) \exp\left(-\tilde{S}[\Phi]\right), \tag{2.17}$$

where $\delta(\mathcal{D}\Phi)$ is the variation of the measure and $\delta\tilde{S}$ the variation of the bare action and source terms under the field transformation. Since the path integral contains every field configuration, Z must be invariant under these transformations and therefore $\delta Z = 0$, following the relation :

$$\delta Z = \int \mathcal{D}\Phi(\delta\mathcal{D}\Phi - \delta\tilde{S}) \exp\left(-\tilde{S}[\Phi]\right) = 0. \tag{2.18}$$

In this case, identities for transformed operators are found. Let $\langle\mathcal{O}\rangle$ be a correlator defined under the presence of the source which transforms as $\mathcal{O} \to \mathcal{O}' = \mathcal{O} + \delta\mathcal{O}$. Under the assumption that the system is symmetric under the infinitesimal field transformation $\Phi \to \Phi + \delta\Phi$ and requiring that $Z' = Z$, the correlator is transformed as:

$$\begin{aligned}
\langle\mathcal{O}\rangle' &= \frac{1}{Z'[J=0]} \int \mathcal{D}\Phi'\mathcal{O}' \exp\left(-\tilde{S}'[\Phi']\right) \\
&= \frac{1}{Z[J=0]} \int \mathcal{D}\Phi \left(1 + \delta\mathcal{D}\Phi\right) \left(\mathcal{O} + \delta\mathcal{O}\right) \left(1 - \delta\tilde{S}\right) \exp\left(-\tilde{S}[\Phi]\right) \\
&= \langle\mathcal{O}\rangle + \langle\delta\mathcal{O} + \mathcal{O}\delta(\mathcal{D}\Phi) - \mathcal{O}\delta\tilde{S}\rangle.
\end{aligned} \tag{2.19}$$

The correlators are required to be invariant under transformations, leading to the other identity $\langle\delta\mathcal{O} + \mathcal{O}\delta(\mathcal{D}\Phi) - \mathcal{O}\delta\tilde{S}\rangle = 0$. This relation and expression (2.19) are the general form of the Ward-Takahashi identities (WTI[1]) and need to be always satisfied [47, 48]. Such statement is not trivial: the functional equations used need to satisfy the WTIs, even when a truncation is required. On the other hand, the WTIs allow a consistent parametrisation of the interaction kernel with the truncation, in a way that they are, at least approximately, satisfied.

[1] The generalisation of a Ward-Takahashi identity in a non-Abelian gauge theory is called Slavnov-Taylor identity.

2.2 Functional Approach in QCD using DSE-BSE

The non-perturbative behaviour of bound states and QCD requires sophisticated tools. Access to fundamental properties of the bound states should be guaranteed with these tools, and the comparison of theoretical observables with expertiments should be possible. The usual functional approach to properties of bound states has been done using the DSE-BSE formalism, a continuous non-perturbative method that has been very successful in determining fundamental properties of QCD and bound states, and has been greatly developed both theoretically and numerically, see, e.g. [49–51].

In this subsection, QCD is briefly derived as a non-Abelian gauge theory, emphasizing some of its fundamental properties and how it is placed within the path-integral. Afterwards, a short application of these functional equations will be shown.

2.2.1 Foundations of QCD

Gauge field theories have proven to provide an accurate description of the subatomic world. Quarks, gluons and colours - the main entities in this theory - are introduced into a fermionic system requiring $SU(3)$ gauge invariance [52]. The resulting classical Euclidean action follows the expression:

$$S_{QCD}[\bar{\psi}, \psi, A] = \int_x \bar{\psi} \left(-\not{D} + m_q\right) \psi + \frac{1}{2}\mathrm{Tr}\left(G_{\mu\nu}G^{\mu\nu}\right). \tag{2.20}$$

The ψ is a fermionic triplet in the fundamental representation denoting quarks, being m_q their mass. The term $\not{D} = \gamma^\mu D_\mu$ includes the contracted covariant derivative $D_\mu = \partial_\mu + igA_\mu$, where $A_\mu = A^a_\mu\, t^a$ denotes the gauge fields, including the gluons A^a_μ living in the adjoint representation of $SU(3)$, and t^a are the generators of the Lie algebra. Finally, the field-strength tensor is defined as $G_{\mu\nu} = \partial_\mu A_\nu - \partial_\nu A_\mu + ig\left[A_\mu, A_\nu\right]$, with the relation $G_{\mu\nu} = G^a_{\mu\nu} t^a$.

The QCD action includes quark-gluon vertices, as well as interactions of 3 and 4 gluons. QCD, both in its theoretical formulation as well as in phenomenology, includes several properties relevant for the purpose of this work:

- *Gauge invariance*: As a gauge theory, QCD must be invariant under local SU(3) gauge transformations. The physics described under different gauge choices shall be equivalent. Therefore, observables should be independent of the gauge, although correlators may still be dependent. Let $U(x) = e^{it^a\theta^a(x)} \in SU(3)$ be a gauge transformation operator. The QCD action is invariant under the transformation of the fields according to:

$$\begin{aligned} \psi \to U\psi \quad &, \quad A_\mu \to U\left[A_\mu - \frac{i}{g}U^\dagger(\partial_\mu U)\right]U, \\ D_\mu\psi \to UD_\mu\psi \quad &, \quad G_{\mu\nu} \to UG_{\mu\nu}U^\dagger. \end{aligned} \tag{2.21}$$

- *Asymptotic freedom*: This property relates the asymptotically decreasing magnitude of the QCD coupling g with the increasing energy scale [53]. At very large energies the coupling is very weak, allowing calculations using perturbation theory, in the same manner as in QED. In this regime, it can be said that the degrees of freedom of QCD, quarks and gluons, are free in the infinite energy limit. On the other hand, at very low energies the strong coupling becomes large and perturbation theory can no longer be applied and non-perturbative methods are required.

- *Confinement*: Free quarks and gluons -the degrees of freedom of QCD- have not yet been experimentally detected. Every strongly interacting particle observed is *colourless* or *white* [54] and is classified in the form mesons and baryons (and recently, in larger composite states). This phenomenon is still not completely understood, but plays a capital role within the low-energy QCD scale, where the degrees of freedom change into hadrons.

- *Dynamical chiral symmetry breaking*: Chiral transformations become exact in QCD only if fermions were massless. When the system evolves dynamically, quarks become massive, breaking the symmetry [55].

Once the bare action of QCD is obtained along its properties, the next step is the formulation into its path integral. Gauge field theories require a thorough treatment when introduced into the generating functional. In this section we will follow the derivation described in [56].

By its definition, the path integral is an infinite sum over all possible field configurations. Gauge theories state that some field configurations are equivalent to others -related by gauge transformations- and therefore shall not be counted twice. In this regard, the gauge fields included in the path integral shall be not $A_\mu \in \mathcal{A}$, being $\mathcal{A}$ the space of all the gauge fields, but the ones belonging to the equivalence class:

$$\mathcal{C} = \frac{\mathcal{A}}{\mathcal{U}}, \tag{2.22}$$

where $\mathcal{U}$ consists in the space of all gauge transformations that lead to equivalent physical fields. Under this consideration, the measure of the path integral needs to be modified according to $d\hat{\mu}(\mathcal{A}) = d\hat{\mu}\left(\frac{\mathcal{A}}{\mathcal{U}}\right) d\hat{\mu}\left(\mathcal{U}\right)$, where $\hat{\mu}$ represents a general measure. The path integral formulation is modified with the introduction of the new measure:

$$\begin{aligned} Z[J] &= \int d\hat{\mu}\left(\frac{\mathcal{A}}{\mathcal{U}}\right) \exp\left(-S[A] + \int J^{\boldsymbol{a}} A^{\boldsymbol{a}}\right) = \\ &= \int d\hat{\mu}(\mathcal{A}) \delta(f(A) - h) \left|\det(\Delta_{FP})\right| \exp\left(-S[A] + \int J^{\boldsymbol{a}} A^{\boldsymbol{a}}\right). \end{aligned} \tag{2.23}$$

Locally, the measure $d\hat{\mu}(\mathcal{U})$ is written in function of the infinitesimal gauge-transformation factor θ following $d\hat{\mu}(\mathcal{U}) \approx d\hat{\mu}(\theta)$ and the missing steps involve the use of the identity:

$$1 = \int d\hat{\mu}(f)\delta(f-h) = \int d\hat{\mu}(\theta)\,|\det(\Delta_{FP})|\,\delta(f-h) \tag{2.24}$$

having defined $\delta(f-h)$ as a gauge fixing condition and the Faddeev-Popov determinant as:

$$|\det(\Delta_{FP})| = \left|\det(\Delta^{ab}_{FP})\right| = \left|\det\left(\frac{\partial f^a}{\partial \theta^b}\right)\right| \tag{2.25}$$

The equation (2.23) formulates the standard quantisation of non-Abelian gauge field theories by introducing a gauge-fixing term and a determinant. However, the procedure is incomplete as the commonly known Gribov copies affect observable quantities at low energies [57,58]. Nevertheless, this formulation is useful to understand which entities play a role in QCD. This equation can be further simplified by redefining the new delta distribution and determinant terms included. Green's functions from the path integral remain unchanged by multiplying Z by extra constant terms as seen in (2.2). Since h is arbritary, it can be chosen so that these constant terms appear from the Gaussian integral form $\int d\hat{\mu}(h)\exp\left(-\frac{1}{2\zeta}\int h^2\right)$. After this inclusion and integrating out the delta distribution, the generating functional becomes:

$$Z[J] = \int d\hat{\mu}(\mathcal{A})\,|\det(\Delta_{FP})|\exp\left(-S[A] - \frac{1}{2\zeta}\int f(A)^2 + \int J^{\boldsymbol{a}}A^{\boldsymbol{a}}\right) \tag{2.26}$$

The last term remaining is the Faddeev-Popov determinant [59]. Ideally, the determinant should be expressed within the exponential by completing squares of a Gaussian, but this identity yields, for general fields, the inverse of the determinant of a matrix instead. The way-out is the use of Grassmann valued fields $\bar{c}$ and c, satisfying the identity:

$$\int d\hat{\mu}(\bar{c},c)\exp\left(\int \bar{c}Mc\right) = \det(M) \tag{2.27}$$

Thus, the Faddeev-Popov determinant can be expressed as an exponential term using the fields $\bar{c}$ and c and therefore introduced into the generating functional following:

$$Z[J] = \int d\hat{\mu}(\mathcal{A},\bar{c},c)\exp\left(-S[A] - \frac{1}{2\zeta}\int f(A)^2 - \int \bar{c}^a\Delta^{ab}_{FP}c^b + \int J^{\boldsymbol{a}}A^{\boldsymbol{a}}\right). \tag{2.28}$$

And this is the generalisation of the construction of the path integral of a gauge theory. In QCD in particular, it becomes:

$$Z[J] = \int d\hat{\mu}(\bar{\psi},\psi,\mathcal{A},\bar{c},c)\exp\left(-S_{QCD} - S_{GF} - S_{FP} + S_{ST}\right), \tag{2.29}$$

where all the action terms are defined as:

$$S_{QCD}[\bar{\psi},\psi,A] = \int_x \bar{\psi}\left(-\not{D}+m\right)\psi + \frac{1}{2}\mathrm{Tr}\left(G_{\mu\nu}G^{\mu\nu}\right), \tag{2.30}$$

$$S_{GF}[A] = \frac{1}{2\zeta}\int_x f(A)^2, \tag{2.31}$$

$$S_{FP}[A,\bar{c},c] = \int_x \bar{c}^a \partial^\mu D^{ab}_\mu c^b, \tag{2.32}$$

$$S_{ST}[\Phi,J] = \int_x \Phi^{\boldsymbol{a}} J^{\boldsymbol{a}}. \tag{2.33}$$

Expression (2.29) is indeed the correct generalisation of the QCD path integral, but some properties of QCD are not reflected in it. In particular, due to the gauge-fixing term, the sum of $S_{QCD} + S_{GF} + S_{FP}$ is no longer gauge invariant. As a direct consequence, Green's functions derived from the generating functional are also gauge-dependent, although observables must be independent of the gauge choice. The remaining symmetry of the path integral is the BRST symmetry [60–62] which is important for the quantisation and renormalisability of the path integral. The ghost fields are simply mathematical tools manually introduced and therefore are unphysical, even though their correlators may contribute in the functional equations of the other fields Green's functions.

2.2.2 Derivation of the Dyson-Schwinger equations

The Dyson-Schwinger equations are the equations of motion of the Green's functions within quantum field theories. They are derived directly from the properties of the path integral, after requiring invariance under a field transformation $\Phi \to \Phi + \delta\Phi$. The cancellation of the path integral under a total derivative is assumed:

$$\int \mathcal{D}\Phi \frac{\delta}{\delta\Phi_{\boldsymbol{i}}} \exp\left(-S[\Phi] + \int_x J_{\boldsymbol{a}}\Phi_{\boldsymbol{a}}\right) = 0. \tag{2.34}$$

Applying the field derivative explicitly in the exponential term and using the properties of the generating functional, it is easy to show the relation:

$$\left(\frac{\delta S}{\delta\Phi_i}\left[\frac{\delta}{\delta J}\right] - J_i\right) Z[J] = 0 \tag{2.35}$$

This expressions generates the Dyson-Schwinger equations for the generating functional $Z[J]$. It is straightforward to derive the DSEs for the other functionals [14], yielding the expression for the generating functional of connected correlators $W[J]$:

$$\frac{\delta S}{\delta\Phi_i}\left[\frac{\delta W[J]}{\delta J} + \frac{\delta}{\delta J}\right] - J_i = 0 \tag{2.36}$$

And from the use of the properties mentioned in expression (2.6), the Dyson-Schwinger equations for the 1PI effective action follow:

$$\frac{\delta\Gamma[\varphi]}{\delta\varphi_i} - \frac{\delta S}{\delta\varphi_i}\left[\varphi_i + \left(\frac{\delta^2\Gamma[\varphi]}{\delta\varphi_i\delta\varphi_j}\right)^{-1}\frac{\delta}{\delta\varphi_j}\right] = 0 \tag{2.37}$$

For the purpose of this work, only expression (2.37) will be used, yielding the DSE for the 1PI Green's functions. Rewriting the DSE for the effective action using a vertex expansion following (2.10), a $(n-1)$-field derivative leads to the DSE of the n-point function, containing all the non-perturbative contributions within.

As the equation itself suggests, higher order vertices appear in every DSE. For any n-point function DSE, contributions involving $n+1$ or higher order correlators appear, normally included in loop diagrams. The solution only makes sense when all these higher order correlators DSE are solved self-consistently. The main problem is that this leads to an infinite tower of Dyson-Schwinger equations which can not be solved unless some truncation or approximation is used. Furthermore, the equations are not limited to one-loop diagram contributions, but up to two and higher order loops which need to be included in a full solution. A reformulation of the DSE in terms of nPI diagrams is in this case required and the solution is laborious and numerically demanding.

As a last remark, the DSE shown in expression (2.37) includes not only dressed, full 1PI correlators, but also bare propagators and vertices given by the free theory, appearing in the equations from the $\frac{\delta S}{\delta\varphi}$ term. They introduce the renormalisation constants into the system, which need to be calculated from subtraction of terms at certain scale, performed analogously as in the renormalisation procedure of perturbation theory.

2.2.3 Dyson-Schwinger equations in QCD

In QCD, Dyson-Schwinger equations are derived from the path integral described in expression (2.29), where the gauge fixing term and the Faddeev-Popov determinant are already included. Therefore, the derivative of the bare action in equation (2.37) does not consist only of the QCD action S_{QCD}, but also of the gauge fixing term component S_{GF} and the Faddeev-Popov S_{FP} terms. As a consequence, not only quark and gluon n-point function Dyson-Schwinger equations need to be formulated, but also ghost-including correlators as well as their contributions in the corresponding quark and gluon DSEs. Figure 2.2 shows the set of some of the lowest-order Dyson-Schwinger equations in QCD.

The DSE formalism is particularly convenient in QCD, as it holds access to a wide range of scales distancing several orders of magnitude and includes both perturbative and non-perturbative contributions. Furthermore, it successfully reproduces QCD properties like dynamical chiral symmetry breaking. The main drawback of the method is the type of approximations needed for the infinite tower of self-coupled integral equations. Some of the calculations use some ansätze for the vertices following the symmetries of the system given by the WTIs and STIs, and some other approaches neglect the contribution of some terms following adequate assumptions.

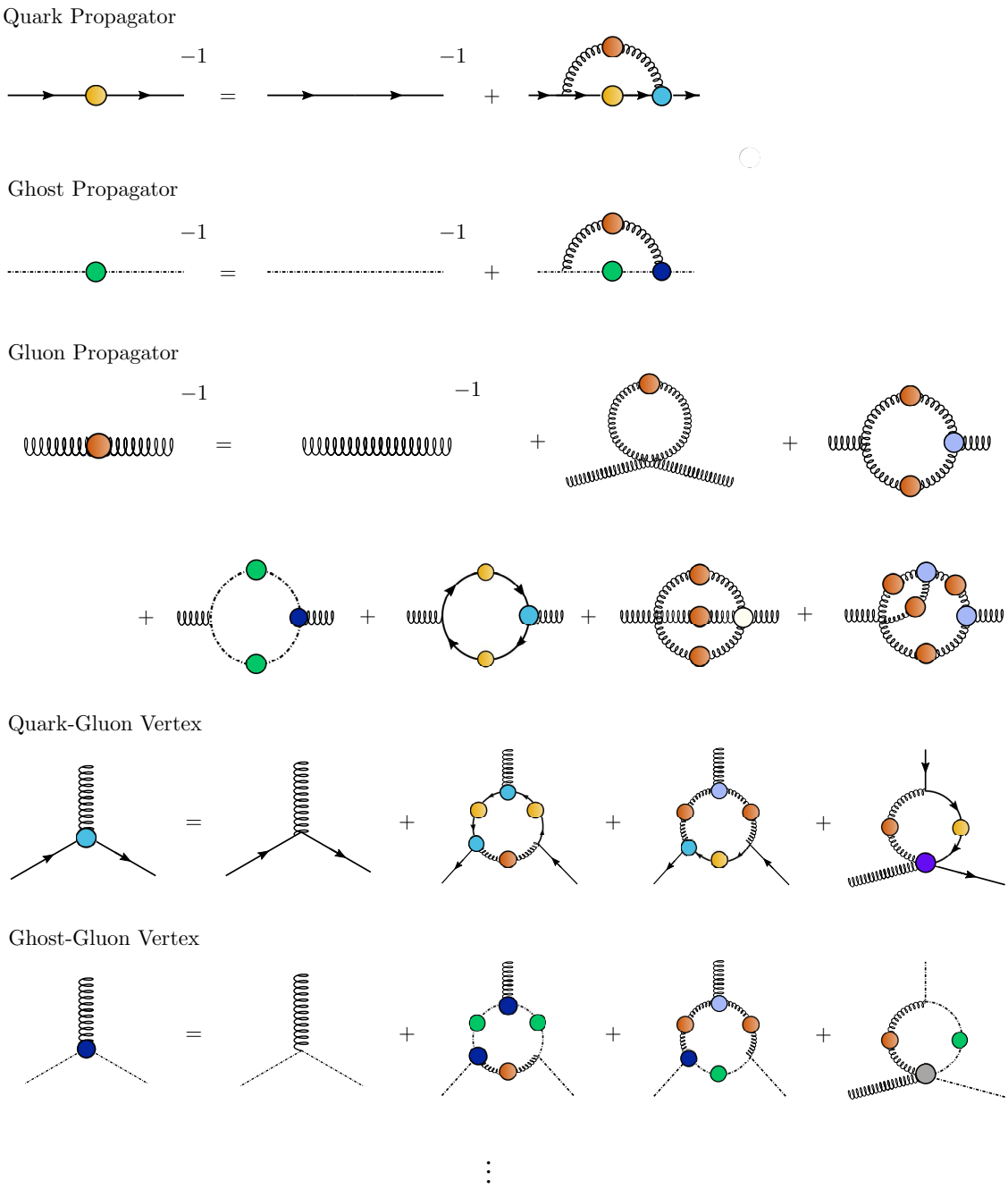

Figure 2.2: DSEs of full QCD. The plus sign in front of each diagram indicates the contributing diagram, not the actual sign according to the conventions. Further DSEs related to the three-gluon vertex and n-point vertices with $n \geq 4$ are omitted.

The simplest approach known to solve the system self-consistently and able to reproduce dynamical chiral symmetry breaking is the use of the *Rainbow-Ladder* truncation [63,64]. This approach manages to reduce the system into only a self-coupled quark-propagator equation. The starting point is the Dyson-Schwinger equation of the quark propagator that diagrammatically follows:

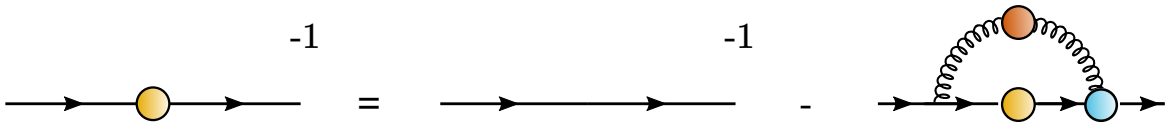

Figure 2.3: Dyson-Schwinger equation for the quark propagator in QCD.

As it can be observed, the equation involves full quark and gluon propagators as well as the dressed quark-gluon vertex. These objects are obtained from the parametrisation of the n-point functions described in the Appendix C. For the purpose of this section, the correlators, chosen in Landau gauge, are explicitly shown:

$$\text{Free Quark 2-point function:} \qquad S_0(p) = Z_2 i\not{p} + Z_2 Z_m m_q, \tag{2.38}$$

$$\text{Quark Propagator:} \qquad S^{-1}(p) = \left(-i\not{p}A(p^2) + B(p^2)\right) G^{\psi}(p^2), \tag{2.39}$$

$$\text{Gluon Propagator:} \qquad D^{\mu\nu}(k) = \frac{Z(k^2)}{k^2}\left(g^{\mu\nu} - \frac{k^\mu k^\nu}{k^2}\right), \tag{2.40}$$

$$\text{Free Quark-Gluon Vertex:} \qquad -iZ_{1f}^{\frac{1}{2}} g\gamma^\mu, \tag{2.41}$$

$$\text{Quark-Gluon Vertex:} \qquad -i\Gamma^\mu_{\psi A}(p,k), \tag{2.42}$$

where $G^{\psi}(p^2) = (A(p^2)^2 p^2 + B(p^2)^2)^{-1}$. The solution of the Dyson-Schwinger equations give values to the dressings $A(p^2), B(p^2), Z(p^2)$ and $\Gamma^\mu_{\psi A}(p,k)$. Naturally, the DSEs of the gluon propagator and quark-gluon vertex come into play and shall be, in principle, consistently solved. The Rainbow-Ladder truncation allows to solve the system using only the quark propagator DSE by the approximation:

$$Z_{1f} g^2 \frac{Z(k^2)}{k^2}\Gamma^\mu \qquad \longrightarrow \qquad Z_2^2 4\pi \frac{\alpha(k^2)}{k^2}\gamma^\mu, \tag{2.43}$$

where $\alpha(k^2)$ is an effective momentum dependent coupling that includes every non-perturbative contribution of both gluon propagator and quark-gluon vertex. Consequently, with the inclusion of the coupling $\alpha(k^2)$ left to be parametrised, the gluon propagator and quark-gluon vertex become free in the quark propagator DSE, yielding a self coupled equation solvable iteratively for the dressings $A(p^2)$ and $B(p^2)$ only.

Leaving the explicit derivation of the equations in Appendix C, the final expressions for $A(p^2)$ and $B(p^2)$ are, in the Rainbow-Ladder truncation:

$$A(p^2) = Z_2 + \frac{4}{3} Z_2^2 \int_q \frac{4\pi\alpha(k^2)}{k^2 p^2} \frac{A(q^2)}{A^2(q^2)q^2 + B^2(q^2)} \left(3(p \cdot q) - \frac{2p^2q^2 - 2(p \cdot q)^2}{k^2} \right), \quad (2.44)$$

$$B(p^2) = Z_2 Z_m m_q + \frac{4}{3} Z_2^2 \int_q \frac{4\pi\alpha(k^2)}{k^2} \frac{3\, B(q^2)}{A^2(q^2)q^2 + B^2(q^2)}. \quad (2.45)$$

The values Z_2 and Z_m are renormalisation constants that are determined once the value of $A(\mu^2)$ and $B(\mu^2)$ are fixed in the renormalisation scale μ. The remaining term required to obtain a numerical solution is the parameter $\alpha(k^2)$. Maris and Tandy suggested for $\alpha(k^2)$ the expression [65]:

$$\alpha(k^2) = \pi\eta^7 \left(\frac{k^2}{\Lambda^2} \right) e^{-\eta^2 \left(\frac{k^2}{\Lambda^2} \right)} + \alpha_{UV}(k^2), \quad (2.46)$$

where η and Λ are real numbers and $\alpha_{UV}(k^2)$ is set to agree with the ultraviolet behaviour. Further details are found in Appendix C. Using the historically set renormalisation scale $\mu = 19$ GeV and $A(\mu^2) = 1$ and $B(\mu^2) = m_q$, the system is solved in both chiral $(m_q = 0)$ and non-chiral $(m_q \neq 0)$ limits yielding:

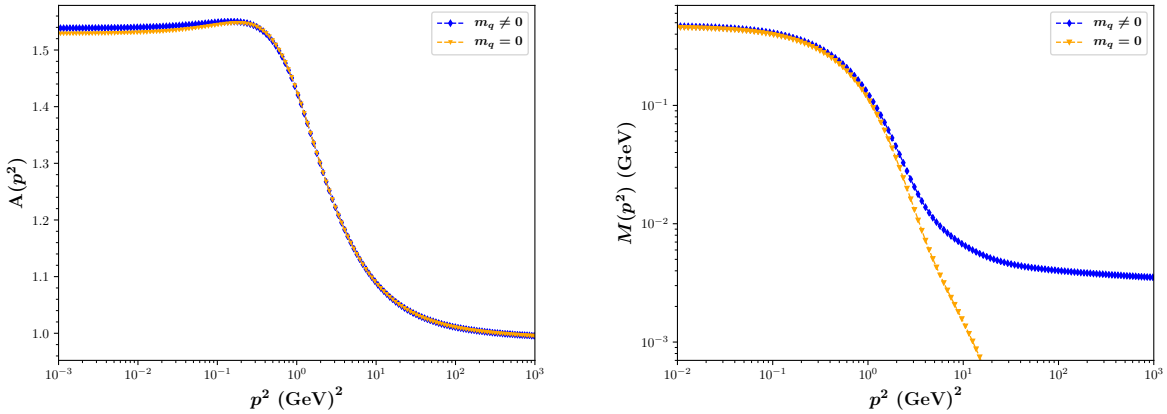

Figure 2.4: Dressings $A(p^2)$ (left) and $M(p^2) = B(p^2)/A(p^2)$ (right) in function of the momentum p^2, computed for the massive case $m_q = 0.0037$ GeV and for the zero fermionic mass.

Figure 2.4 explicitly shows how the Rainbow-Ladder truncation includes the dynamical spontaneous chiral symmetry breaking property of QCD by generating a non-zero mass function even in the chiral limit. Furthermore, both dressing functions collapse to their value at very large energies, as expected. The procedure for general approximations is analogous to the Rainbow-Ladder truncation, but further diagrams, momentum dependence and tensor structures are included, thus making the solution of the system non-trivial and numerically far more demanding.

2.2.4 Bethe-Salpeter Equation in QCD

The Dyson-Schwinger equations formalism provides numerical solution of the full quark propagator and, in addition, of the disconnected fermionic 4-point function. With this information one can attempt to solve the homogeneous Bethe-Salpeter equation for amputated Green's functions (2.16). There are, however, some remarks to be mentioned beforehand.

First of all, the exact form of the interaction kernel K needs to be parametrised according to the STIs, which is highly non-trivial. The simplest known case follows also the Rainbow-Ladder truncation [66], in which the interaction kernel is reduced to a free gluon exchange, with also undressed quark-gluon vertices as shown in Figure 2.5.

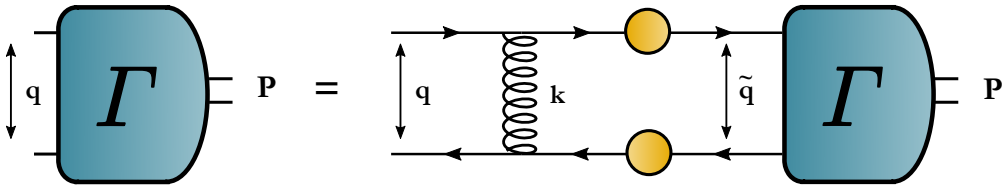

Figure 2.5: Bethe-Salpeter equation in the Rainbow-Ladder truncation.

Under this consideration, every involved object in the equation is known and the system can be solved. In Figure 2.5, some momenta are indicated following the relations:

$$q = \tilde{q} + k \qquad\qquad p_{1,2} = \tilde{q} \pm \frac{P}{2}, \tag{2.47}$$

where q is the relative momentum between quarks before the gluon exchange, $\tilde{q}$ is the relative momenta after the exchange and P is the total momentum of the bound state. The problem appears when the meson momentum P is on-shell, satisfying $P^2 = -M^2$. In can easily be checked that, in the reference frame $P = (0, 0, 0, iM)$, quark momenta $p^2_{1,2}$ follow:

$$p^2_{1/2} = \tilde{q}^2 - \frac{M^2}{4} \pm iMz\sqrt{\tilde{q}^2}, \tag{2.48}$$

consequently making the dressings $A(p^2)$ and $B(p^2)$ complex-valued and dependent on complex momenta. In order to be perfectly consistent, an analytic continuation of the dressings is required. The DSE formalism allows complex calculations by first principle, see Appendix B. Once every dressing is calculated also with complex momentum, the BSE can be solved [21, 67]. Under the Rainbow-Ladder truncation, the form bound state equation follows:

$$\Gamma(q,\, P) = \int_{\tilde{q}} \gamma^\mu S(p_1)\Gamma(\tilde{q}, P)S(p_2)\gamma^\nu D_{\mu\nu}(k). \tag{2.49}$$

The Bethe-Salpeter amplitudes Γ have their own tensor structures, related to the characteristics of the mesons. Hence, the Bethe-Salpeter amplitude is expanded according to an orthonormal basis. For the particular case of the pion, the basis τ is defined as:

$$\tau = \gamma_5\{\ \mathbb{I}\ ,\ \hat{q}\!\!\!/_T\ ,\ \hat{P}\!\!\!/\ ,\ i\hat{q}\!\!\!/_T\hat{P}\!\!\!/\ \}, \tag{2.50}$$

where $\hat{P}$ is the unitary vector in the same direction as P, and $\hat{q}_T$ is the unitary transverse vector to P, therefore $\hat{q}_T \cdot P = 0$. The amplitude Γ is then expanded in terms of this new basis:

$$\Gamma(q, P) = \sum_{i=0}^{3} f^i(q^2, P^2, q \cdot P)\tau^i. \tag{2.51}$$

This expansion splits the amplitude in several functions according to its tensor structure, and lets the system be solved after tracing every index. With a proper treatment of the resulting expressions and using a grid, the system can be written in terms of an eigenvalue problem:

$$\vec{f}(P^2, q^2, q \cdot P) = \lambda\ \ X\ \ \vec{f}(P^2, \tilde{q}^2, \tilde{q} \cdot P). \tag{2.52}$$

Where indeed, λ is set to be $\lambda = 1$ and the matrix X is given by the trace of every tensor structure in the right hand side of the bound state equation and includes momentum integration as well. Once the eigenvector $\vec{f}$ is obtained, the Bethe-Salpeter equation is finally solved and the wave function of the bound state (the Bethe-Salpeter amplitude) is completely known. This procedure can be used also to determine, in the case of the pion, the pseudoscalar vertices via the inhomogeneous BSEs [68] in the form $\Gamma^{(5)} = \Gamma_0^{(5)} + KG\Gamma^{(5)}$ which, in addition to physical information regarding vertices, it provides consistency checks, particularly in the position of the physical pole as shown in Figure 2.6. Further details are shown in the Appendix C.

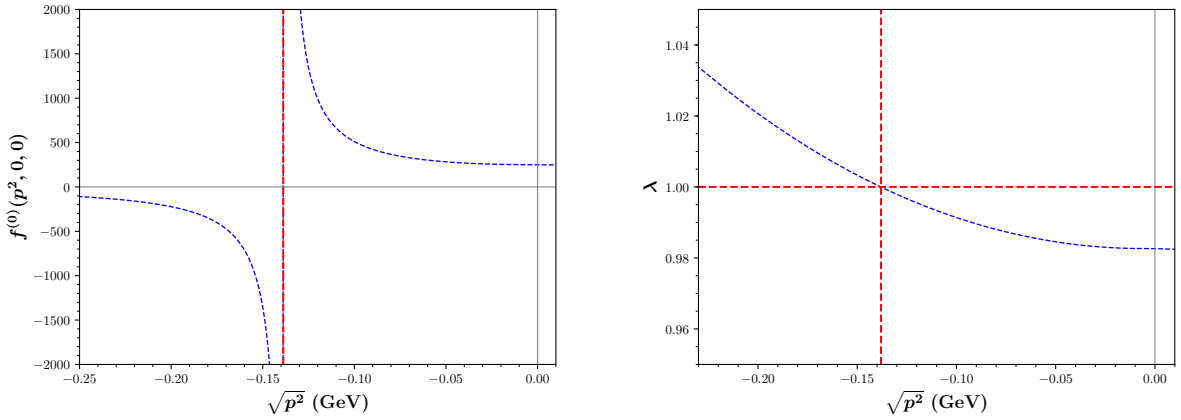

Figure 2.6: Dominant term $f^{(0)}(P^2, 0, 0)$ of the solution of the inhomogeneous BSE (left) with $\Gamma_0^{(5)} = (Z_2\gamma_5, 0, 0, 0)$ and evolution of the eigenvalues of the matrix X, both in terms of $\sqrt{P^2}$.

2.3 The Functional Renormalisation Group

Wilson's approach to quantum field theories led to the alternative interpretation of physical quantities as scale-dependent objects [69], the scale dependence of which is described by the renormalisation group equations. Such approach does not consist in integrating the path integral as a whole, but in infinitesimal steps ruled by the scale parameter k that acts as an infrared cutoff. The physical contributions of the fields whose momenta are lower than the scale k are neglected and only quantum fluctuations with momenta $k < p \leq \Lambda$ are integrated, being Λ an ultraviolet cutoff. By integrating over every momentum shell by reducing the scale $k \to k + dk$ until $k \to 0$, the full path integral is completely solved.

The use of the averaged effective action $\Gamma[\varphi]$ as a functional shown in the previous sections has proven to be convenient for the derivation of functional equations, as well as for numerical calculations. Instead of integrating the full path-integral at once like in the DSE formalism, we would like to implement of Wilson's idea into the $\Gamma[\varphi]$ to treat vertex functions in a RG-like approach. Introducing the scale parameter into the path integral the effective action is promoted into a scale dependent functional $\Gamma \to \Gamma_k$ that agrees, up to corrections, with the bare action S in the ultraviolet and includes all quantum fluctuations at $k \to 0$ [13]:

$$\Gamma_{k\to\Lambda} \approx S_{bare}, \qquad \Gamma_{k\to 0} \to \Gamma. \tag{2.53}$$

The definition of the scale dependent effective action is not unique. The method in which infrared contributions are neglected changes the flow $\partial_k \Gamma_k$ in theory space, analogously as the choice of the renormalisation scheme to renormalise perturbatively a quantum field theory. Nevertheless, given a ultraviolet cutoff Λ, the system shall independently converge to the same fixed point $\partial_k \Gamma_k^* = 0$ in which the full quantum effective action is recovered.

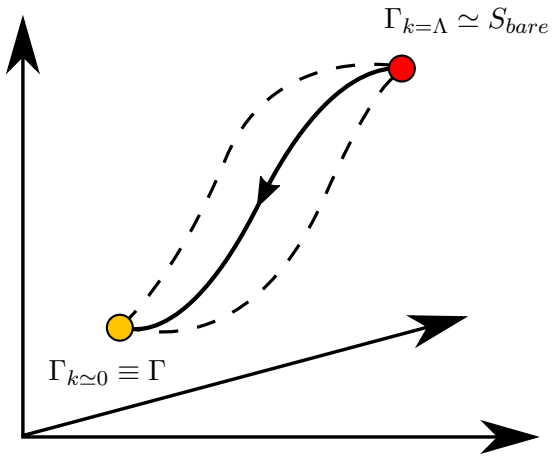

Figure 2.7: Pictorial representation of the application of Wilson's idea of integrating quantum fluctuations over momentum shells. The picture shows the evolution of the scale-dependent effective action in theory space. Dashed lines indicate alternative flow trajectories, with virtually fixed UV and IR points.

The scale-dependent effective action is formally derived from the definition of the scale-dependent generating functional. In order to force the scale-dependent effective action to satisfy the properties mentioned above, it is convenient to introduce a term with k whose properties lead to the proper behaviour. Following [26], this is achieved by promoting $Z[J]$ into the scale-dependent generating functional $Z_k[J] = \exp\left(-\Delta S_k\left[\frac{\delta}{\delta J}\right]\right) Z[J]$. In terms of the path integral formulation, this is translated into

$$Z_k[J] = e^{W_k[J]} = \int \mathcal{D}\Phi \exp\left\{-S[\Phi] - \Delta S_k[\Phi] + \int_x J^{\boldsymbol{a}}\, \Phi^{\boldsymbol{a}}\right\}. \tag{2.54}$$

Here ΔS_k is a regulator term, also known as infrared cutoff, that depends on the scale parameter and on the fields. The regulator is, in principle, free of choice as long as it satisfies certain properties, in particular $\Delta S_{k\to 0} = 0$ where the full quantum functional is recovered. The flows of the functionals are already attainable under this definition. Nevertheless, interesting properties and great numerical success have been achieved for the particular choice of a quadratic regulator in the fields:

$$\Delta S_k[\Phi] = \frac{1}{2}\int_x \Phi^{\boldsymbol{a}}(x)\; R_k^{\boldsymbol{ab}}(x)\; \Phi^{\boldsymbol{b}}(x), \tag{2.55}$$

where the regulator function $R_k^{\boldsymbol{ab}}$ encodes all the scale dependence. Its matrix notation, which includes correct signs for the fermionic case, is shown in the Appendix A. The function R_k must satisfy three general properties in momentum space:

$$\lim_{q^2/k^2\to 0} R_k(q) > 0, \qquad \lim_{k\to 0} R_k(q) = 0, \qquad \lim_{k\to\infty} R_k(q) \to \infty. \tag{2.56}$$

The first of the properties is related to the infrared cutoff implementation. When R_k is positive definite, the regulator function acts as a mass term which suppresses contributions below the scale k [70]. The other two limits are set in order to satisfy the conditions indicated in expression (2.53). The definition of the effective action under this choice of regulator is done similarly as in expression (2.3), yielding:

$$\Gamma_k[\varphi] = \sup_J \left(\int_y J_{\boldsymbol{a}}\varphi_{\boldsymbol{a}} - W_k[J]\right) - \Delta S_k[\varphi]. \tag{2.57}$$

Now this modified Legendre transform is not necessarily convex. Nevertheless, its convexity is only required in the limit $k \to 0$, agreeing with the general definition of the quantum effective action. For the case of quadratic regulator in the fields, it can be shown that

$$\varphi_{\boldsymbol{a}} = \frac{\delta W_k}{\delta J_{\boldsymbol{a}}}, \qquad J_{\boldsymbol{a}} = \frac{\delta \Gamma_k}{\delta \varphi_{\boldsymbol{a}}} + R_k^{\boldsymbol{ab}}\varphi_{\boldsymbol{b}}. \tag{2.58}$$

These identities lead to an important conclusion regarding the relation of the derivatives of the effective action and the connected correlators. The expressions lead to:

$$\frac{\delta J_{\boldsymbol{b}}}{\delta \varphi_{\boldsymbol{a}}} = \frac{\delta^2 \Gamma_k}{\delta \varphi_{\boldsymbol{a}} \delta \varphi_{\boldsymbol{b}}} + R_k^{\boldsymbol{ab}}, \qquad \frac{\delta \varphi_{\boldsymbol{b}}}{\delta J_{\boldsymbol{a}}} = \frac{\delta^2 W_k}{\delta J_{\boldsymbol{a}} \delta J_{\boldsymbol{b}}} \equiv G_k^{\boldsymbol{ab}}. \tag{2.59}$$

Here we defined the scale-dependent connected propagator:

$$G_k^{\boldsymbol{ab}} = \frac{\delta^2 W_k}{\delta J_{\boldsymbol{a}} \delta J_{\boldsymbol{b}}} = \langle \Phi_{\boldsymbol{a}} \Phi_{\boldsymbol{b}} \rangle_J - \langle \Phi_{\boldsymbol{a}} \rangle_J \langle \Phi_{\boldsymbol{b}} \rangle_J = \langle \Phi_{\boldsymbol{a}} \Phi_{\boldsymbol{b}} \rangle_J - \varphi_{\boldsymbol{a}} \varphi_{\boldsymbol{b}}. \tag{2.60}$$

An important identity relating both entities is derived by applying the functional chain rule into the identity matrix, expressed as $\delta^{\boldsymbol{ab}}$ to include indices. It follows $\delta^{\boldsymbol{ab}} = \frac{\delta J_{\boldsymbol{b}}}{\delta J_{\boldsymbol{a}}} = \int \frac{\delta J_{\boldsymbol{b}}}{\delta \varphi_{\boldsymbol{c}}} \frac{\delta \varphi_{\boldsymbol{c}}}{\delta J_{\boldsymbol{a}}}$ and it leads to the relation:

$$G_k = \left(\Gamma_k^{(2)} + R_k \right)^{-1}, \tag{2.61}$$

where here the operator notation was used for simplicity. This identity is the scale-dependent version of expression (2.6) and states that the regulator function contributes within the connected propagators. Consequently, every propagator included within the FRG formalism is implicitly a regularised propagator.

The remaining requirement to solve the now known scale-dependent functionals is their flow equations, i.e. the equations that describe how the scale parameter evolves and which momentum shells are integrated in every step. For such purpose the dimensionless scale parameter t is introduced in the usual renormalisation group notation:

$$t = \log\left(\frac{k}{\Lambda}\right), \qquad \partial_t \equiv \frac{d}{dt} = k \frac{d}{dk} = k\, \partial_k. \tag{2.62}$$

The flow equation of the 1PI effective action is obtained from derivating expression (2.57) with respect to t. Since $J_{\boldsymbol{a}} \varphi_{\boldsymbol{a}}$ are, in principle, scale-independent, it follows:

$$\begin{aligned} \partial_t \Gamma_k[\varphi] = & -\partial_t W_k[J] - \partial_t \Delta S_k[\varphi] \\ = & \int_q \frac{1}{2} \partial_t R_k^{\boldsymbol{ab}} \langle \Phi_{\boldsymbol{a}} \Phi_{\boldsymbol{b}} \rangle_J - \frac{1}{2} \partial_t R_k^{\boldsymbol{ab}} \varphi_{\boldsymbol{a}} \varphi_{\boldsymbol{b}} \\ = & \frac{1}{2} \int_q \partial_t R_k^{\boldsymbol{ab}} \left(G_k^{\boldsymbol{ab}} + \varphi_{\boldsymbol{a}} \varphi_{\boldsymbol{b}} \right) - \partial_t R_k^{\boldsymbol{ab}} \varphi_{\boldsymbol{a}} \varphi_{\boldsymbol{b}} \\ = & \frac{1}{2} \int_q \partial_t R^{\boldsymbol{ab}} \left(\Gamma_k^{(2)} + R_k \right)^{-1}_{\boldsymbol{ab}}. \end{aligned} \tag{2.63}$$

The identities during the derivation in expression (2.63) are straightforwardly obtained from the properties of $Z_k[J]$. This expression, written in a more compact way, is called Wetterich's flow equation [13] and reduces to:

$$\partial_t \Gamma_k = \frac{1}{2} \mathrm{STr} \left[\left(\Gamma_k^{(2)} + R_k \right)^{-1} \partial_t R_k \right] \tag{2.64}$$

Here the super-trace STr not only explicitly indicates every traced index and correct bosonic and fermionic signs, but also includes momentum integration within. This exact flow equation describes how the Euclidean effective action evolves in function of the scale parameter k in terms of non-perturbative one-loop contributions that are diagrammatically easily treatable. The one-loop dependence is a direct consequence of the use of quadratic regulators in the fields [71]. In order to properly include the regulator in the regularised propagator term, fermionic regulators include a tensor structure that needs to be carefully treated. Further details are found in the Appendix C. The diagrammatic formulations of the flow equation is shown in Figure 2.8.

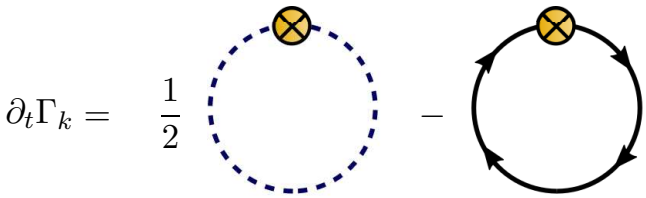

Figure 2.8: Pictorial representation of Wetterich's flow equation as non-perturbative one-loop diagrams. The blue, dashed-line diagram represent every bosonic field whereas the fermionic diagram follows usual convention.

Wetterich's flow equation is in most systems complicated to treat and, in practice, cannot be in general solved exactly. There exist different approaches to the solution of the flow equation, but truncations are usually required. For instance, a vertex expansion used like in the DSE approach leads to an infinite set of coupled flow equations for the n-point correlators. They depend on contributions that include up to $n + 2$ full vertices, given by the derivative of the inverse matrix $\delta_\varphi G_k = -G_k(\delta_\phi \Gamma_k^{(2)})G_k$ relation. Consequently, in order to obtain a numerical solution, the implementation of the truncation of the flow equations is needed. This compromises the independence of the system on the choice of the regulator, as it is satisfied only within the full, untruncated flow. In practical computations, the system starts at a set of initial conditions given by $\Gamma_{k=\Lambda}$ and evolves until $\Gamma_{k\to 0}$ which is, in general in a truncated system, regulator dependent. Although the effect of the truncation is unavoidable, the regulator dependence provides insight on the quality of the truncations used and, in addition, a more adequate regulator can be chosen to numerically optimize the truncation.

2.3.1 Symmetries in the FRG

In the previous sections we explained the importance of symmetries in Quantum Field Theory and the role they play during the calculations. The derivation of the identities that followed the Green's functions and the generating functional were performed on the full, quantum path-integral and considered no regulator dependence. Hence, the behaviour of symmetries in the FRG shall be analysed before the approaches on the Wetterich's flow equation.

Following the same procedure done in section 2.1.3 invariance of the scale dependent path integral is required. Assuming, for simplicity, that the measure is invariant under field transformation, i.e. $\delta\mathcal{D}\Phi = 0$, it can be shown that the invariance of $Z_k \to Z_k' \to Z_k + \delta Z_k$ requires:

$$\delta Z_k = \int \mathcal{D}\Phi \left(-\delta S - \delta\Delta S_k + \int_x J_{\boldsymbol{a}}\delta\Phi_{\boldsymbol{a}}\right) \exp\left(-S - \Delta S_k + \int_x J_{\boldsymbol{a}}\Phi_{\boldsymbol{a}}\right) = 0. \quad (2.65)$$

The expression is rewritten in terms of the effective action performing the modified Legendre transformation. Using the identities obtained during the derivation of the FRG and, in particular, the relation $\delta\Gamma_k = \int \frac{\delta\Gamma_k}{\delta\varphi_{\boldsymbol{a}}}\delta\varphi_{\boldsymbol{a}}$, the following modified WTI (mWTI) is obtained:

$$\delta\Gamma_k = \langle \delta S + \delta\Delta S_k\rangle_J - \delta\Delta S_k[\varphi]. \quad (2.66)$$

The terms including the regulator ΔS_k do not necessarily cancel each other. However, expression (2.66) states that Γ_k is invariant under the symmetries of the bare action ($\delta S = 0$) along the flow only when the regulator is symmetric, i.e., $\delta\Delta S_k = 0$. Consequently, the use of a symmetric regulator is desired in order guarantee that the effective action (and similarly Green's functions) are invariant in every k-step.

As mentioned in the previous section, Wetterich's flow equation cannot be solved exactly and a truncation is needed. Particularly, the regulator may not be invariant in the ultraviolet scale $\Delta S_{k=\Lambda}$ and therefore breaking the effective action invariance from the very starting point. Nevertheless, the regulator is built such that it cancels in the infrared, i.e., $\Delta S_{k\to 0} = 0$, restoring $\delta\Gamma_{k\to 0} = \delta S$. In these cases, the mWTI indicates how the regulator must behave in the ultraviolet so that the UV contributions get cancelled during the flow. As a result, not only does the mWTI give the initial conditions, but also guarantees the symmetric behaviour of the full effective action in the infrared even when non-symmetric regulators are used. A similar analysis for the mWTIs can be done for scale-dependent Green's functions.

For gauge field theories like QCD, the analysis of the now modified Slavnov-Taylor identities (mSTIs) is performed analogously including the gauge-fixing and Faddeev-Popov action terms. The flows of the identities can be formally derived. It is crucial that the mSTI are satisfied in the infrared limit, since it leads to the physical gauge invariance necessary for a proper calculation of observables. For further information, see [26].

2.3.2 Approaches to Wetterich's flow equation

There exist different ways of solving Wetterich's flow equation in a truncated system [24, 72]. The first step is to parametrise the explicit form of the averaged effective action Γ_k. Due to its close relation to the bare action S_{bare}, it should contain, at least, the same degrees of freedom and interactions. However, the way to introduce the scale dependence into the system is not trivial, as it encodes which modes are integrated out. There exist different approaches to parametrise the effective action so that the Wetterich's equation is easily treatable:

- *Local Potential Approximation (LPA)*: all the scale dependence of the system is encoded within a local potential V_k dependent on the fields. For the bosonic case, it reads:

$$\Gamma_k[\varphi] = \int_x \left\{ \frac{1}{2} \left(\partial_\mu \varphi\right)^2 + V_k[\varphi] \right\}. \tag{2.67}$$

  The potential is normally parametrised in a Taylor expansion:

$$V_k[\varphi] = \sum_n \frac{V_k^{(n)}}{n!} \left(\varphi - \varphi_0\right)^n, \tag{2.68}$$

  where the $V_k^{(n)}$ are the potential couplings and Φ_0 is the scale-independent expansion point. In this case it is easy to see that $\partial_t \Gamma_k[\varphi] = \partial_t V_k[\varphi]$. The flow of every coupling $V_k^{(n)}$ can be found by applying n-field derivatives in both sides of Wetterich's equation and evaluating them both at φ_0, yielding:

$$\partial_t V_k^{(n)} = \frac{1}{2} \int_q \frac{\delta^n}{\delta \varphi^n} \left(\frac{\partial_t R_k(q)}{q^2 + R_k(q) + V_k''[\varphi]} \right) \Bigg|_{\varphi=\varphi_0}. \tag{2.69}$$

  Using the LPA approximation, one obtains also an infinite set of flow equations for every coupling of the potential $V_k^{(n)}$, but in most bosonic systems a truncation can be applied at order m when numerical results no longer change. Furthermore, using a potential such like the one previously mentioned allows to introduce a potential that, properly treated, can be used as a chiral symmetry breaking mechanism.

- *Derivative expansion*: the effective action in this case also includes a local potential, but the kinetic term is rewritten into a derivative expansion following:

$$\Gamma_k[\varphi] = \int_x \left\{ V_k[\varphi] + \frac{1}{2} Z_{k,\varphi} \left(\partial_\mu \varphi\right)^2 + \mathcal{O}\left(\partial^4\right) \right\}, \tag{2.70}$$

  where $Z_{k,\Phi}$ is the wave-function renormalisation function which, in general, can depend on the fields and the momentum. On the leading order, it gives scale dependence to the kinetic term and the study of its beta function $\partial_k Z_{k,\Phi}$ provides information regarding the anomalous dimensions of the system, defined analogously as in the RG formulation:

$$\eta_{k,\varphi} = -\frac{\partial_t Z_{k,\varphi}}{Z_{k,\varphi}}. \tag{2.71}$$

The flow $\partial_k Z_{k,\varphi}$ is normally given in momentum space as:

$$\partial_k Z_{k,\varphi} = \frac{d}{dp^2}\int_q \frac{\delta}{\delta\varphi(-p)}\frac{\delta}{\delta\varphi(p)}\left(\frac{\partial_t R_k(q)}{Z_{k,\Phi}q^2 + R_k(q) + V_k''[\varphi]}\right)\Bigg|_{\varphi=\varphi_0}. \tag{2.72}$$

In this case, the regularised propagator was parametrised in its natural form, following $G_k^{\varphi} = \left(Z_{k,\varphi}q^2 + R_k(q) + V_k''[\varphi]\right)^{-1}$. In some cases it is convenient to use a wave-function renormalisation dependent regulator to obtain simplifications in the flow equation, but the flow becomes anomalous-dimension dependent due to the flow of the regulator. For momentum dependent calculations, this approach is not convenient due to the momentum derivative, yielding further contributions which make the calculations more complicated.

- *Vertex expansion*: as similarly done in expression (2.10), the scale-dependent effective action is expanded in n-point functions:

$$\Gamma_k[\varphi] = \sum_{n=0}^{\infty}\frac{1}{n!}\left(\prod_{i=0}^{n}\int_{x_i}[\varphi_i(x_i)-\varphi_0]\right)\Gamma^{(n)}_{k,\varphi_1,\ldots,\varphi_n}(x_1,\ldots,x_n), \tag{2.73}$$

where the expansion is done in this case around the expansion fields φ_0, see [24] for further information. The flow equation of every n-point function is obtained by applying field derivatives and evaluating at φ_0. A general parametrization of the vertex functions is needed to describe these objects, although its behaviour can differ depending on the chosen truncation. The correlators $\Gamma^{(n)}_{k,\varphi_1,\ldots,\varphi_n}$ need to include also their tensor structure. In this work, they are parametrized in momentum space following [73] as:

$$\Gamma^{(n)}_{k,\varphi_1\ldots\varphi_n}(p_1,\ldots,p_{n-1}) = \bar{\Gamma}^{(n)}_{k,\varphi_1\ldots\varphi_n}(p_1,\ldots,p_{n-1})\prod_{i=1}^{n}\sqrt{Z_{k,\varphi_i}(p_i)}, \tag{2.74}$$

which includes all dynamical degrees of freedom involved in the system. The tensor kernel $\bar{\Gamma}^{(n)}_{k,\varphi_1\ldots\varphi_n}$ is written in terms of a basis of tensor structures $\mathcal{T}^{(i)}_{\varphi_1\ldots\varphi_n}$ following:

$$\bar{\Gamma}^{(n)}_{k,\varphi_1\ldots\varphi_n}(p_1,\ldots,p_{n-1}) = \sum_i z^{(i)}_{k,\varphi_1\ldots\varphi_n}(p_1,\ldots,p_{n-1})\mathcal{T}^{(i)}_{\varphi_1\ldots\varphi_n}(p_1,\ldots,p_{n-1}). \tag{2.75}$$

The dressing functions $z^{(i)}_{k,\Phi_1\ldots\Phi_n}$ depend, in general, on the renormalisation wave functions Z_{k,φ_i}. Under this definition, not only are the flows of the (momentum dependent) wave function renormalisation functions required, but also the flows of the dressing functions that allow a formal way of introducing momentum dependence into the system. In this work, the parametrisation of the n-point function will be explicitly specified.

2.3.3 Dynamical Hadronisation

The previous sections described how the FRG is derived and how it can be solved using the Wetterich's flow equation. The whole method can be interpreted as a differential version of the Dyson-Schwinger equations, and it can indeed provide the same information obtained alternatively. Nevertheless, since the FRG includes the scale k as an extra parameter and analyses physics in different scales, it provides some advantages that must be mentioned.

It is particularly convenient to introduce both microscopic and macroscopic degrees of freedom into the effective action. This provides a more efficient description of the physics in different scales and yields, in the particular QCD case, further insight on the conditions in which the low-energy degrees of freedom -hadrons- start contributing more than quarks and gluons. The usual approach to include mesons into the system is to use the Hubbard-Stratonovich (HS) transformation [74, 75], where a 4-Fermi interaction is rewritten in terms of a Yukawa term, see Appendix B.3 for details. Under this consideration, a purely fermionic system $\Gamma_k[\psi, \bar{\psi}]$ becomes half bosonised, i.e., including both fermions and the new degrees of freedom $\Gamma_k[\psi, \bar{\psi}, \sigma, \pi]$. Green's functions of both fermionic and bosonic degrees of freedom are computable through Wetterich's flow equation, but two major problems arise when running the flow.

First of all, although the 4-Fermi interaction with coupling λ_k is rewritten as a Yukawa interaction, the flow $\partial_t \lambda_k$ is in general non-vanishing. In QCD, gluon box diagrams contribute:

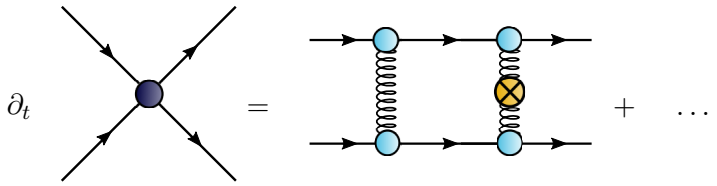

Figure 2.9: Flow of the non-vanishing 4-Fermi coupling in QCD.

In this situation, once an RG-step is performed into the half bosonised system, the 4-Fermi interaction appears, cancelling the effects of the HS transformation. One could attempt iterative HS transformations in every k-step, but this would include, at least, as many extra degrees of freedom as integration steps.

The second problem appears also as a consequence of the HS transformation, where the 4-Fermi coupling is related to the Yukawa coupling h_k following:

$$\lambda_k = \frac{h_k^2}{2m_{k,\phi}^2}. \tag{2.76}$$

where $m_{k,\phi}$ is the mass term of the boson introduced by the HS transformation. The coupling λ_k diverges at the chiral symmetry breaking scale, i.e., when the meson (the pion) becomes massive.

The method introduced within the FRG formalism that deals with these problems and facilitates apparent convergence is the *Dynamical Hadronisation* (DH), see [25, 76–78]. The idea behind this technique consists in promoting the bosonic degrees of freedom ϕ introduced via the HS transformation into scale dependent fields $\phi \to \phi_k$. Consequently, they have a flow of the form:

$$\partial_t \phi_k = \mathcal{C}_k[\varphi]. \tag{2.77}$$

Here $\mathcal{C}_k[\varphi]$ is a scale dependent function that can be parametrised, in principle, freely. Under this consideration, Wetterich's flow equation gets modified, as the left hand side of (2.63) includes the field flow term, yielding:

$$\left(\partial_t + \partial_t \phi_k[\varphi] \frac{\delta}{\delta \phi_k}\right) \Gamma_k[\varphi] = \frac{1}{2} \mathrm{STr} \left[\left(\Gamma_k^{(2)}[\varphi] + R_k\right)^{-1} \partial_t R_k\right]. \tag{2.78}$$

The extra term on the left hand side of the equation includes extra contributions in the flow equation that need to be considered. Under a convenient parametrisation, namely for instance $C_k[\varphi] = \partial_t A_k \bar{\psi}\psi$, the new flow of the 4-Fermi coupling becomes:

$$\partial_t \tilde{\lambda}_k = \partial_t \lambda_k - \partial_t A_k. \tag{2.79}$$

The function $\partial_t A_k$ is, in principle, arbitrary. Nevertheless, we parametrise it such that the flow of the new 4-Fermi coupling vanish in every k-step $\partial_t \tilde{\lambda}_k = 0$. This generalises the HS transformation leading the system into better convergence, including however extra terms in the flow equations. Further interpretations regarding the Dynamical Hadronisation become available once the parametrisation of the scale-dependent fields is explicitly implemented.

The 1PI effective action Γ_k calculated by having employed the dynamical hadronisation is not the same 1PI free energy without the implemented technique. Contributions related to the term $\partial_t \phi_k[\varphi] \frac{\delta}{\delta \phi_k} \Gamma_k[\varphi]$ are subtracted during the implementation of the DH. Consequently, a comparison between 1PI correlators needs to consider this difference. Furthermore, an important feature of this technique is that the new 1PI 4-Fermi interaction is, in every step, cancelled. This is true also for the bound-state calculations, in which the new 1PI 4-Point Green's function is simply replaced for a mesonic exchange, greatly simplifying the tensor structures involved, without any loss of generality.

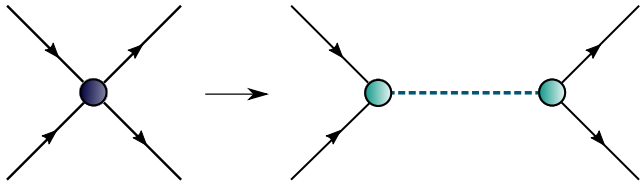

Figure 2.10: Diagrammatic 4-Fermi interaction expressed in terms of a meson exchange after the implementation of the Dynamical Hadronisation technique.

Chapter 3

Bound States in low-energy QCD

Functional methods were introduced in the previous section with the goal of extracting properties of bound states in a non-perturbative approach. In this chapter, the procedure to obtain these properties using the FRG is analysed within a low-energy QCD effective system, the Quark-Meson (QM) model.

First, we discuss the motivation of using effective models to describe low-energy QCD, and how a general expression is derived based on the QCD Lagrangian. Next, we obtain the QM effective action and identify which degrees of freedom are required in the system, depending on every FRG approach. Finally, results in Euclidean momenta will be analysed and observables will be obtained by employing analytic continuation methods, described in detail in Appendix B.

This chapter follows [79], which includes general results obtained in the QM model and comparisons with QCD calculations from the fQCD collaboration [73, 80–82].

3.1 Low-energy QCD effective models

QCD as a gauge theory has shown to provide an accurate description of the Physics of strong interactions. Non-perturbative approaches to QCD yielded many features and followed further understandings of Nature, but newer calculations are becoming both numerically and theoretically more demanding. Since we are interested on the low-energy regime, hadrons are colourless and gluons become decoupled [83, 84], we can reduce the complexity of QCD to an effective field theory, which is easier to treat. In order to achieve such feat, the QCD action shall be first split in terms regarding their gluon field dependence. Hence, the QCD action (2.20) is written explicitly:

$$S_{QCD} = \int_x \bar{q}\left(-\not{\partial} + m_q\right) q + g\,\bar{q}\,t^a A^a_\mu \gamma^\mu q + \frac{1}{2}\mathrm{Tr}\left(G_{\mu\nu}G^{\mu\nu}\right), \tag{3.1}$$

where we use the $(q, \bar{q})$ notation to emphasize the reference to QCD quarks, and m_q is their bare mass. A summation over flavour and colour indices is implied.

In order to attempt to eliminate gluons from the action, the QCD generating functional Z_{QCD} is written in its path integral formulation as described in [85]:

$$Z_{QCD} = \int \mathcal{D}q\mathcal{D}\overline{q} \exp\left(-\int_x \bar{q}\left(-\not{\partial} + m_q\right) q + \Gamma[j]\right), \tag{3.2}$$

where $\Gamma[j]$ is an effective action containing every gluonic contribution, expressed as:

$$\Gamma[j] = \log\left(\int \mathcal{D}A \exp\left(-\int_x \frac{1}{2} G_{\mu\nu}G^{\mu\nu} - g\int_x A^a_\mu\, j^\mu_a\right)\right). \tag{3.3}$$

Here the summation over Lorentz indices is implicit and j^a_μ is the colour current of the quarks defined as $j^\mu_a = \overline{q}\, t^a\gamma^\mu q$. Notice that the gauge-fixing and Faddeev-Popov terms of the QCD path-integral have been omitted from the formulation. Even though they may contribute in the low-energy systems, they are neglected during this derivation for simplicity.

Expression (3.3) encodes the gluon contributions of the path integral. The gluonic effective action $\Gamma[j]$ can be rewritten applying by field identities, see [85] for further details and a step-by-step procedure. One can show that the newly rewritten effective action $\Gamma[j]$ can be included into the QCD generating functional as:

$$\Gamma[j] = -\int_x \frac{\kappa g^2}{2} j^a_\mu j^\mu_a, \tag{3.4}$$

where κ is a constant. Under this expression, the gluon contribution gets reduced to a 4-Fermi interaction in the vector channels, i.e., terms proportional to $(\overline{q}\gamma^\mu q)(\overline{q}\gamma_\mu q)$. The idea behind this new interacting term is analogous to Fermi's theory of weak interaction, where weak processes are effectively described by a fermionic system, even when only the vector channel is present. The greatest advantage of this reformulation is the reduction of the number and type of degrees of freedom involved in the system, working only with fermions. Using a Fierz identity, the 4-Fermi interaction is expressed in the scalar-pseudoscalar channel $S - P$ and leads, in the massless case, to the Nambu-Jona-Lasinio (NJL) model [86, 87], the action of which follows:

$$S_{NJL}[\overline{\psi}, \psi] = \int_x -\overline{\psi}\not{\partial}\psi - \frac{\lambda}{4}\left((\bar{\psi}\psi)^2 + (\overline{\psi}i\gamma_5\psi)^2\right), \tag{3.5}$$

where $\lambda = \kappa g^2$. Notice that the $(\psi, \overline{\psi})$ notation is used for the fermions fields to distinguish them from the QCD fermions, as they do not necessarily carry the same indices. In expression (3.5), corresponding to the $U(1) \times U(1)$ formulation of a NJL model, summation of the corresponding indices of the theory is understood. The NJL model successfully introduced a mechanism to describe QCD's spontaneous chiral symmetry breaking with the introduction of light pseudoscalars [87]. Hence, it is a potential candidate for a low-energy QCD effective model. Its non-renormalisability requires a momentum cutoff, therefore limiting the range of predictability of this model. In this work, several different versions of the NJL action will be used.

3.1.1 The half-bosonised NJL model

A convenient starting point to describe QCD using the NJL model, which includes the mechanism to describe spontaneous chiral symmetry breaking, is the $U(2) \times U(2)$ symmetric model instead of the $U(1) \times U(1)$ introduced in the expression (3.5). The associated bare action follows:

$$S_{NJL}[\overline{\psi}, \psi] = \int_x -\overline{\psi}\partial\!\!\!/\psi - \lambda \left(\frac{(\bar{\psi}\psi)^2}{2N_f} + (\overline{\psi} i\gamma_5 \vec{\tau}\psi)^2 \right) \tag{3.6}$$

Here the fields are implicitly summed over colour and flavour indices, with the number of colours $N_c = 3$ and number flavour indices $N_f = 2$, which are left unchanged for the sake of notation. The generators of the $U(2) = SU(2) \times U(1)$ symmetry are represented within the 4-Fermi interaction, τ^i being the generators of $SU(2)$ with $\tau^i = \frac{1}{\sqrt{2N_f}}\sigma^i$ and σ^i the Pauli matrices.

It is desirable, for more efficient FRG calculations, to introduce macroscopic degrees of freedom into the system. This is usually performed by applying the Hubbard-Stratonovich transformation, the implementation of which is detailed in Appendix B. Following the same notation described in the appendix, the pseudoscalar $\vec{O}_5$ and scalar O_1 composite operators are defined:

$$O_1 = -i \left(\frac{h\bar{\psi}\psi}{\sqrt{2N_f}} \right) \qquad\qquad O_5^z = -i \left(h\bar{\psi} i\gamma_5 \tau^z \psi \right), \tag{3.7}$$

where the parameter h is introduced through the HS transformation as a Yukawa coupling together with the mesonic mass term m under the relation $\lambda = \frac{h^2}{2m^2}$. These operators are used in the transformation yielding the half-bosonised NJL model:

$$S[\psi, \overline{\psi}, \sigma, \vec{\pi}] = \int_x -\bar{\psi}\partial\!\!\!/\psi + \frac{1}{2}m^2 \left(\sigma^2 + \vec{\pi}^2\right) + h\bar{\psi} \left(\frac{\sigma}{\sqrt{2N_f}} + i\gamma_5 \vec{\tau}\vec{\pi} \right) \psi, \tag{3.8}$$

where σ and $\vec{\pi}$ are the auxiliary fields introduced by the transformation, and are named after the physical particles due to the quantum numbers they carry. The HS transformation is identical, and therefore the expressions 3.6 and 3.8 describe the same system.

Despite having introduced further degrees of freedom, obtaining their associated correlators becomes easier. However, there are some remarks to be mentioned. First of all, the half-bosonised system is apparently renormalisable, whereas the NJL model is not. The divergences are hidden in the auxiliary fields and the system becomes renormalisable only when interpreting the auxiliary fields as mean-fields. Furthermore, both σ and $\vec{\pi}$ have no kinetic term, and therefore are unphysical.

3.1.2 The Quark-Meson model

In the previous section the half-bosonised NJL model was derived in form of its bare action. In its formulation, the mesonic fields are auxiliary and carry no kinematics, they share the same mass term and the chiral symmetry breaking mechanism has yet to be implemented. Deriving the DSEs of the system, one can see that not only does the meson two point function get momentum dependence - and therefore include kinematics - but also generates multi-meson interactions dynamically. In order to include all these features, the scale-dependent effective action of the Quark-Meson (QM) model [27, 81, 88] is parametrised following:

$$\begin{aligned}\Gamma_k\left[\overline{\psi},\psi,\sigma,\vec{\pi}\right] = & \int_p \Big\{ Z_{k,\psi}\overline{\psi}\, i\not{p}\,\psi + \frac{p^2}{2}\left(Z_{k,\sigma}\sigma^2 + Z_{k,\pi}\vec{\pi}^2\right) + U_k[\rho] \\ & + \int_q h_k\overline{\psi}\left(\frac{\sigma}{\sqrt{2N_f}} + i\gamma_5\tau_z\pi^z\right)\psi \\ & - \int_q\int_r \lambda_k\left(\frac{\left(\overline{\psi}\psi\right)^2}{2N_f} + \left(\overline{\psi}i\gamma_5\vec{\tau}\psi\right)^2\right)\Big\}.\end{aligned} \tag{3.9}$$

The effective action includes the original fermionic terms, i.e. the kinetic term and 4-Fermi interaction term. The latter is dynamically generated, therefore it must be included in Γ_k. Moreover, its flow equation is necessary to properly implement dynamical hadronisation.

Here a potential $U_k[\rho] = V_k[\rho] - c\sigma$ was introduced in function of $\rho = \frac{1}{2}\left(\sigma^2 + \vec{\pi}^2\right)$. In comparison to the half-bosonised NJL model, the mass term is encoded within the potential term and, additionally, a kinetic term for the meson fields was introduced. The mass terms of the mesons are computed by performing a 2-meson derivative of the potential V_k. Choosing $\langle\sigma\rangle = \sigma_0$ and $\langle\pi^z\rangle = 0$, being σ_0 a value to be determined, it is easy to check that the meson masses obtained through the curvature of the potential satisfy:

$$m^2_{k,\pi} = \frac{\delta^2}{\delta\pi\delta\pi}V_k[\rho]\Big|_{\langle\Phi\rangle} = V_k'[\rho_0], \tag{3.10}$$

$$m^2_{k,\sigma} = \frac{\delta^2}{\delta\sigma\delta\sigma}V_k[\rho]\Big|_{\langle\Phi\rangle} = V_k'[\rho_0] + \sigma_0^2 V_k''[\rho_0], \tag{3.11}$$

where $\rho_0 = \frac{\sigma_0^2}{2}$. In order to provide mesons with different masses, it is necessary that, at least, 3-meson interactions are present in the potential. Commonly, a potential of the form $V_k = \mu\rho + \frac{\tilde{\lambda}}{2}\rho^2$ is used such that mesons may have different masses and multi-meson interactions are included into the system. The missing requirement is the determination of σ_0, which is obtained after minimising $U[\rho]$:

$$\frac{\delta}{\delta\rho}U_k[\rho]\Big|_{\langle\Phi\rangle} = 0. \tag{3.12}$$

Here the explicit chiral symmetry breaking term $-c\sigma$ plays a key role. In its expectation value, the chiral symmetry breaking term is proportional to the fermion condensate $\langle\overline{\psi}\psi\rangle$. When the condensate is different from zero, quarks become massive and so do the pions as Goldstone bosons. Hence, the minimised potential U_k under the presence of $-c\sigma$ obtains a non-zero value for $\langle\sigma\rangle$ and, consequently, breaks chiral symmetry. Summarising, not only does U_k split mesonic masses, but also provides the system with a chiral symmetry breaking mechanism.

The mentioned mechanism gives mass to quarks, and therefore the fermion propagator needs to include a mass term. It is clear from expression (3.9) that the fermion mass becomes proportional to the Yukawa coupling in the form:

$$\overline{m}_F \propto \frac{h_k}{\sqrt{2N_f}}\sigma_0, \tag{3.13}$$

where $\overline{m}_F$ denotes the renormalised fermion mass which is proportional, up to renormalisation constants, to the minimum of the potential σ_0.

3.2 FRG approach to the Quark-Meson model

As explained in Chapter 2, a system can be treated in the FRG using several approaches and approximations. We studied the system under different considerations and evaluated which setting corresponds to a better low-energy description of QCD. In the following subsections the different approximations as well as the technical details involved in every case are discussed. The explicit expressions of the flow equations of every parameter treated, as well as their diagrammatic form, are explicitly shown in Appendix C.

3.2.1 Approximations

- *LPA*: The wave functions are set to unity $Z_{k,i} = 1$, the Yukawa coupling is scale and momentum independent $h_k = h$ and the 4-Fermi coupling λ is set to zero in every k-step. The whole scale dependence is encoded in the potential V_k which is parametrised as:

$$V_k[\rho] = \sum_{n=0}^{8} \frac{V_k^{(n)}}{n!}(\rho - \rho_{exp})^n. \tag{3.14}$$

  The scale independent expansion point follows $\rho_{exp} = \frac{\sigma_{exp}}{2}$ and is set at the beginning of the calculation. The flow of every potential coupling $V_k^{(n)}$ is obtained by plugging the potential at both sides of the flow equation and evaluating the resulting expression at ρ_{exp} at both sides. Notice that the defined potential contains nine coefficients to be determined. This particular choice comes from the fact that, numerically, the contribution of higher order terms is negligible, with relative error to the current result of $< 10^{-8}$.

- *LPA + Y*: The previous equations are complemented with a running Yukawa coupling which remains momentum independent. Its flow equation can be derived equivalently from the flow of the quark two-point function:

$$\partial_t h_k = \frac{1}{4N_c N_f} \frac{\sqrt{2N_f}}{\langle\sigma\rangle} \frac{\delta^2 \partial_t \Gamma_k}{\delta\psi\delta\overline{\psi}}. \tag{3.15}$$

  The flow of the Yukawa coupling can also be obtained from the flow of the three-point function by performing a three-field derivative. The expressions are equivalent, therefore we decided to more conveniently work with two-field derivative case.

- *LPA + Y'*: The Yukawa coupling includes additional momentum dependence. In terms of computation, an additional set of grid points, as well as their flow equations need to be included. The momentum dependent Yukawa coupling used in this approximation is evaluated at the average of relative and total momentum following the parametrisation:

$$h(p,q) = h\left((p+q)^2 + \frac{(p-q)^2}{4}\right). \tag{3.16}$$

  The choosing of this parametrisation is based on the dominant behaviour of the relative momenta in the three-point function [79, 80]. Using this formulation, the Yukawa coupling becomes a one parameter function, simplifying computations and interpolations.

- *Full case (+ DH)*: The wave function renormalisations are explicitly included and carry explicit momentum dependence $Z_{k,i}(p^2)$. Their flow equations are directly derived from the fermion and meson inverse propagators that need to be parametrised before running the system. The flow equation of the momentum dependent $Z_{k,i}$ become more complicated in the case where the regulator is also wave function dependent. For further details on how to proceed in this case, see Appendix C.

  When DH is present, some flow equations obtain additional contributions and thus the system is modified. The initial consideration is the parametrisation of scale dependent mesons. In this work, they are parametrised as:

$$\partial_t \sigma_k = \frac{1}{\sqrt{2N_f}} \dot{A}_k \overline{\psi}\psi, \qquad \partial_t \vec{\pi}_k = \dot{A}_k \overline{\psi} i\gamma_5 \vec{\tau}\psi. \tag{3.17}$$

  Here A_k is associated to the flow of the scale-dependent field within the dynamical hadronisation and shall not be mistaken with the quark propagator dressing $A(p^2)$. This notation was chosen to follow literature such as [73, 79].

  Explicitly, the flow of the scale-dependent fields in momentum space satisfy:

$$\partial_t \sigma_k(p) = \frac{1}{\sqrt{2N_f}} \int_q \dot{A}_k(p-q,q)\overline{\psi}(p-q)\psi(q) \tag{3.18}$$

$$\partial_t \pi_k(p) = \int_q \dot{A}_k(p-q,q)\overline{\psi}(p-q) i\gamma_k \vec{\tau}\psi(q) \tag{3.19}$$

Notice that $\dot{A}_k$ behaves like a Yukawa coupling. For this reason, its momentum dependence is parametrised equivalently, following:

$$\dot{A}_k(p,q) = \dot{A}_k\left(\frac{(p-q)^2}{4}\right). \tag{3.20}$$

Under this consideration, the flow of the 4-Fermi interaction can be set to zero in every k-step. In principle, a full momentum dependence requires the four-point function to depend on three momenta. For convenience, the system is set in the t-channel:

$$\lambda_k(p,-p,p) = \lambda_k(p^2), \tag{3.21}$$

reducing the momentum dependence of the four-point function to a single argument. Under this consideration, the flow of the 4-Fermi coupling can be set to zero according to:

$$\partial_t \lambda_k(p,-p,p) = \text{Flow}\,\lambda_k - \dot{A}_k(p^2)h_k(p^2) = 0. \tag{3.22}$$

Setting the flow $\dot{A}(p^2)$ as:

$$\dot{A}_k(p^2) = \frac{\text{Flow}\,\lambda_k}{h_k(p^2)}. \tag{3.23}$$

The effect of the scale-dependent mesons is reflected on the flow of the Yukawa coupling, which gets an additional contribution reading:

$$\partial_t h_k(p^2) = \text{Flow}\,h_k - \frac{1}{\langle\sigma\rangle}\dot{A}_k(p^2)\Gamma^{(2)}_{k,\pi}(0), \tag{3.24}$$

where $\Gamma^{(2)}_{\pi}(0)$ is the two-point function of the pion that appears from the additional term on left hand side of expression (2.78).

- *Full case with full momentum dependence and DH*: in addition to the presence of the renormalisation wave functions and, depending on the case, of the DH terms, here the Yukawa coupling includes its full momentum dependence in the form:

$$h_k(p,q) = \hat{h}_k(p^2,q^2,z), \tag{3.25}$$

where z is the relative angle between p and q. Consequently, the momentum dependence of the four-point function and $\dot{A}_k$ are also modified:

$$\lambda_k(p,q,-p) = \lambda_k(p^2,q^2,z), \tag{3.26}$$
$$\dot{A}_k(p,q) = \dot{A}_k(p^2,q^2,z). \tag{3.27}$$

In this case, the calculation of this approximation requires more computational power and also requires a large grid of points for h_k, $\dot{A}_k$ and λ_k and three-dimensional interpolation. Results involving the full momentum dependence are not shown in this chapter.

3.2.2 Definition of vertex functions

One of the key points in order to work consistently in the FRG and to facilitate the calculation of observables is the definition of the vertex functions. As long as they satisfy the tensor structures corresponding to the correlators, their parametrisation can be chosen freely. This is particularly convenient for two reasons: both scale and momentum dependence are encoded in the correlator according to the requirements of the system, and may simplify, together with the choice of regulator, the flow equations considerably.

Throughout the calculations involving the QM model, the same parametrisation for the n-point functions will be used. The meson correlators are parametrised following:

$$\Gamma^{(2)}_{k,\pi}(p^2) = Z_{k,\pi}(p^2)p^2 + m^2_{k,\pi}, \tag{3.28}$$

$$\Gamma^{(2)}_{k,\sigma}(p^2) = Z_{k,\sigma}(p^2)p^2 + m^2_{k,\sigma}, \tag{3.29}$$

where $m^2_{k,\pi} = V_k'[\rho]$ and $m^2_{k,\sigma} = V_k'[\rho] + 2\rho V_k''[\rho]$. The bare masses are momentum independent and are obtained directly from the curvature of the potential. In the case where wave functions are set to unity, the momentum dependence in the propagators is solely dominated by the free kinetic term. Similarly done for the quark correlator, we parametrise its two-point function as:

$$\Gamma^{(2)}_{k,\psi\bar{\psi}}(p) = Z_{k,\psi}(p^2)i\not{p} + m_{k,\psi}(p^2), \tag{3.30}$$

where again, the momentum dependence is hidden in the quark wave function renormalisation and becomes relevant only when the wave functions are not set to unity. In this case, $m_{k,\psi} = \frac{h_k\sigma}{\sqrt{2N_f}}$. The definitions of the vertex functions allow an easy computation of the flow of the wave function renormalisations:

$$\partial_t Z_{k,\phi}(p^2) = \frac{1}{p^2}\left(\partial_t\Gamma^{(2)}_{k,\phi}(p^2) - \partial_t\Gamma^{(2)}_{k,\phi}(0)\right), \tag{3.31}$$

$$\partial_t Z_{k,\psi}(p^2) = \frac{-i\not{p}}{p^2}\left(\partial_t\Gamma^{(2)}_{k,\psi\bar{\psi}}(p^2)\right), \tag{3.32}$$

for $\phi = (\sigma, \pi)$. Notice, however, that the expressions (3.31) and (3.32) are not straightforward to solve when the regulator is proportional to $Z_{k,i}$. In such case, iterative procedure or the method shown in Appendix C is required.

3.2.3 Renormalised parameters

Despite the FRG being built such that initial and final conditions are independent of the regulator, different truncations lead to different IR values in practical calculations of an approximated system. Furthermore, in Quantum Field Theory the quantities that have physical meaning are not necessarily the ones appearing in the effective action. For this reason, the concept of renormalised parameters and renormalised fields needs to be defined.

In a quantum field theory, the Lagrangian of the system is modified by rescaling the fields according to $\Phi = Z_{\Phi}^{\frac{1}{2}}\bar{\Phi}$, where we use the over line to denote renormalised fields. In the FRG, the usual convention to obtain the renormalised fields follows:

$$\bar{\Phi} = Z_{k,\Phi}^{\frac{1}{2}}\Phi. \tag{3.33}$$

Here, the scale dependence of the renormalised field is made implicit. Under this definition, the effective action of the QM model can be rewritten in terms of renormalised fields:

$$\begin{aligned}\Gamma_k = \int_p \Big\{ \bar{\bar{\psi}}\, i\not{p}\, \bar{\psi} + \frac{p^2}{2}\left(\bar{\sigma}^2 + \vec{\bar{\pi}}^2\right) + \bar{U}_k[\bar{\rho}] + \int_q \bar{\bar{\psi}}\left(\frac{\bar{h}_{k,\sigma}\bar{\sigma}}{\sqrt{2N_f}} + i\bar{h}_{k,\pi}\gamma_5\tau_z\bar{\pi}^z\right)\bar{\psi} \\ - \int_q\int_r \bar{\lambda}_k\left(\frac{\left(\bar{\bar{\psi}}\bar{\psi}\right)^2}{2N_f} + \left(\bar{\bar{\psi}}i\gamma_k\vec{\tau}\bar{\psi}\right)^2\right)\Big\}.\end{aligned} \tag{3.34}$$

Under this definition, every $Z_{k,i}$ is absorbed within the fields and in the now renormalised couplings. Particularly, the ones appearing in the rewritten effective action follow:

$$\bar{h}_{k,\phi} = \frac{h_k}{Z_{k,\psi}Z_{k,\phi}^{\frac{1}{2}}}, \qquad \bar{\lambda}_k = \frac{\lambda_k}{Z_{k,\psi}^2}. \tag{3.35}$$

Similarly as in perturbation theory, renormalised parameters are the ones related to physical quantities. There is, however, more than one way of parametrising the renormalised quantities, depending on the renormalisation scheme chosen. For instance, one can define the momentum dependent renormalised meson masses as $\bar{m}_{k,\phi}^2(p^2) = \frac{m_{k,\phi}^2}{Z_{k,\phi}(p^2)}$. This definition leads to the interpretation of a mass function, similar to the mass functions obtained in the DSE approach. Furthermore, this particular definition may be convenient for the simplification of terms in the flow equations.

In this work, the renormalised parameters are defined according to the following conventions. The renormalised fields follow:

$$\bar{\overline{\psi}} = \bar{Z}_{k,\psi}^{\frac{1}{2}}\overline{\psi}, \qquad \bar{\psi} = \bar{Z}_{k,\psi}^{\frac{1}{2}}\psi, \tag{3.36}$$

$$\bar{\pi}^i = \bar{Z}_{k,\pi}^{\frac{1}{2}}\pi^i, \qquad \bar{\sigma} = \bar{Z}_{k,\pi}^{\frac{1}{2}}\sigma, \tag{3.37}$$

where we defined:

$$\bar{Z}_{k,\pi} = Z_{k,\pi}(p^2 = 0), \qquad \bar{Z}_{k,\psi} = Z_{k,\psi}(p^2 = 0). \tag{3.38}$$

Accordingly, the renormalised average meson field follows $\bar{\rho} = \bar{Z}_{k,\pi}\rho$. This allows also to renormalise the terms of the potential consistently:

$$\bar{V}_k^{(n)} = \frac{V_k^{(n)}}{\bar{Z}_{k,\pi}^n}, \qquad \bar{c}_k = \frac{c}{\bar{Z}_{k,\pi}^{\frac{1}{2}}}. \tag{3.39}$$

Notice that in its renormalised version, $\bar{c}$ becomes scale dependent. This property plays an important role when the system is treated only with renormalised parameters. For completeness the rest of the relevant renormalised quantities follow:

$$\bar{h}_k = \frac{h_k}{\bar{Z}_{k,\psi}\bar{Z}_{k,\pi}^{\frac{1}{2}}}, \qquad \bar{\lambda}_k = \frac{\lambda_k}{\bar{Z}_{k,\psi}^2}, \tag{3.40}$$

Under these definitions, the masses obtained by the potential and the quark mass are simply $\bar{m}_{k,\phi}^2 = \frac{m_{k,\phi}^2}{\bar{Z}_{k,\pi}}$ and $\bar{m}_\psi = \frac{m_\psi}{\bar{Z}_{k,\psi}}$. It should be kept in mind that alternative definitions of the renormalised parameters require different interpretations of the physical quantities. Calculation-wise, the method in which parameters are renormalised dictates which set of initial conditions needs to be taken. In some systems, it is more convenient to work with scale dependent renormalised parameters. Given the fact that the $\bar{Z}_{k,i}$ are scale dependent, the flow equations are modified. For instance, in the flow equation of the renormalised potential couplings, additional terms coming from the scale dependence of the renormalised expansion point appear:

$$\delta_\rho^n \partial_t \bar{V}[\bar{\rho}] = (\partial_t - n\eta_{k,\pi})\bar{V}_k^{(n)} - \bar{V}_k^{(n+1)}(\partial_t + \eta_{k,\pi})\bar{\rho}_{k,exp} \tag{3.41}$$

where $\eta_i = -\frac{\partial_t \bar{Z}_{k,i}}{\bar{Z}_{k,i}}$ is the anomalous dimension. This approach and the one solving the unrenormalised variables and renormalising afterwards are exactly equivalent and their use is strongly dependent on the renormalisation scheme defined, see [81]. In this work, every parameter involved is calculated in their unrenormalised form, and all the flow equations derived correspond to the scale-dependent bare quantities. Their renormalised counterparts are obtained afterwards.

3.2.4 Results and discussion

The results are organised in two main sections. First of all, the results obtained after solving the Quark-Meson model in different approximations are shown. Curves comparing the behaviour of the most relevant quantities in terms of the scale and momentum are displayed. Secondly, analytic continuation is implemented in the results of the approximations that include dynamical hadronisation, showing the predictions of the observables obtained.

The comparison between the different approximations has been implemented under several conditions. As a low-energy model, the range of validity of the QM model is limited. Normally, it is bounded within the region $0 < \sqrt{p^2} < 0.3$ GeV. Hence, the UV cutoff is chosen to be $\Lambda = 0.95$ GeV, allowing the system to evolve including all the dynamics involved until reaching the infrared values. Furthermore, the renormalised minimum of the effective potential is expected to agree with the pion decay constant at the IR cutoff as $\bar{\rho}_0 = \frac{\bar{\sigma}_0{}^2}{2}$, with $\bar{\sigma}_0 = f_\pi = 0.093$ GeV [1]. This condition is also useful for the determination of the parameter c, which in its renormalised value must satisfy $\bar{c}_0 = f_\pi \bar{m}^2_{\mathrm{IR},\pi}$. These conditions are still insufficient to solve the system uniquely. In order to agree with the IR known values, which are the ones compatible with experimental data, the following quantities are also desired:

- $\bar{m}_{\mathrm{IR},\pi} = 0.138$ GeV
- $\bar{m}_{\mathrm{IR},\sigma} \approx 0.550$ GeV
- $\bar{m}_{\mathrm{IR},\psi} = 0.297$ GeV
- $\bar{h}_{\mathrm{IR},\psi} = \bar{m}_{\mathrm{IR},\psi} \frac{\sqrt{2N_f}}{f_\pi} = 6.387$

The assumption of $N_f = 2$ was used in the last identity. The physical mass of the sigma meson is not exact. According to the PDG, the f_0 or σ meson have a mass laying between $400 \sim 550$ MeV. As a result, the mass of the sigma is set to this particular value for convenience.

Before indicating the set of initial conditions, the explicit form of the regulator is required. Different types of regulators have been used to obtain the results. For instance, in [79] we used dressed regulators. In this work only calculations with undressed regulators are shown, in the form:

$$R_k^B = p^2 r_k^B\left(\frac{p^2}{k^2}\right), \qquad R_k^F = i\not{p} r_k^F\left(\frac{p^2}{k^2}\right), \tag{3.42}$$

where the bosonic $r_k^B(x)$ and fermionic $r_k^F(x)$ relate as:

$$1 + r_k^F(x) = \sqrt{1 + r_k^B(x)}. \tag{3.43}$$

[1] The identity is only true in the chosen renormalisation scheme. Generally, $\bar{\sigma}_0 = \sqrt{\frac{\bar{Z}_\sigma}{\bar{Z}_\pi}} f_\pi$ is satisfied, see [89] for further details.

For $r_k^B(x)$ we choose the form of the exponential regulator with $m = 2$, i.e. the expression:

$$r_k^B(x) = \frac{x}{e^{x^2} - 1}. \tag{3.44}$$

Under this choice, the regulator drops its value rapidly for values of p^2 reaching k^2. The one-loop equations involved in the resolution of the system involve contributions of parameters depending on $(p \pm q)^2$. For this reason, the momentum integration is performed in every flow from the IR cutoff until $(2.5\,k)^2$. Contributions of q^2 greater than $(2.5\,k)^2$ are negligible due to the effect of the regulator. In other words, the momentum integral follows:

$$\partial_t F_k(p) = \int_0^\infty dq^2 \tilde{F}_k(p-q) \quad \rightarrow \quad \partial_t F_k(p) = \int_{\text{IR}}^{(2.5\,k)^2} dq^2 \tilde{F}_k(p-q). \tag{3.45}$$

The computation of the momentum and angular integrals is performed using an adaptive quadrature which, in this work, was performed using the hcubature c++ package. The detailed description of this package can be found in in https://github.com/stevengj/cubature.

Finally, the remaining pieces are the initial conditions, the values set at the UV cutoff. The non-trivial initial conditions used in every approach are exposed in table 3.1. The remaining scale-dependent parameters from the potential $V_\Lambda^{(i)}$ with $i > 2$ are set identically to zero, and every initial wave function renormalisation is set to the unit $Z_{\Lambda,i} = 1$.

	LPA	LPA+Y	LPA+Y'	Full	Full+DH
σ_{exp}	93	93	93	30.7	28.5
$\tilde{V}_\Lambda^{(1)}$	820.75	612.8	607.1	2491.65	2795.75
$V_\Lambda^{(2)}$	17	40	40	350	15
h_Λ	6.387	5.09	5.095	16.75	18.9

Table 3.1: Table of the non-zero initial ultraviolet conditions in function of every approximation used. $\tilde{V}_\Lambda^{(1)}$ is related to the original $V_\Lambda^{(1)}$ according to $V_\Lambda^{(1)} = \left(\tilde{V}_\Lambda^{(1)}\right)^2$. The values σ_{exp} and $\tilde{V}_\Lambda^{(1)}$ correspond to dimensionful parameters, both in MeV.

The system evolves until reaching the infrared value IR$= 0.0001$ GeV by solving the system of differential equations using the Runge-Kutta-Cash-Karp 54 method, implemented numerically thanks to the Boost c++ package, found in https://www.boost.org/, chosing -0.0001 GeV as the integration step and a relative error of 10^{-6}.

The infrared values obtained in every approximation are shown in table 3.2.

	LPA	LPA+Y	LPA+Y'	Full	Full+DH
$\bar{m}_{\mathrm{IR},\pi}$	138.054	137.955	137.984	138.073	138.052
$\bar{m}_{\mathrm{IR},\sigma}$	549.970	550.051	547.976	547.952	556.011
$\bar{m}_{\mathrm{IR},\psi}$	296.97	297.029	297.013	297.027	297.393
$\bar{\sigma}_{\mathrm{IR},0}$	92.995	93.004	93.0013	93.100	93.130
$\bar{h}_{\mathrm{IR}}$	6.387	6.387	6.387	6.381	6.387
$\bar{Z}_{\mathrm{IR},\psi}$	1.000	1.000	1.000	9.207	10.680
$\bar{Z}_{\mathrm{IR},\pi}$	1.000	1.000	1.000	7.257	8.205
$\bar{Z}_{\mathrm{IR},\sigma}$	1.000	1.000	1.000	1.062	1.056

Table 3.2: Table of the infrared values of the dominant parameters in function of every approximation used. The values of the renormalised masses $\bar{m}_{\mathrm{IR},i}$ and renormalised minimum of the potential $\bar{\sigma}_{\mathrm{IR},0}$ are implicitly expressed in MeV units.

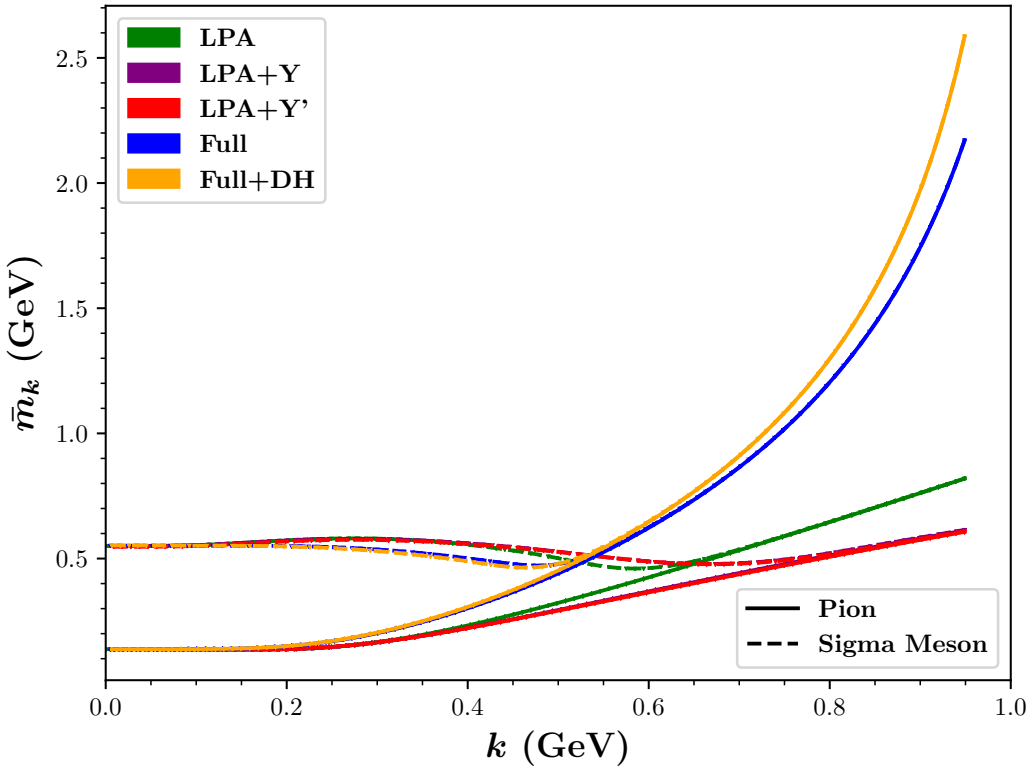

Figure 3.1: Renormalised meson masses $\bar{m}_{k,\phi}$ in function of the running scale k in every approximation used. Solid lines represent pion masses, whereas dashed lines are associated to the masses of the sigma meson.

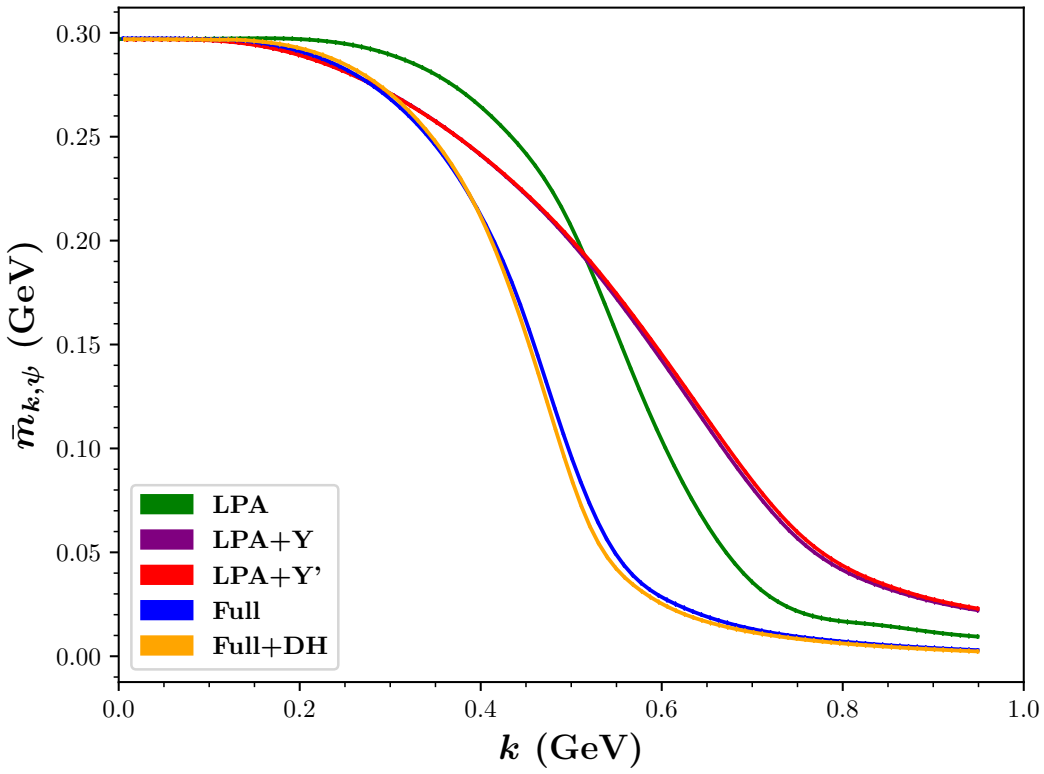

Figure 3.2: Renormalised quark mass $\bar{m}_{k,\psi}$ in function of the running scale k in every approximation used, obtained from the values of the renormalised scale dependent Yukawa coupling $\bar{h}_k$ and the renormalised minimum of the potential $\bar{\sigma}_{k,0}$ in every RG-step, following the expression $\bar{m}_{k,\psi} = \frac{\bar{h}_k \bar{\sigma}_{k,0}}{\sqrt{2N_f}}$.

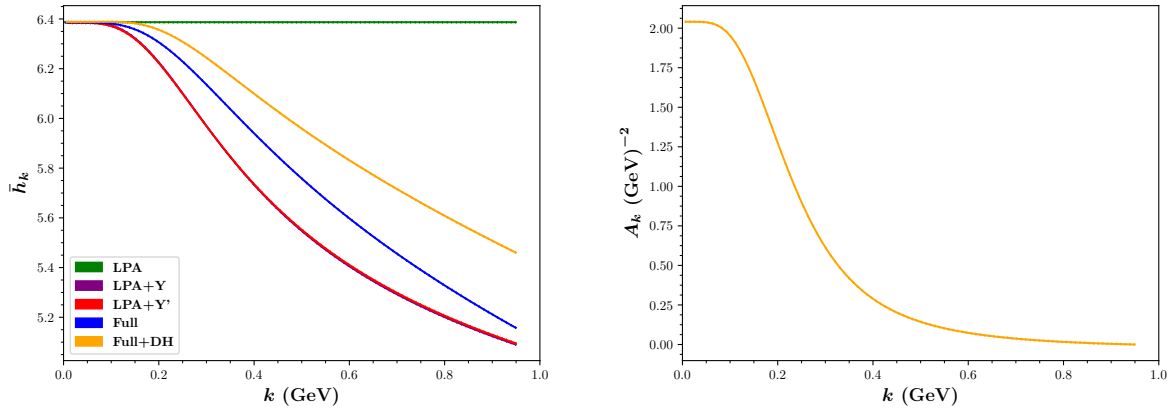

Figure 3.3: Scale dependent flows of renormalised Yukawa coupling in the different approximations used (left) and the value of the unrenormalised dynamical hadronisation term A_k (right).

Scale-dependent flows in the FRG shall be read from right to left, i.e., understanding that the scale decreases until reaching the infrared. In this sense, Figure 3.1 shows the flow of the renormalised meson masses obtained from the curvature of the potential. Every curve shows a splitting around $0.5 \sim 0.7$ GeV, depending on the approximation. When the curves split, the mass of the sigma meson becomes larger than the mass of the pion due to the additional $\sigma_0^2 V_k^{(2)}$ term, which becomes larger once the minimum of the potential increases. This fact occurs precisely at the symmetry breaking scale, and hence the curves displayed provide hints on which is the chiral symmetry breaking scale, which at the best approximations used surrounds 0.45 GeV. The main difference in this plot can be seen in the initial ultraviolet values of the masses, which get considerably larger due to the running of $\bar{Z}_{k,i}$. Results behave qualitatively similar to [79, 90, 91]

This recently mentioned fact is complemented by the plot of the quark mass shown in Figure 3.2. The quark mass in the ultraviolet has a small value due to the minimum of the potential, and at certain scale it begins generating mass. Considering this energy scale the value where the generated mass is half the infrared one, the full cases obtain a value of 0.45 GeV, consistent with the mesonic curvature masses. A particular feature of this plot can be seen in the LPA+Y amd LPA+Y' approximations, in which the initial renormalised quark mass is not that close to zero, but with a value close to 0.025 GeV. This occurs due to the selection of initial conditions, being $V_\Lambda^{(2)}$ larger than in the LPA and therefore shifting the minimum of the potential to a higher value.

In Figure 3.3 the running of the renormalised Yukawa and running of the dynamical hadronisation function A_k are shown. The latter is defined in a way that when the positive 4-Fermi coupling decreases, so does A_k in order to cancel the flow identically according to expression (3.22). As expected from the behaviour of the 4-Fermi coupling from NJL-like models [73, 92, 93], the flow of λ gets higher magnitude while decreasing the scale. Correspondingly, the slope of A_k is also more accentuated while reaching lower scales, and collapses when the system starts to converge.

As many scale dependent plots as parameters involved in the system can be shown. Nevertheless, our interest resides in the quantities living in the low-energy regime in which every quantum correction is included. The following figures show the behaviour of the relevant momentum dependent quantities involved in the correlators in function of the momentum $p \equiv \sqrt{p^2}$.

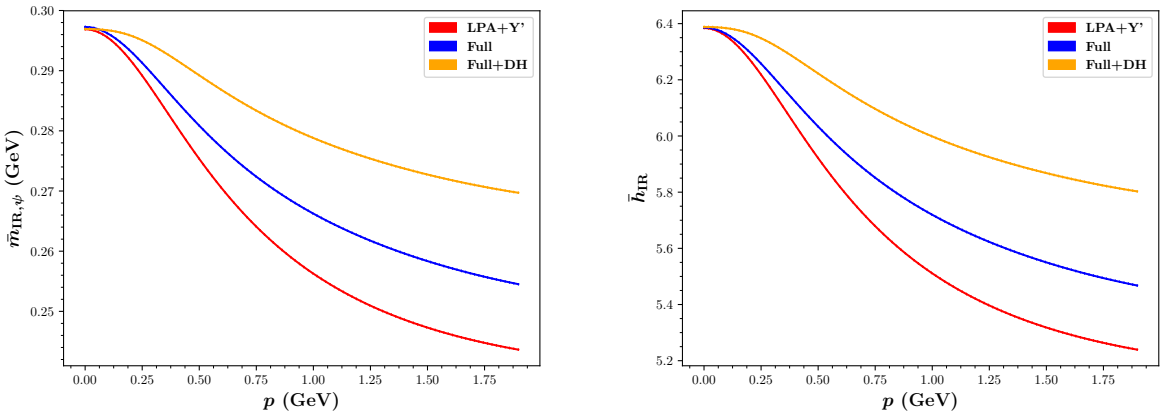

Figure 3.4: Momentum dependent quark mass function (left) and renormalised Yukawa coupling (right) in the different approximations used.

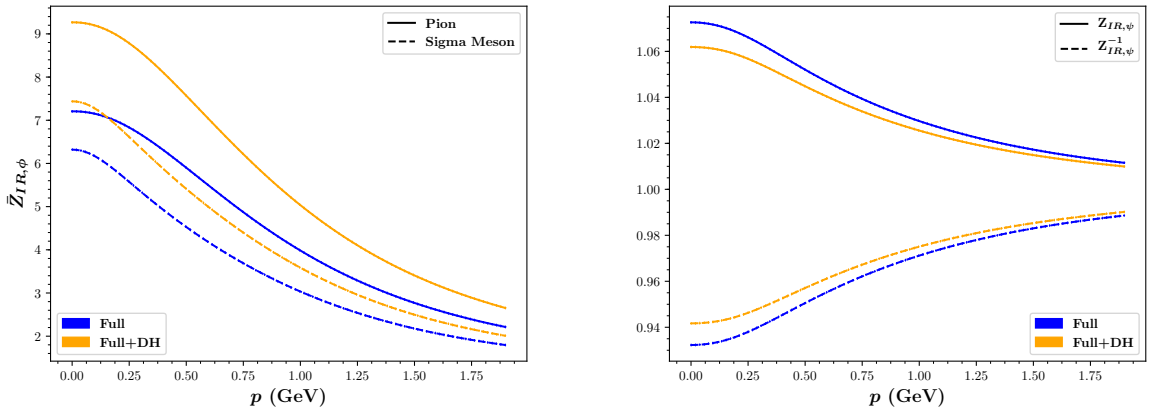

Figure 3.5: Momentum dependent renormalisation wave functions of the mesons (left) and of the fermions (right) for the full case and the full case with dynamical hadronisation. The sigma meson quantities are shown with dashed lines, whereas pions are shown with solid lines. $Z^{-1}_{\mathrm{IR},\psi}$ is also displayed. The figure concerning fermions shows also the inverse renormalisation wave function, for simpler comparison with the standard Z_ψ in the QFT notation.

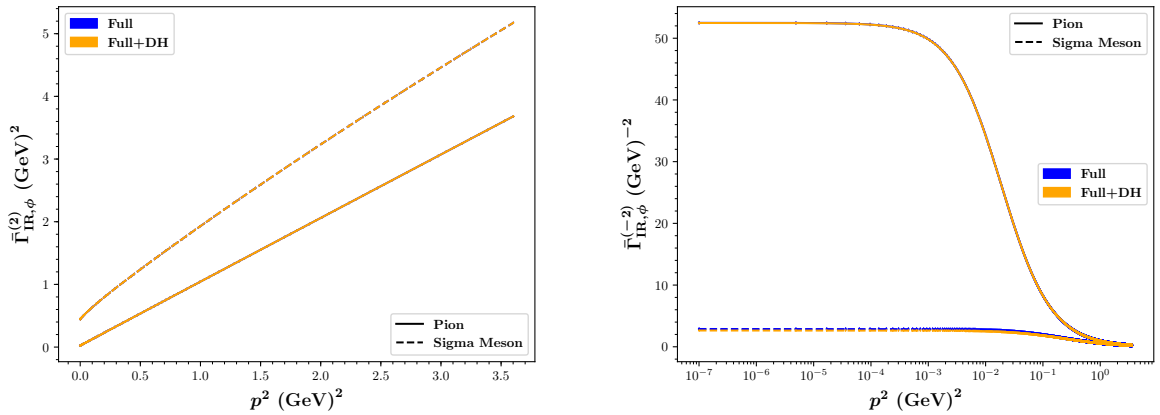

Figure 3.6: Momentum dependent renormalised two-point function (left) and renormalised propagator in logarithmic scale (right) for the pion and sigma meson in the full systems with and without the presence of the dynamical hadronisation effects. The sigma meson correlators are shown in dashed lines, whereas all the pion quantities are displayed in solid line.

In Figure 3.4 the renormalised quantities involved in the renormalised momentum dependent quark mass function are shown for the approximations that implement momentum dependence. Despite behaving the renormalised Yukawa coupling similarly as its scale-dependent counterpart, the quark mass function does not reduce its value to smaller masses in the region where chiral symmetry is restored. This is a consequence of the limitation of the QM model in the approximations used an requires further investigation.

Wave function renormalisations in Figure 3.5 reduce their value with increasing momentum, but never reach the initial ultraviolet value $Z_{k,i} = 1$ at $p = \Lambda$. Mesonic $Z_{IR,i}$ behave similarly in every approximation, but the presence of the dynamical hadronisation changes their values significantly, particularly in $p = 0$. The same occurs in the fermionic case, but with a smaller difference due to their low values. In the case of quarks, the wave function renormalisation drops in agreement to $A(p^2)$ in the DSE notation, despite not agreeing in general shape and value. In comparison to the QCD results shown in [79], the slope of $Z_{\mathrm{IR},\pi}$ should become far more accentuated than the ones obtained in the QM model.

Lastly, the renormalised meson correlators are analysed in Figure 3.6. The picture on the left shows the renormalised meson two-point functions, defined simply as:

$$\bar{\Gamma}^{(2)}_{\mathrm{IR},\phi}(p^2) = \frac{\Gamma^{(2)}_{\mathrm{IR},\phi}(p^2)}{Z_{\mathrm{IR},\phi}(p^2)}. \tag{3.46}$$

The meson propagators are straightforwardly obtained through the inverse of the two-point function. The presence of the wave function renormalisations makes the slopes of both lines different for pions and sigma meson, which are on top of each other in all the approximations. Knowing the behaviour of these parameters, we proceed to obtain observables using the Euclidean results as input. Our aim is to obtain the values of the pole masses and spectral functions:

$$\rho_\phi(p_0) = -\frac{1}{\pi}\mathrm{Im}\left(G_\phi(p_0 - i\epsilon)\right), \tag{3.47}$$

where G_ϕ is the meson propagator with $\phi = (\sigma, \pi)$. The parameter p_0 represents momentum in Minkowskian space. We perform extrapolation via Padé approximant and the Schlessinger Point method based Padé, see [94] and Appendix B for further details. In this extrapolation, we identify $p_0 = ip_4$, where p_4 is the Euclidean rest-energy. By virtue of Lorentz invariance we can choose our Euclidean results to be true in the rest-frame, therefore obtaining $p_4 = \sqrt{p^2}$. The continuation using the Padé methods is required to be done using p^2 for the pole masses, and positive p_4 instead of p^2 for the spectral functions. Otherwise, if we used p^2 there would double-counting and the extrapolation would fail.

The results obtained for the pole masses are shown in table 3.3

Particle	Curvature mass	Pole mass Padé	Pole mass Modified Padé	Decay width
Pion	138.053	137.1 ± 0.5	137.6 ± 0.4	0.5 ± 0.5
Sigma meson	551.843	340 ± 20	330 ± 15	30 ± 6

Table 3.3: Table of masses and decay widths obtained from the curvature of the potential (reduced to curvature mass) and pole masses obtained from analytic continuation using the Padé approximant $R^{(5,5)}(x)$ and the modified Padé approximant performed with 100 data points in the Full+DH approximation. Values are displayed both for pion and sigma mesons and every quantity is shown in MeV.

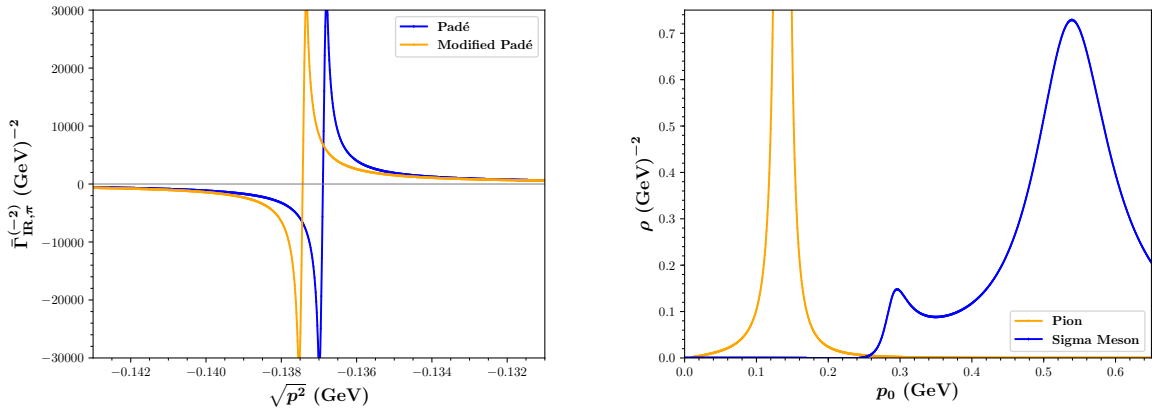

Figure 3.7: Analytical continued pion propagator into real-time momentum around the region of the physical pole computed using both Padé approximants (left) and the spectral function of the sigma meson (right) using the modified Padé. Every input data comes from the Euclidean Full+DH approximation.

The pole masses are compared with the masses obtained by the curvature of the potential given their close relation shown in [95]. The results show that the pion pole masses agree with the value of the masses obtained from the curvature of the potential with a difference smaller than 1%. Furthermore, the modified Padé method gives a slightly preciser result given by the number of points used, since further error is carried by the fit performed in the usual Padé. The position of the pion pole found in both of the methods is shown in Figure 3.7. A similar analysis is performed with the sigma meson, with completely different results. Despite the mass being obtained from the curvature of the potential close to 550 MeV, the pole masses obtained in both of the approaches are close to 330 MeV. This result is nevertheless expected since the process $\sigma \to \pi\pi$ is allowed in the system. Consequently, the pole is found in the second Riemann sheet [96], where p^2 is allowed to be complex. This procedure determines not only the pole in the real axis, but also its decay rate looking at their imaginary counterparts. The value of the decay width of the pion is compatible with 0, in agreement with its nature as stable particle in this model. On the other hand, the sigma meson is allowed to decay and therefore a non-zero value for the decay width is found.

Figure 3.7 also displays the spectral function of the mesons involved. The spectral function of the sigma meson shows a threshold at exactly $2m_\pi$ as predicted by QFT [97] and a peak (resonance) at the corresponding physical mass. Despite the spectral functions describing the correct physics, the exact values of the spectral functions are very sensitive to numerics and require very precise calculations. Further calculations of spectral functions using the FRG can be found in [98–101]. As shown in [94], a numerical noise of 10^{-6} may change the magnitude or even the behaviour of the spectral function. Hence, an approach that directly computes real time correlation functions from first principle, similarly done as in [101, 102], is desired to deal with spectral functions.

Chapter 4

Comparison between methods

The previous chapter showed how the Functional Renormalisation Group works within the Quark-Meson model in different approximations and truncations, some of them being the dynamical-hadronisation technique in which the 4-point Green's functions are solely expressed as a meson exchange. Furthermore, observables were obtained performing analytic continuation as proof that the FRG is a convenient tool to derive properties of bound states, see also [103].

In this chapter both FRG and DSE-BSE approaches will be used and compared in different approximations and low-energy QCD systems. The aim of the chapter is to analyse both approaches in terms of effectiveness of the numerical resolution and the methodological difficulties given by the functional equations. In addition, we will discuss which features are uniquely obtainable in each one of the approaches and what can be learnt from it.

4.1 Formal comparison

The FRG approach is based on the scale-dependent effective action, set to contain every quantum contribution of the full theory once the scale parameter reaches the infrared. Right at this point, the regulator terms cancel and the full effective action is, in principle, recovered. Nevertheless, some remarks need to be clarified.

First of all, the previous statement is not enough to guarantee that the solution of the FRG equations yields the same results as in the DSE-BSE approach. On the one hand, the FRG starting point Γ_Λ is required to be similar to the bare action, whereas DSEs use the bare S to derive the full effective action. Furthermore, in practical cases in the FRG the scale parameter may not reach the exact value $k = 0$ and the final results depend on an apparent convergence of the system. In the DSE approach the system is solved iteratively and the final results are obtained once the relative difference between the values of subsequent iterations is lower than a certain value.

The connection between the DSEs and the FRG flow equations is well-known, see [25] for a detailed review. In this section, the FRG-BSE relation within fermionic systems and the renormalisation procedure in both methods will be analysed.

4.1.1 Relation between BSEs and FRG flow equations

The results obtained in the FRG approach serve, in general, as input in the Bethe-Salpeter equations equivalently as the DSEs would do. Nevertheless, a truncation is still necessary in the BSEs in order to solve them. The FRG approach allows, in particular approximations, to solve the BSEs without any additional calculation. Furthermore, such approximations are related to the ones used in the usual DSE-BSE formalism, see [29, 104]. In this work we have focused on different systems involving fermionic degrees of freedom exclusively, such that the Gross-Neveu model, NJL model and their bosonised versions. In this section it will be shown that, for fermionic systems under a particular approximation, the solution of the BSE can be formally obtained from the solution of the flow equations.

Let us consider the system effective action expressed within a vertex expansion:

$$\Gamma_k[\overline{\psi},\psi] = \Gamma^{(2)}_{k,\psi\bar{\psi}}\ \overline{\psi}\psi + \Gamma^{(4)}_{k,\psi\bar{\psi}\psi\bar{\psi}}\ (\overline{\psi}\psi)^2 + \dots, \tag{4.1}$$

where summation of flavour and colour indices is implied. Higher order vertex functions are, in principle, permitted within the expansion. In our present approximation the four-point function is the higher order vertex function in the system. Under the presence of flavour and colour numbers, the four-point function is obtained through:

$$\frac{\delta^4\partial_t\Gamma_k}{\delta\psi_{\boldsymbol{d}}\delta\overline{\psi}_{\boldsymbol{c}}\delta\psi_{\boldsymbol{b}}\delta\overline{\psi}_{\boldsymbol{a}}} = 2\left(\delta^{\boldsymbol{ab}}\delta^{\boldsymbol{cd}} - \delta^{\boldsymbol{ad}}\delta^{\boldsymbol{cb}}\right)\partial_t\Gamma^{(4)}_{k,\psi\bar{\psi}\psi\bar{\psi}} \equiv \partial_t\Gamma^{(4)\,\boldsymbol{abcd}}_{k,\psi\bar{\psi}\psi\bar{\psi}}, \tag{4.2}$$

where the term $2\left(\delta^{\boldsymbol{ab}}\delta^{\boldsymbol{cd}} - \delta^{\boldsymbol{ad}}\delta^{\boldsymbol{cb}}\right)$ appears from the flavour and colour content of the fields.

Leaving the index structures untouched, we can relate the $\Gamma^{(4)\,\boldsymbol{abcd}}_{k,\psi\bar{\psi}\psi\bar{\psi}}$ matrix to the elements of the Bethe-Salpeter equation. In this section, we will work in an approximation involving two important remarks. First of all, we will neglect the contributions of the flow of the 2-point function so that all the focus will be put on the 4-point function. As a consequence, the derivative of the regulator term can be expressed in a compact notation:

$$\partial_t G_k = -G_k(\partial_t R_k)G_k, \tag{4.3}$$

Secondly, Green's functions of order equal or larger than 6 will be neglected, making the system only dependent on 2-point functions and 4-point functions. Under this assumption, the flow of the four-point function is easily derived from Wetterich's flow equation leading, diagrammatically, to the expression shown in Fig 4.1.

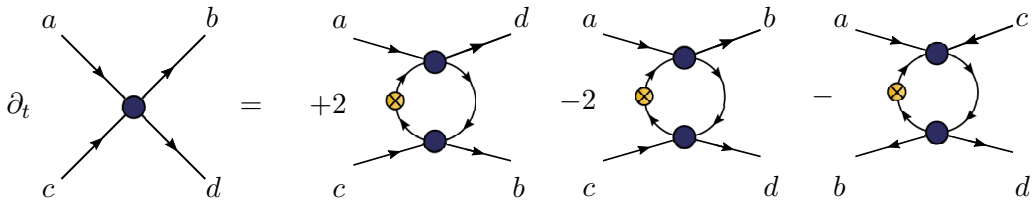

Figure 4.1: Diagrammatic flow of the fermion four-point function in the current approximation corresponding to $\partial_t \Gamma^{(4)\,\boldsymbol{abcd}}_{k,\psi\bar{\psi}\psi\bar{\psi}}$.

If we were to calculate the flow $\partial_t \Gamma^{(4)\,\boldsymbol{adcb}}_{k,\psi\bar{\psi}\psi\bar{\psi}}$, which corresponds to interchanging the indices $b \leftrightarrow d$, we would see that the flow equation would be the same with only the first two diagrams with opposite sign. Using this knowledge and the fact that $\partial_t \Gamma^{(4)\,\boldsymbol{adcb}}_{k,\psi\bar{\psi}\psi\bar{\psi}} = -\partial_t \Gamma^{(4)\,\boldsymbol{abcd}}_{k,\psi\bar{\psi}\psi\bar{\psi}}$, it easy to show that the flow equation becomes:

$$\begin{aligned}\partial_t \Gamma^{(4)\,\boldsymbol{abcd}}_{k,\psi\bar{\psi}\psi\bar{\psi}} = &+ 2\,\Gamma^{(4)\,\boldsymbol{abij}}_{k,\psi\bar{\psi}\psi\bar{\psi}}\;\partial_t G^{\boldsymbol{jJ}}_k\;\Gamma^{(4)\,\boldsymbol{JIcd}}_{k,\psi\bar{\psi}\psi\bar{\psi}}\;G^{\boldsymbol{Ii}}_k \\ &- 2\,\Gamma^{(4)\,\boldsymbol{adij}}_{k,\psi\bar{\psi}\psi\bar{\psi}}\;\partial_t G^{\boldsymbol{jJ}}_k\;\Gamma^{(4)\,\boldsymbol{JIcb}}_{k,\psi\bar{\psi}\psi\bar{\psi}}\;G^{\boldsymbol{Ii}}_k\end{aligned} \tag{4.4}$$

Here there appears a global minus sign given by the use of expression (4.3). The expression is reduced further by defining the matrix of the two-particle propagator $G^{(2)}_k$ in the form:

$$\left(G^{(2)}_k\right)^{\boldsymbol{abcd}} \equiv G^{\boldsymbol{ab}}_k G^{\boldsymbol{cd}}_k. \tag{4.5}$$

Using this notation and considering that the terms are traced and every correlator is fermionic, we can express the flow equation as:

$$\left(\partial_t \Gamma^{(4)}_k\right)^{\boldsymbol{abcd}} = \left(\Gamma^{(4)}_k \dot{G}^{(2)}_k \Gamma^{(4)}_k\right)^{\boldsymbol{aicj}} \left(\delta^{\boldsymbol{ib}}\delta^{\boldsymbol{jd}} - \delta^{\boldsymbol{id}}\delta^{\boldsymbol{jb}}\right) \tag{4.6}$$

The four-point function that satisfies this flow equation follows:

$$\left(\Gamma^{(4)}_k\right)^{\boldsymbol{abcd}} = -\frac{1}{2}\left(\frac{\Gamma^{(4)}_\Lambda}{1 + G^{(2)}_k \otimes \Gamma^{(4)}_\Lambda}\right)^{\boldsymbol{aicj}} \left(\delta^{\boldsymbol{ib}}\delta^{\boldsymbol{jd}} - \delta^{\boldsymbol{id}}\delta^{\boldsymbol{jb}}\right), \tag{4.7}$$

where $\Gamma^{(4)}_\Lambda$ is the four-point function at the cutoff. This solution is true for the 4-point function, but it is convenient to write it in its not amputated form $\tilde{\Gamma}^{(4)}_k$ as:

$$\tilde{\Gamma}^{(4)}_k = G^{(2)}_k - G^{(2)}_k \otimes \Gamma^{(4)}_k \otimes G^{(2)}_k. \tag{4.8}$$

This expression needs to satisfy Dyson's equation (2.12), with the formal solution:

$$\tilde{\Gamma}_k^{(4)} = G_k^{(2)} + \frac{G_k^{(2)} \otimes K \otimes G_k^{(2)}}{1 - G_k^{(2)} \otimes K}. \tag{4.9}$$

Comparing this expression to the solution obtained from the fermionic system, we can derive its relation with the interaction kernel involved in the BSEs:

$$(K)^{\boldsymbol{abcd}} = \frac{1}{2}\left(\left(\Gamma_\Lambda^{(4)}\right)^{\boldsymbol{abcd}} - \left(\Gamma_\Lambda^{(4)}\right)^{\boldsymbol{adcb}}\right), \tag{4.10}$$

which corresponds to the free 4-point function in the same two channels involved in the flow equations. Since this is the lowest-order free interaction possible between quark-antiquark within the effective action used, this approximation corresponds to a Rainbow-Ladder truncation in the DSE-BSE approach. For more sophisticated truncations a similar but more complicated proof of equivalence can be given.

4.1.2 Renormalisation procedure

One distinctive feature of Quantum Field Theory is the renormalisation procedure performed in order to deal with divergences and to extract physical quantities from them. The method employed to subtract divergences is not unique and different schemes are used depending on the properties of the system. Nevertheless, physical quantities shall be independent of how the system is renormalised.

Functional methods deal with divergences differently due to the way the approaches are defined. Because of this, a complete comparison between methods requires also a comparison on how renormalisation is applied in every method.

In the DSE-BSE approach, divergences appear within loop terms corresponding to Feynman diagrams of dressed and bare correlators. When the systems are non-renormalisable, divergences cannot be properly subtracted and the system is only treatable by imposing a cutoff. On the other hand, when the system is renormalisable, subtraction is performed through the calculation of renormalisation constants Z_i that appear in the system's $S[\Phi]$ at a given momentum scale. The usual procedure is the following:

- The full and free correlators are parametrised in function of their tensor structure. The free correlators must include the renormalisation constants Z_i introduced by the presence of counterterms. As an example, a two-point function DSE can be written as:

$$\Gamma^{(2)}(p^2) = \Gamma_0^{(2)}(p^2, Z_i) + \Sigma(p^2, Z_i), \tag{4.11}$$

  where $\Gamma_0^{(2)}$ is the bare two-point function and Σ represents the loop terms.

- The renormalisation conditions are set by imposing fixed values to the correlators at certain renormalisation scale μ, yielding:

$$\Gamma^{(2)}(\mu^2) = \Gamma_0^{(2)}(\mu^2, Z_i) + \Sigma(\mu^2, Z_i) \tag{4.12}$$

  The expression becomes an equation for the Z_i (or set of equations in the case of coupled equations) which is numerically solved. Expression (4.11) is then solved with the values of Z_i which encodes the subtraction of divergences.

- When the system requires iterative procedure to be solved, a recalculation of Z_i is required in every iteration.

The parameters Z_i play a key role in the renormalisation in the DSE approach as, due to their presence, every quantity involved is finite. There exist some subtleties involving the nature of Σ and the approximation used in every system, but the general approach is to follow these steps to make quantities finite.

The FRG renormalisation procedure works differently. In order to illustrate it, it is convenient to start with Wetterich's flow equation in its compact form:

$$\dot{\Gamma}_k = \frac{1}{2} G_k \dot{R}_k, \tag{4.13}$$

where the right hand side of the equation is traced over all the indices. The expression can be rewritten by making use of the property:

$$\partial_t \left(\ln \left(\mathrm{Tr} \left(\Gamma_k^{(2)} + R_k \right) \right) \right) = \partial_t \ln \mathrm{Tr} \left(G_k \right)^{-1} = G_k \dot{R}_k + G_k \dot{\Gamma}_k^{(2)}, \tag{4.14}$$

where again the terms on the right hand side are traced over all the indices. Consequently, the new flow equation reads:

$$\dot{\Gamma}_k = \frac{1}{2} \partial_t \left(\ln \left(\mathrm{Tr} \left(G_k^{-1} \right) \right) \right) - \frac{1}{2} G_k \dot{\Gamma}_k^{(2)} \tag{4.15}$$

The flow equation can be formally integrated within the interval (k', Λ), where Λ is the ultraviolet cutoff and k' is a particular scale lower than Λ. The resulting expression reads:

$$\Gamma_{k'} = \Gamma_\Lambda - \frac{1}{2} \ln \left(\mathrm{Tr} \left(G_k \right) \right) \Big|_\Lambda^{k'} - \frac{1}{2} \int_\Lambda^{k'} dt \, G_k \dot{\Gamma}_k^{(2)} \tag{4.16}$$

Expression (4.16) represents the integrated flow of Wetterich's flow equation. There are some important features of this expression that require analysis involving renormalisation. First of all, since the integrated interval is finite, the boundary condition Γ_Λ is also finite and therefore no ultraviolet divergences are present. In other words, the choice of initial conditions in the ultraviolet cutoff renormalises the theory implicitly. Furthermore, the renormalisation conditions usually defined in the DSE in a particular renormalisation scale are implemented differently: the choice of renormalisation conditions in the infrared, i.e. at $k \to 0$, relates to a particular set of boundary conditions at $k = \Lambda$. Due to this fact, the choice of initial conditions renormalises the theory and fixes a set of renormalisation conditions. For further details regarding renormalisation procedure in the FRG, see [25].

4.2 Practical comparison

Even though both functional approaches have been proven to be formally equivalent, the behaviour of the solutions in different truncated systems needs to be analysed. Such study shall explicitly show the difference between the solutions dealt in different systems.

The main systems of interest are low-energy QCD models. Hence, the NJL, Gross-Neveu and Quark-Meson models will be treated in both functional approaches.

4.2.1 The NJL model

The NJL model analysed consists of quark kinetic and mass terms and a global $U(2)$-symmetric four-Fermi interaction, with fermion fields living in a space with $N_f = 2$ flavours and $N_c = 3$ colours. The mass term breaks chiral symmetry explicitly. The associated bare action follows:

$$S[\overline{\psi}, \psi] = \int_p \overline{\psi} \left(i\not{p} + m_q \right) \psi + \int_{p,q,r} \frac{\lambda}{2N_f} \left(\overline{\psi}\psi \right)^2 , \tag{4.17}$$

where the field momentum dependence and colour, Dirac and flavour indices are implied. Notice that this expression differs from the ones defined in (3.5) and (3.6): there is a fermion mass and the four-Fermi interaction includes only one of the terms. Due to the non-renormalisability of the model in four dimensions, the system requires a truncation from the very beginning. Ultraviolet divergences cannot be subtracted and therefore cutoffs will be used to make integrals finite. The four-Fermi interaction introduces two-loop diagrams in the lowest order DSE. There exists no unambiguous way to solve such diagrams under the presence of a cutoff without modifying the system intrinsically. Hence, the usual DSE approach is to neglect two-loop contributions. Under this assumption, the quark DSE shown in Figure 4.2 consists only on the free inverse quark propagator and the tadpole diagram dependent on the free 4-Fermi coupling. Consequently, the quark DSE can be solved self-consistently and higher-order DSEs are irrelevant in this approach.

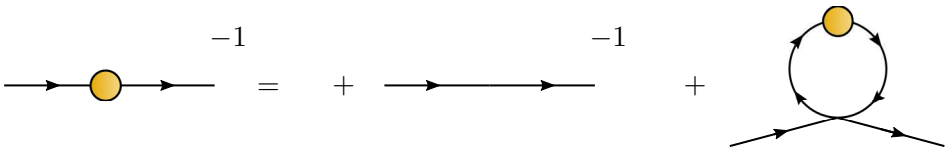

Figure 4.2: Diagrammatic quark DSE in the NJL model.

In the usual parametrisation, the dressed two-point function follows:

$$\Gamma^{(2)}_{\psi\bar{\psi}}(p) = A(p^2)i\not{p} + B(p^2) \tag{4.18}$$

The solution of the system shall provide the description of the explicit behaviour of $A(p^2)$ and $B(p^2)$, related to the quark mass function as $B(p^2) = A(p^2)M(p^2)$. It is easy to show that the tadpole diagram contribution is momentum independent, and therefore we can safely establish $A(p^2) = 1$ and $B(p^2) = M$. The DSE related to the quark mass function term yields:

$$M = m_q + cM\left(1 - a\ln\left(1 + \frac{1}{a}\right)\right), \tag{4.19}$$

where $a = \left(\frac{M}{\Lambda}\right)^2$, Λ is a sharp ultraviolet cutoff and c is a constant related to the 4-Fermi coupling and other numerical constants. For further details, see Appendix C and [20, 86, 87]. Equation (4.19) is solved iteratively, both in the massive and chiral case:

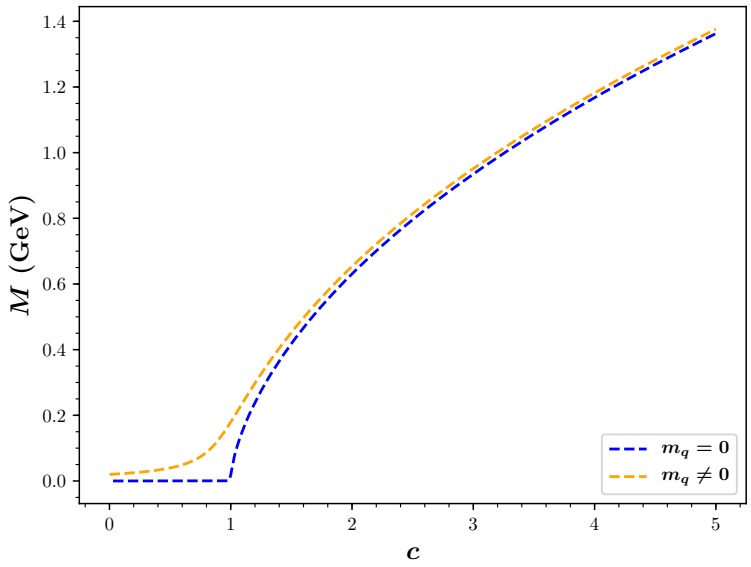

Figure 4.3: Solutions for the mass function of the quark DSE in the NJL model for massive quarks ($m_q = 0.02$ GeV) and in the chiral limit in function of the parameter c, with $\Lambda = 1$ GeV.

Figure 4.3 shows two solutions for M. Once c reaches the critical value 1, the mass function generates a mass, growing logarithmically with Λ. The exact numerical values of the curves depend both on Λ and m_q, therefore only the qualitative behaviour is shown.

Next, we would like to compare the results obtained previously within the DSE formalism with the FRG. The NJL model has been treated in the FRG in several works, see e.g, [28,92,93,105–107] and references therein. However, the truncations employed in the DSE approach are difficult to reproduce in the FRG, as we need to understand the role that the scale parameter plays in this truncation. Furthermore, we need to clearly distinguish which of the parameters are related to physical quantities.

Similarly as in the DSE approach, the starting point is the scale-dependent effective action Γ_k:

$$\Gamma_k[\overline{\psi},\psi] = \int_p \overline{\psi}\left(Z_{k,\psi} i\not{p} + m_k\right)\psi + \int_{p,q,r} \frac{\lambda_k(p,q,r)}{2N_f}\left(\overline{\psi}\psi\right)^2 . \tag{4.20}$$

The quantities in the effective action are understood to include flavour, Dirac and colour indices as well. The scale dependence is encoded in the wave-function renormalisation $Z_{k,\psi}$, in the quark mass m_k and in the four-point function λ_k, which depends on three arguments by virtue of momentum conservation. The flow equations involved are displayed in Figure 4.4:

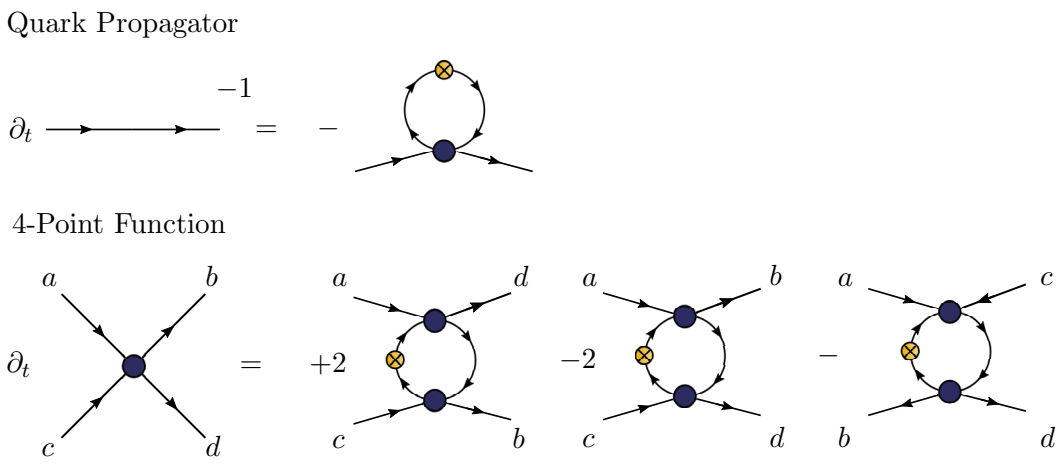

Figure 4.4: Diagrammatic quark DSE in the NJL model.

Since the previously obtained results only involved the momentum independent mass term of the quark propagator DSE, there exist only two possible truncations which may be related to the previous results. In order to make the flow of the quark propagator momentum independent, the 4-point function is required to be momentum independent as well. Only in this case, the flow of $Z_{k,\psi}$ is cancelled and $Z_{k,\psi} = 1$ in every scale, in agreement with the DSE results. Thus, the two choices are scale dependent four-point function $\lambda_k(p,q,r) \equiv \lambda_k$ or scale and momentum independent four-point function $\lambda_k(p,q,r) \equiv \lambda$.

The next step is to understand which variables represent physical quantities. In order to illustrate it, it is convenient to work in the constant four-point function case. Following the same idea as

derived in [104], we define the two-point function as:

$$\Gamma^{(2)}_{k,\psi\bar{\psi}}(p) = -i\not{p}(1 + r_k^F(p)) + m_b, \tag{4.21}$$

where m_b is the scale independent bare mass. From the diagram shown in Figure 4.4, it is easy to show that the flow of the mass term satisfies:

$$\partial_k m_k = 2(4N_f N_c - 1)\frac{\lambda}{2N_f} m_b \int_p \frac{p^2(1 + r_k^F)\partial_k r_k^F}{(p^2(1 + r_k^F)^2 + m_b^2)^2}. \tag{4.22}$$

The flow of the mass term is positive and increases with the scale. In this particular case and with the use of the optimised regulator, it is easy to show that $m_k \propto k^2$. This fact leads us to the understanding that m_k is an unrenormalised mass whose ultraviolet divergences are not yet subtracted. Indeed, by defining

$$2\tilde{c} \equiv 2(4N_f N_c - 1)\frac{\lambda}{2N_f}, \tag{4.23}$$

expression (4.22) is reduced to a total scale derivative:

$$\partial_k m_k = -\partial_k \left(\tilde{c}\, m_b \int_p G_k^{\psi} \right) \equiv \partial_k \Sigma_k. \tag{4.24}$$

where we used $G_k^{\psi} = \left(\Gamma^{(2)}_{k,\psi\bar{\psi}}\right)^{-1}$ for simplicity. Σ is the contribution of the tadpole diagram and is, as expected, momentum independent. The integration of this differential equation is straightforward and yields the definition of the scale dependent mass term:

$$m_k = M + (\Sigma_k - \Sigma)\,, \tag{4.25}$$

where $M = m_{k=0}$ and $\Sigma = \Sigma_{k=0}$. When the scale is taken to the infrared, it is clear that the tadpoles (initially divergent diagrams) cancel and the remaining m is finite. Hence, we understand M to be the physical mass, and not m_k. Lastly, we need to understand how the physical mass is obtained from the flow, that is, from the choice of initial conditions in the ultraviolet Λ. From the definition of the scale dependent mass m_k, it is clear that $m_\Lambda = M - (\Sigma - \Sigma_\Lambda)$ and therefore expression (4.25) is easily rewritten to:

$$m_k = m_\Lambda - (\Sigma_\Lambda - \Sigma_k) \qquad \Longrightarrow \qquad M = m_\Lambda - (\Sigma_\Lambda - \Sigma)\,. \tag{4.26}$$

Here m_Λ is simply a finite value which is chosen at the initial scale to satisfy renormalisation conditions in the IR since the tadpole contributions cancel at Λ. The difference between tadpole diagrams is obtained from integrating the flow and needs to be subtracted from m_Λ in order to extract the physical mass M and is the value that is compared with the NJL results.

Taking this definition for the physical mass M, one can attempt to solve the flow equation in the usual way and obtain similar results as in the DSE approach. Nevertheless, the solution will differ completely as both systems are not yet in the same approximation. In order to achieve this, we rewrite λ as $\lambda = \frac{c'}{\Lambda^2}$, where Λ is a sharp ultraviolet cutoff. When Λ is large enough, the system can be treated perturbatively.

At this point, we treat the flow equations in a similar way as in Chapter 3. Hence, we define the two point function as:

$$\Gamma^{(2)}_{k,\psi\bar{\psi}}(p) = -i\not{p}(1 + r_k^F(p)) + m_k, \tag{4.27}$$

where now the quark mass is scale dependent. The associated flow equation follows:

$$\partial_k m_k = 2\frac{\tilde{c}}{\Lambda^2} m_k \int_p \frac{p^2(1 + r_k^F)\partial_k r_k^F}{(p^2(1 + r_k^F)^2 + m_k^2)^2}, \tag{4.28}$$

where now $\tilde{c}$ encodes all the numerical constants in a similar way as (4.23), with the only difference that Λ is left untouched. The next step is to rewrite the expression as a total derivative using the properties of the derivative chain rule, but it is clear that terms involving $\partial_k m_k$ on the right hand side of the equation will appear due to the running mass in the propagator. Nevertheless, replacing these new $\partial_k m_k$ terms with the flow equation iteratively will yield terms proportional to $\left(\frac{\tilde{c}}{\Lambda^2}\right)^2$. Consequently, the flow equation is rewritten as:

$$\partial_k m_k = -\partial_k \left(\frac{\tilde{c}}{\Lambda^2} m_k \int_p \frac{1}{p^2(1 + r_k^F)^2 + m_k^2} \right) + \mathcal{O}\left(\left(\frac{\tilde{c}}{\Lambda^2} \right)^2 \right). \tag{4.29}$$

Under the assumption that $\Lambda >> \tilde{c}$, the $\mathcal{O}\left(\left(\frac{\tilde{c}}{\Lambda^2}\right)^2\right)$ terms become negligible and play no further role in the flow. Furthermore, using the same reasoning and the relation shown in expression (4.25), the quantities m_k can be safely replaced by the physical mass M without loss of generality in this approximation, since the additional terms become also proportional to $\left(\frac{\tilde{c}}{\Lambda^2}\right)^2$. The numerical constants are encoded together by defining $c \equiv \frac{1}{2}\tilde{c}\int \frac{d\Omega}{(2\pi)^4}$. Finally, the flow equation becomes:

$$\partial_k m_k = -\partial_k \left(\frac{c}{\Lambda^2} M \int_0^{\Lambda^2} \left(\frac{1}{p^2(1 + r_k^F)^2 + M^2} \right) p^2 dp^2 \right). \tag{4.30}$$

Here c is exactly the same as the one in expression (4.19) and the momentum integral is performed within the interval $(0, \Lambda)$.

The remaining step is to integrate the scale parameter. The scale integration is performed from $k = 0$ to $k \to \infty$. Taking into consideration that $r_0^F = 0$ by the properties of the regulator function and the interpretation of the renormalised dynamical mass function satisfying $\partial_k \overline{m}_k = -\partial_k m_k$ from the extraction of divergences, the integrated flow yields the equation:

$$M = \overline{m}_{k\to\infty} + \left(\frac{c}{\Lambda^2} M \int_0^{\Lambda^2} \frac{p^2}{p^2 + M^2} dp^2 \right), \tag{4.31}$$

which agrees exactly with the expression derived in the NJL section of Appendix C, identifying $m_q = \overline{m}_{k\to\infty}$ and $M = m_0 = \overline{m}_0$. The approximation required in the FRG was the assumption of the perturbative behaviour of a constant four-Fermi coupling λ, The proof shown and the same reasoning cannot be easily applied for a running λ_k, as it can grow to large values.

4.2.2 The Gross-Neveu model

Despite the NJL model describing spontaneous chiral symmetry breaking in terms of the scale, the behaviour cannot be obtained in function of the momentum due to the neglected two-loop term in the used approximation. In order to include these terms, the dimension d of the system is reduced to $d = 2$, in which the system becomes renormalisable and two-loop terms are solvable unambiguously. The model in this case is the Gross-Neveu model in two dimensions and is described with the following bare action:

$$S[\overline{\psi}, \psi] = \int_{\tilde{p}} \overline{\psi} \left(i\not{p} + m \right) \psi + \int_{\tilde{p},\tilde{q},\tilde{r}} \frac{\lambda}{2N_f} \left(\overline{\psi}\psi \right)^2, \tag{4.32}$$

where $\int_{\tilde{p}} = \int \frac{d^2p}{(2\pi)^2}$, field momentum dependence and summation of colour, Dirac and flavour indices are implied. Two-loop terms are formally included in the DSEs and the coupled system to be solved is displayed in Figure 4.5, where six-point functions are neglected. Calculations involving the Gross-Neveu model in the two functional approaches can be found in two and three dimensions, see respectively [108–113] and [108, 114–116].

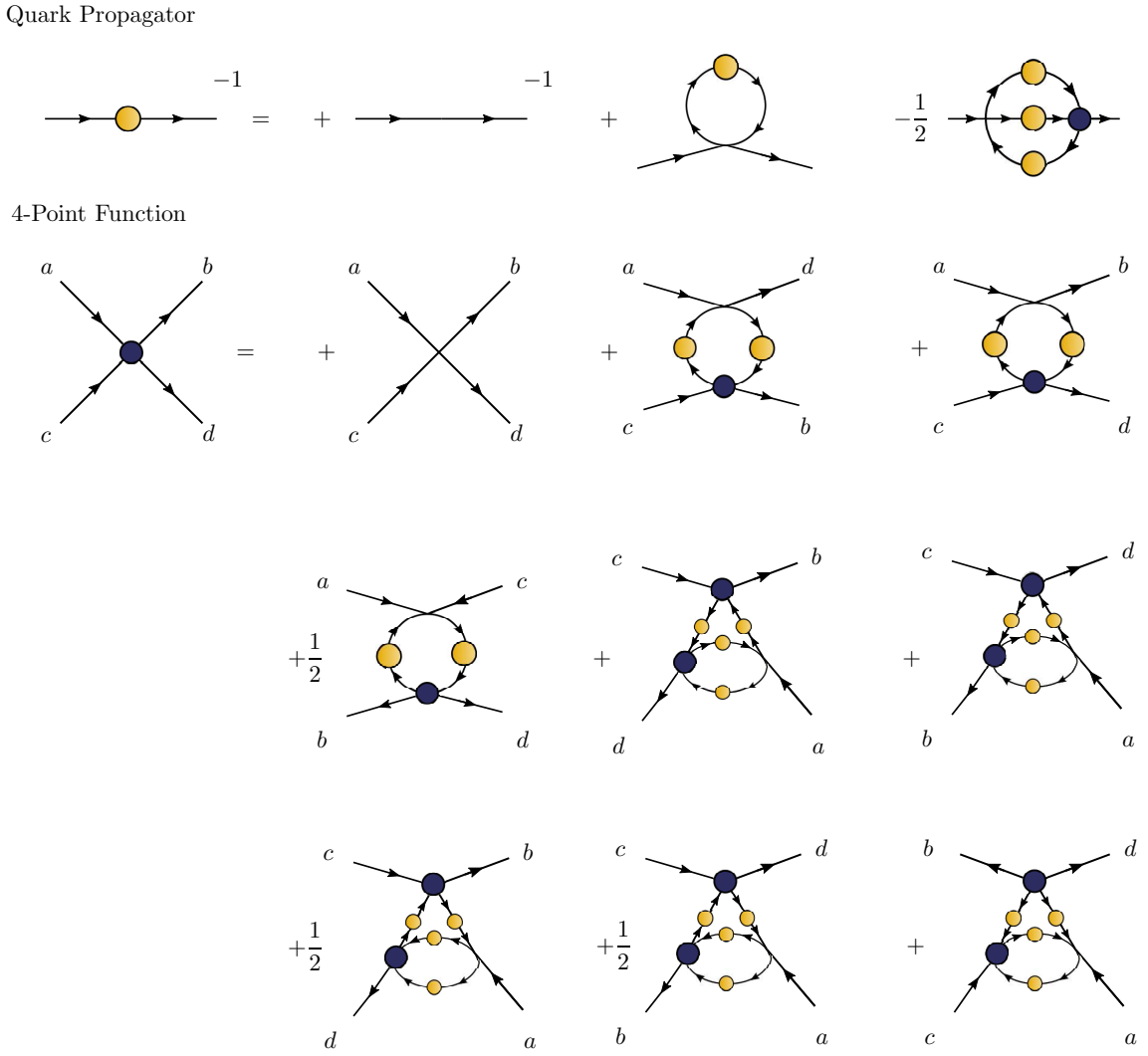

Figure 4.5: Dyson-Schwinger equations of the two-point function and four-point function in the Gross-Neveu model.

Similarly as in the NJL model, the tadpole diagram is momentum independent. However, the sunset diagram is momentum dependent and provides momentum dependence to the $A(p^2)$ and $B(p^2)$ dressings from the two-point function. Furthermore, the dressed four-point function plays a role in the two-loop term. Hence, the DSE of the four-point function, dependent also on two-loop diagram terms, is required. For simplicity, the momentum of the four-point function is averaged following:

$$\Gamma^{(4)}_{\psi\bar{\psi}\psi\bar{\psi}}(p_1,p_2,p_3,p_4) \equiv \Gamma^{(4)}_{\psi\bar{\psi}\psi\bar{\psi}}\left(\left(\frac{p_1-p_2+p_3-p_4}{2}\right)^2\right). \tag{4.33}$$

Here $p_4 = -p_1 - p_2 - p_3$ due to momentum conservation.

The flow equations associated to the GN model are exactly the same as the ones displayed in the NJL one. Comparing the equations of the quark propagator, it is clear that the two-loop sunset diagram appearing in the DSE approach is encoded within the dressed four-point function of the FRG tadpole diagram. Similarly, all the information of two-loop terms in the the four-point function DSE is also hidden within the dressed four-point functions of the flow of the four-point function. Hence, the FRG equations succeed in reducing the complexity of the necessary equations by construction.

Since both methods are equivalent, the same solution in both approaches given the full four-point function is expected. In order to check this statement, we parametrise the momentum dependent four-point function in a similar way as in [108], where the shape of the function is obtained perturbatively, following:

$$\Gamma^{(4)}_{\psi\bar{\psi}\psi\bar{\psi}}(p^2) = \frac{\pi}{\sqrt{1+\frac{p^2}{\mu^2}}\ \sinh^{-1}\left(\sqrt{\frac{p^2}{4\mu^2}}\right)} \tag{4.34}$$

Here μ is a dimensionful parameter of units of momentum $\sqrt{p^2}$. In the DSE approach, this corresponds to the renormalisation scale μ, which in our solution is 1 GeV. In the FRG, however, μ does not correspond to the renormalisation scale but we leave it as the same dimensionful parameter to guarantee proper units.

In the present approximation, we impose $A(p^2) = 1$ in the DSE approach, whereas $Z_{k,\psi}(p^2) = 1$ in the FRG. Consequently, the only variable of interest that plays a role, both in terms of momentum and scale, is the mass function M and m_k. The calculations were set such that they satisfy:

$$M_{DSE}(\tilde{\mu}^2) = M_{FRG}(\tilde{\mu}^2), \tag{4.35}$$

being $\tilde{\mu}$ the renormalisation scale of the DSE calculations. We used the initial conditions:

$Z_{k=\Lambda,\psi}$	$m_{k=\Lambda}$ (GeV)	Λ (GeV)	IR (GeV)
1	0.6	31.62	0.1

Table 4.1: Initial conditions used in the FRG calculations for the Gross-Neveu model. The IR cutoff was taken such that the system reaches apparent convergence before reaching this value.

$A(\mu^2)$	$M(\mu^2)$ (GeV)	μ (GeV)	Λ_{UV}(GeV)	Λ_{IR}(GeV)
1	0.6205	1	316.2	10^{-4}

Table 4.2: Renormalisation conditions used in the DSE calculations for the Gross-Neveu model. Λ_{IR} and Λ_{UV} represent the momentum integral lower and upper limits, respectively.

After the solutions were obtained with these initial conditions, the FRG results were rescaled in order to satisfy condition (4.35). The results are shown in Figure 4.6:

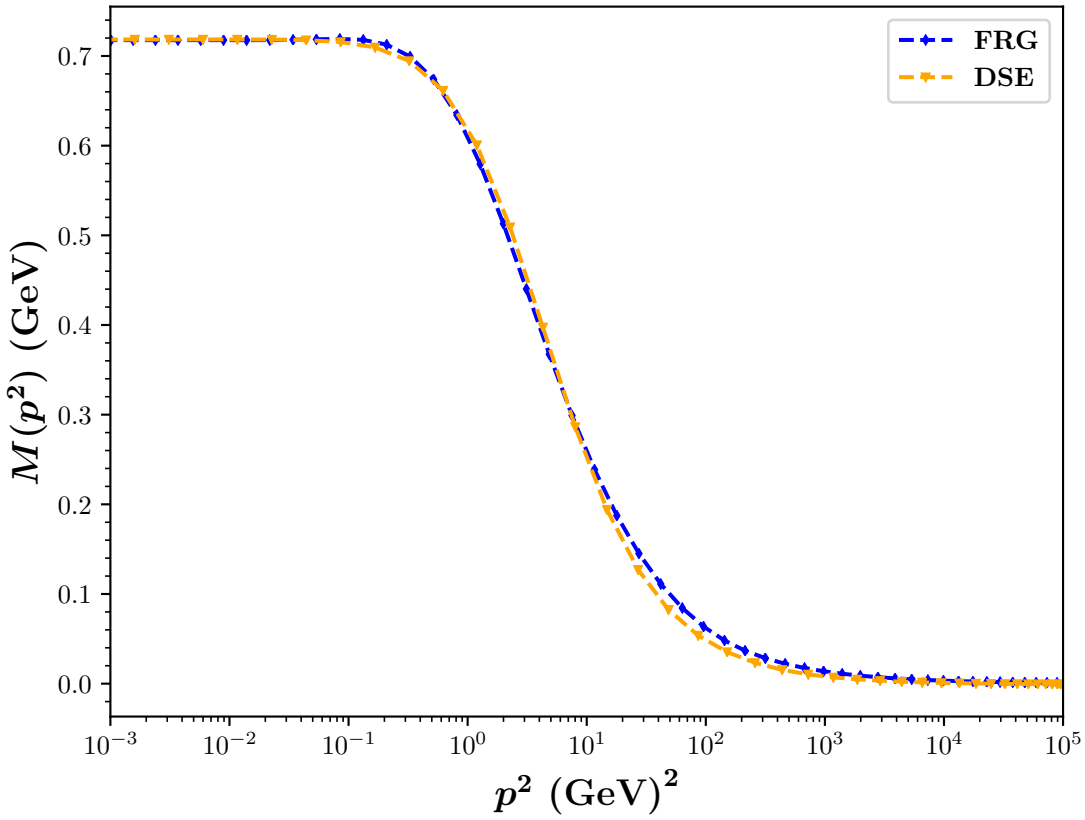

Figure 4.6: Momentum dependent mass functions within the DSE and FRG approaches given the same four-point function.

The curves displayed are almost identical. Using the same 4-point function and the same approximation in which the wave function renormalisation $Z_{k,\psi}(p^2) = A(p^2) = 1$, the mass functions $M(p^2)$ behave the same way, although there are some minor numerical discrepancies caused by the differences between the methods.

The solutions obtained in this method emphasise that equivalent results can be obtained from the use of the both different methods. Nevertheless, there exist fundamental differences between both approaches: in the FRG, the presence of the regulator make numerics faster and stable, whereas the DSE calculations require two-loop terms, which are more expensive in terms of computational time. If different approximation had been used, for instance, a system with unknown full four-point function, additional or different terms would have appeared, complicating thus the calculation. Figure 4.5 already indicate the level of technical difficulty that would appear due to the two-loop terms. Hence, the FRG reduces the complexity of the diagrams involved, facilitating the calculation.

4.2.3 The Quark-Meson model

Another system treated in this work is the bosonised version of the NJL model, leading to the Quark-Meson model in the FRG. The results obtained in Chapter 3 shall be compared to the ones obtained in the DSE approach. For this reason, this section will exclusively make use of the Dyson-Schwinger equations formalism.

The starting point is the classical action of the bosonised NJL model. Its explicit form in euclidean momentum space follows:

$$\begin{aligned} S[\psi,\bar{\psi},\sigma,\vec{\pi}] = \int_p \Bigg(& \bar{\psi}\, Z_2\, i\not{p}\, \psi + \frac{m^2}{2}\left(Z_\sigma\, \sigma^2 + Z_\pi\, \vec{\pi}^2 \right) \\ & + \int_q \bar{\psi} h \left(\frac{Z_{h_\sigma}}{2}\sigma + i\, Z_{h_\pi}\, \gamma_5\, \vec{\tau}\, \vec{\pi} \right) \psi \Bigg), \end{aligned} \tag{4.36}$$

where the summation over colour, Dirac and flavour indices is implied. Under this notation, every quantity and field is renormalised. The momentum dependence of the fields follows the convention defined in the Appendix A. The term m represent the mass of the meson fields and h is associated to their Yukawa couplings. A renormalisation constant term is associated to every action term, which shall be calculated during the computation after setting a renormalisation scale.

Expression (4.36) is in essence different from the FRG effective action at the ultraviolet $\Gamma_{k=\Lambda}$, but it should generate the same vertex functions. Hence, compared to the initial non-zero terms used in the previous chapter, we expect it to generate multi-meson vertex functions up to fourth order associated to the potential $V[\rho]$, as well as momentum dependent quark-meson three-point functions. In this section, the latter vertex functions are referred to H_i and are momentum dependent. Given the interaction:

$$\overline{\psi}\left(q-\frac{p}{2}\right)\psi\left(-q-\frac{p}{2}\right)\mathcal{T}_i\Phi_i, \tag{4.37}$$

where Φ_i is a pion or sigma fields together with their tensor structure $\mathcal{T}$, the associated three-point function follows:

$$\Gamma^{(3)}_{\Phi\psi\bar{\psi}}(p,q) = H_\Phi(p^2,q^2,z), \tag{4.38}$$

where p is the quark total momentum, q is the relative momentum and z is the relative angle between them. Other three-point vertex functions share similar definition of momenta.

Using the definition of the DSEs derived in (2.37), the lowest order functional equations to solve are displayed in Figure 4.7.

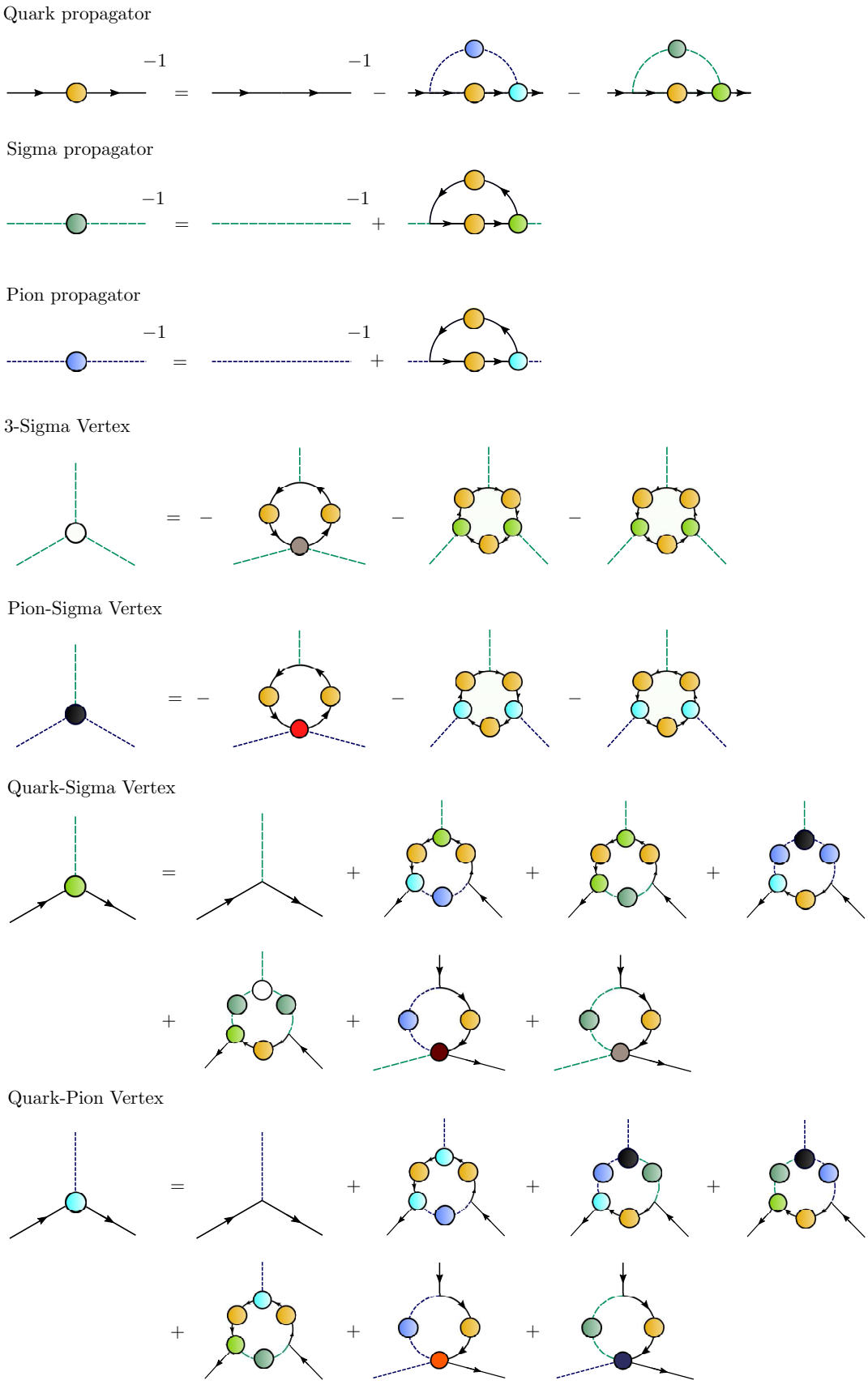

Figure 4.7: Dyson-Schwinger equations of the bosonised NJL.

Figure 4.7 shows that higher order n-point functions appear rapidly in the system while increasing the order of the correlator DSEs. Finding an approximation or truncation compatible with the FRG results is a non-trivial task and a thorough treatment of the equations is required.

In this work, we analysed different approximations and truncations that allow us to solve the system of DSEs self-consistently. In the best of these, we compare the results with the FRG data obtained in the previous chapter. Some of the most interesting cases treated are the following:

- *Rainbow truncation*: the most simple case given by figure (4.8), where only the quark propagator is dressed and every other quantity is free. The values of the vertices in this case are given by h, and the meson inverse propagators are momentum independent and proportional to the mass squared, following m^2. These quantities are related to the four-fermi coupling $\lambda = \frac{h^2}{2m^2}$ from the non-renormalisable NJL model after being bosonised via the Hubbard-Stratonovich transformation.

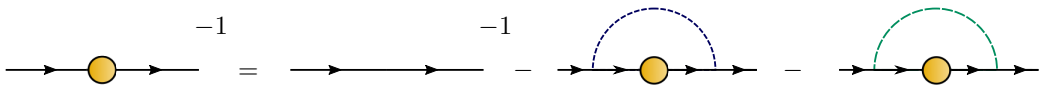

Figure 4.8: Dyson-Schwinger equation for the quark propagator of the bosonised NJL model under the rainbow-like approximation.

A short analysis of the loop terms in the first iteration leads to an important conclusion involving renormalisability of the system. Using m as the mesonic mass and M_q as the generated quark mass, it is easy to show that the loop terms in this truncation follow the proportionality relation:

$$\int d^4q \,\mathrm{Tr}\left(S(q)G_{\pi,\sigma}(p-q)\right) \propto \frac{1}{m^2}\int_0^\infty dq^2 \frac{q^2}{q^2+M_q^2}, \tag{4.39}$$

which are quadratically divergent. Despite the Quark-Meson model being renormalisable, renormalisability is not possible in this approximation. Since it is derived from the non-renormalisable NJL model, divergences arise when the relation $\lambda = \frac{h^2}{2m^2}$ is satisfied. For this reason, this Rainbow-Ladder-like truncation is equivalent to the NJL model treatment and can only be solved using a cutoff. This truncation shows the importance of the presence of bosonic kinetic terms, which shall be encoded within the full momentum dependent meson propagator.

- *Propagator approximation*: in this case, the system only includes the propagator equations, setting the couplings of the quark-meson 3-field interactions to a constant value h. Although this system can provide some information of the pole masses of the mesons, the three-point function can not be completely accessed through BSE, therefore this system is solved only to get a preliminary input of the initial conditions to be used.

- *Full case truncation*: by imposing a vanishing quark-multi-meson four-point function, the set of DSEs shown in Figure 4.7 can be solved self-consistently. In this truncation, four-Fermi interaction plays no role in the solution of the DSEs and will be set to zero for simplicity. Consequently, the solution of the system needs to be compared to the FRG Full Case without dynamical hadronisation, as only then the 1PI correlators are comparable.

  We have treated this truncation using two different approximations for the three point functions. In the first case, total and relative quark momenta are included in the three-point function as an only reason, following:

$$H_\sigma(p,q) = H_\sigma\left((p+q)^2 + \frac{(p-q)^2}{4}\right), \tag{4.40}$$

  and similarly as the other three-point functions. This approach already provides an almost complete description of the system, yielding a first approximation of the three-point vertices in the BSE. This approach, in addition to close to the complete value, is cheaper in evaluation time. In the other approximation used, the three point function keeps its three argument untouched, following:

$$H_\sigma(p,q) = H_\sigma(p^2, q^2, z). \tag{4.41}$$

In this section, only results involving the full momentum dependent three-point functions in the full case will be shown and compared with the Full Case FRG results with also full momentum dependence.

Parametrisation of correlators

Correlators in their dressed and free form need to be parametrised in order to use them in the DSEs. In this section, we use:

$$\Gamma^{(2)}_{\psi\bar{\psi}}(p) = A(p^2)i\not{p} + B(p^2), \qquad \Gamma^{(2)}_{0,\psi\bar{\psi}}(p) = Z_2 i\not{p} + Z_2 Z_m m_q, \tag{4.42}$$

$$\Gamma^{(2)}_{\pi}(p^2) = D^\pi(p^2)p^2 + m_\pi^2, \qquad \Gamma^{(2)}_{0,\pi}(p^2) = Z_\pi p^2 + m_\pi^2, \tag{4.43}$$

$$\Gamma^{(2)}_{\sigma}(p^2) = D^\sigma(p^2)p^2 + m_\sigma^2, \qquad \Gamma^{(2)}_{0,\sigma}(p^2) = Z_\sigma p^2 + m_\sigma^2. \tag{4.44}$$

In a similar way as in the FRG, quarks get mass through the minimum of the potential. Nevertheless, since there is no easy way to minimise potential in the DSE, it is convenient to work with the $B(p^2)$ with the relation:

$$\frac{\sigma}{2} H_\sigma(0, p^2, 0) \equiv B(p^2). \tag{4.45}$$

The remaining required correlators are three-point functions that include their full momentum dependence. They correspond to the quark-meson three-point functions H_σ and H_π, the sigma-pion three-point function $G_{\sigma 2\pi}$ and the three-sigma three-point function $G_{3\sigma}$.

Renormalisation conditions and regularisation

The first step before solving the system is to determine the values of the renormalisation constants Z_i. In order to achieve this, we must choose a renormalisation scale so that the divergence subtraction is performed accordingly. This allows us to fix the renormalisation constants:

$$Z_2 = A(\mu^2) - \Sigma_A(\mu^2), \tag{4.46}$$
$$Z_\pi = D^\pi(\mu^2) - \Sigma_\pi(\mu^2), \tag{4.47}$$
$$Z_\sigma = D^\sigma(\mu^2) - \Sigma_\sigma(\mu^2), \tag{4.48}$$

where Σ_i represents the sum of loop terms. The other three renormalisation conditions need care. The three-point functions, in particular, include both total and relative momenta and relative angle within their parameters. The renormalisation condition has been set at the point where the Yukawa coupling reads $H_i(0, \mu^2, 0)$. As a consequence, the remaining set of equations to determine the values of the renormalisation constants follows:

$$Z_m = \frac{b_0 - \Sigma_B(\mu^2)}{Z_2 m_q}, \tag{4.49}$$
$$Z_{h_\pi} = \frac{H_\pi(0, \mu^2, 0)}{h} - \frac{\Sigma_{h_\pi}(0, \mu^2, 0)}{h}, \tag{4.50}$$
$$Z_{h_\sigma} = \frac{H_\sigma(0, \mu^2, 0)}{h} - \frac{\Sigma_{h_\sigma}(0, \mu^2, 0)}{h}, \tag{4.51}$$

being $m_q = B(\mu^2)/A(\mu^2)$. Once the renormalisation conditions are fixed, the system will be iterated until convergence is reached.

In order to solve the system in the DSE, regularisation was needed to cancel logarithmic behaviour in the ultraviolet. The usual approach to cancel these high energy contributions follows the introduction of the Pauli-Villars regulator in the form:

$$R^{PV}(p^2) = \left(1 + \frac{p^2}{\mu^2}\right)^{-1}, \tag{4.52}$$

which suppresses the logarithmic behaviour when the momentum is larger than the renormalisation scale. This object is included in every propagator involved in the system.

Results

Using the fact that the FRG calculations were performed from an initial ultraviolet scale $\Lambda = 0.950$ GeV, we wanted to choose this value for the renormalisation scale so that $\mu = \Lambda$. By doing this, we wanted to establish a relation between FRG initial conditions and the DSE renormalisation conditions. Nevertheless, since the momentum dependent quantities in the infrared solution

obtained from the FRG do not in general agree with their counterparts in the ultraviolet, that is, $f_{k=\Lambda}(\mu) \neq f_{k=0}(\mu)$, the relation is not straightforward. Hence, we decided to use the FRG results at vanishing k to fix the DSE renormalisation conditions: the renormalised parameters obtained in both methods had to agree at the renormalisation scale $\mu = 0.950$ GeV.

However, the comparison with this choice of results could not be performed. The reason: the DSE results would never converge under these conditions. The values of the dressings would suddenly change sign or unreasonably large values for certain parameters would be obtained during the iteration. Different attempts were done using different renormalisation conditions and initial values in both methods but no stable behaviour could be found.

We could conclude from these attempts that the approximations used in both methods are incompatible. The requirement of vanishing quark-multi-meson interaction is not enough to relate results, even though the DSEs could be solved self-consistently. We believe that, since no four-point function was required in the DSEs, relevant information was missing.

Even if the results are not comparable in this approximation, we would like to understand the behaviour of the correlators with the setting of conditions that allow the convergence of the system. The approach employed is the following: the DSE calculations are performed choosing a particular renormalisation scale μ and the values at this scale are set such that the renormalised pion mass and quark mass agree at the infrared (and $p^2 = 0$).

With the choice of $\mu = 0.95$ GeV, tables 4.3 and 4.4 show the renormalisation and initial conditions used in the calculations of both DSE and FRG approaches.

Parameter	m (GeV)	h	$A(\mu^2)$	$B(\mu^2)$ (GeV)	$D^\pi(\mu^2)$	$D^\sigma(\mu^2)$
Value	1.0841	6.4	1	0.288	1	2

Table 4.3: Table of values of initial and renormalisation conditions in the QM model using the DSE formalism.

Parameter	$\tilde{V}_k^{(1)}$ (GeV)	h_Λ	σ (GeV)	$Z_{\Lambda,\psi}$	$Z_{\Lambda,\phi}$
Value	2.5085	17.03	0.307	1.011	1

Table 4.4: Table of values of initial and renormalisation conditions in the QM model using the FRG. The remaining potential couplings are set to 0.

The renormalised masses at the infrared are such that $m_\pi = 0.138$ GeV and $m_q = 0.297$ GeV. The renormalised values of the three-point functions are set such that $H_i(0, \mu^2, 0) = h$. The results obtained are shown in Figures 4.9 and 4.10.

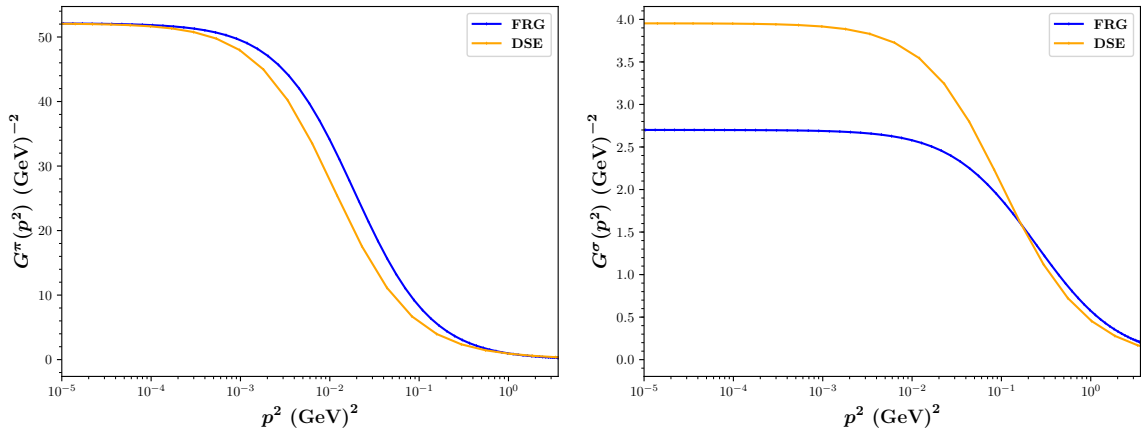

Figure 4.9: Comparison of the propagators of both approaches for a small evolution of the quark mass term.

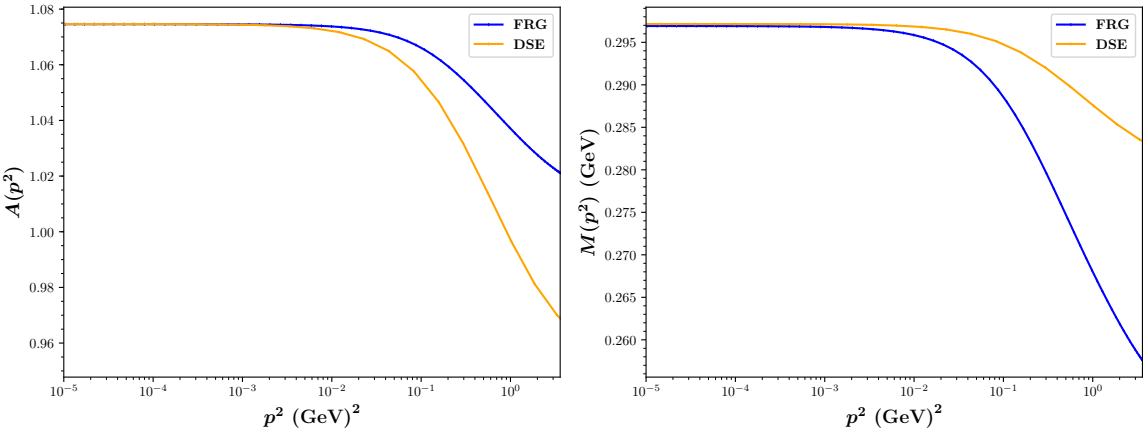

Figure 4.10: Comparison of the dressings of the quark-propagator in both approaches approaches.

Overall, the general behaviour of the curves agree with the FRG results, although there is a clear numerical discrepancy. The pion propagator is slightly shifted, showing that a rescaling is still necessary. This is not surprising as the renormalisation schemes are different. The infrared values of the sigma meson masses could not be tuned to agree. In the case of the quark dressings, the infrared values agree, but the behaviour is quite different. Particularly, there is clearly less mass generated, and the system cannot be set such that it generates much more mass.

From this results, our conclusion is that the approximation used in the DSE is not compatible with the FRG one. The dressed four-point functions would be necessary and this clearly increases the amount and difficulty of the diagrams involved.

In comparison to the previous sections, it is clear that the procedure of bosonising the system increases the complexity of the diagrams involved as more interactions appear. Nevertheless, an analysis of the QM equations and the ones obtained from the NJL should be analysed, in order to understand the main difference between NJL and QM model. This is done in Appendix C.

4.2.4 Distinctive features

In this chapter, a great emphasis has been put on the fact that approximations, truncations and results are equivalent in both of the functional methods treated along this work. Even though a vast amount of new, alternative calculations become accessible due to all the possible approximations of the FRG, we analysed the existence of features exclusive to one of the methods.

A particularly interesting behaviour that could be found only in the FRG is the evolution of the kinetic terms in fermionic and bosonic systems. Properly treated, the system reflects how low-energy degrees of freedom are dynamically generated and which amount of fermionic kinetic energy is transferred to mesons. Furthermore, by relating kinetics to the wave function renormalisations, one can study the probability amplitude conservation in the system. In order to analyse such behaviour, we work in the Quark-Meson model using the Full+DH approximation.

Every kinetic term appears in the effective action of the QM model together with the wave-function renormalisation. Hence, the objects of interest in this section are $Z_{k,i}$. We consider a pure fermionic system in the ultraviolet by setting $Z_{\Lambda,\phi} = 0$ and $Z_{\Lambda,\psi} = 1$, letting the flow evolve. It is important not to use dressed regulators during this calculations, as this setting complicates numerics. The parameters to be analysed are the wave-function renormalisation at zero momentum, and we define the total wave function renormalisation $Z_{k,s}$ as:

$$Z_{k,s} \equiv \sqrt{Z_{k,\psi}^{-2} + \frac{1}{4} Z_{k,\sigma}^{2} + \frac{3}{4} Z_{k,\pi}^{2}}, \tag{4.53}$$

which, ideally, should be $Z_{k,s} = 1$ for every value of the scale k. The parameter $Z_{k,\psi}^{-2}$ is set in this way as it agrees with the probability amplitude in the standard notation, and the meson factors are averaged according to their weight in the system. The set of initial conditions used are shown in the Table 4.5

Parameters	$\tilde{V}_k^{(1)}$ (GeV)	h_Λ	σ_{exp} (GeV)	$Z_{\Lambda,\psi}$	$Z_{\Lambda,\phi}$
Values	0.7	4	0.1	1	10^{-10}

Table 4.5: Table of values of initial conditions in the QM model under the Full+DH approximation.

The rest of initial parameters, including the remaining potential terms are set to zero. The ultraviolet scale is chosen to be $\Lambda = 0.95$ GeV. The set of values was chosen to better accentuate the behaviour of $Z_{k,\psi}$.

Figure 4.11 shows the behaviour of the $Z_{k,i}$ using an undressed, exponential regulator:

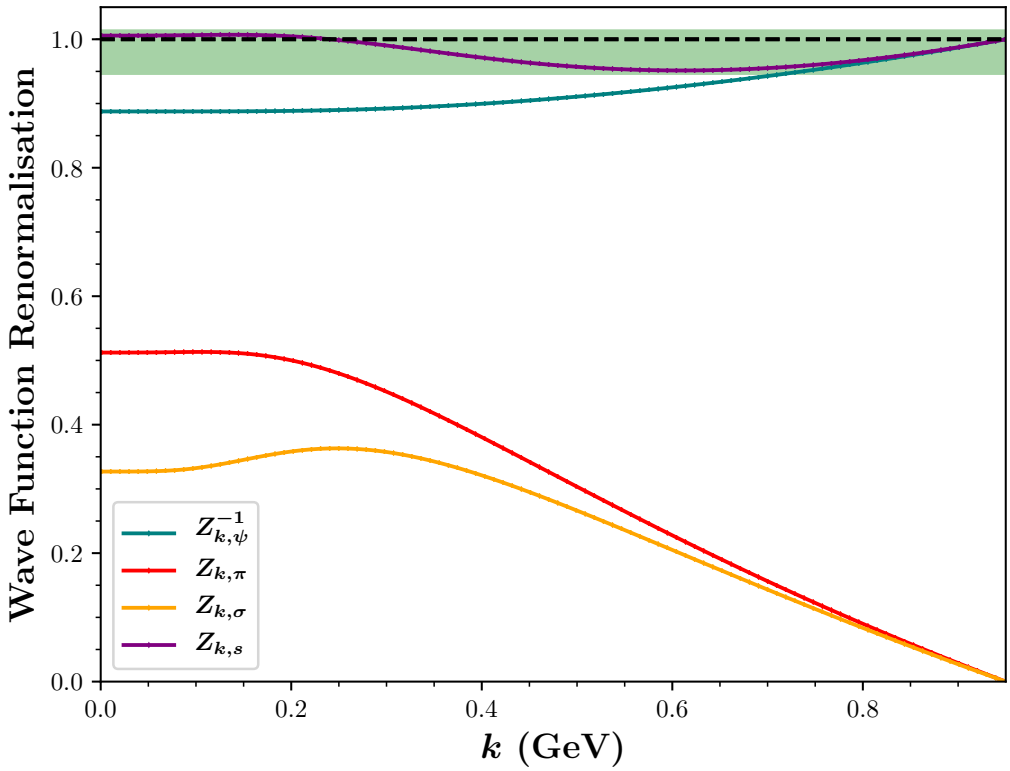

Figure 4.11: Wave function renormalisations in terms of the scale.

This plot shows the evolution of the wave-function renormalisation in terms of the scale. In the ultraviolet point, all the probability amplitude belongs to the fermions, while mesons do not propagate. The probability amplitude of fermions diminishes with the scale and is transferred to the mesons, which start contributing into the system at lower energies as expected. The total $Z_{k,s}$ in (4.53) shows a 5% error against the expectation $Z_{k,s} = 1$, presumably caused by the approximations used.

Further information can be extracted from this figure. First of all, together with the probability amplitude, the propagating degrees of freedom are preserved. Moreover, this behaviour might be related to confinement: while lowering the energy scale, quarks couple to hadrons. In a fully confined system, $Z^{-1}_{k,\psi}$ would drop to zero in the infrared, yielding a purely hadronic system at low energies. The fact that $Z^{-1}_{k,\psi}$ remains shows that the Quark-Meson model is not suitable, at least in the approximations used, to describe confinement. Future calculations should aim to a full calculation including gluons.

4.3 Numerical comparison

The remaining aspect to analyse is the behaviour of numerics in each of the methods. The efficiency and relatively short evaluation time that Functional Methods provide in comparison to other non-perturbative methods makes the former a tool of interest. In a similar way, we would like to study whether one of the functional methods is more optimal for calculation and, in the positive case, in which situations. In this section, we summarise all the observations made during all the calculations performed.

While the DSEs are a set of coupled integral equation, the flow equations from the FRG are differential equations including integrals. Consequently, the approaches used to reach convergence to the full solution of the effective action are completely different. In the DSE approach iteration is required, whereas in the FRG additional ordinary differential equation solving is present. Since two kinds of equation-solving methods are needed in the FRG, additional numerical and methodical errors are carried. For this reason, it is strongly recommended the use of optimised routines in order to have complete control of the numerical errors and minimise uncertainties. The routines involve adaptive quadratures and Runge-Kutta integration with adaptive stepper, the latter of which is very convenient to shorten the integration time. For simple approximations, adaptive quadrature in the DSE approach becomes counterproductive, as the routine takes longer that usual quadrature with no noticeable gain in precision.

Naturally, the more precision is desired, the longer it takes to converge. This is quite accentuated in the DSE case, where iterations are required. Normally, the iteration is finished once the difference between all the values of two subsequent iteration steps is smaller that certain ϵ. When ϵ becomes too small, the evaluation time increases exponentially and the system becomes, in comparison to FRG calculations with same ϵ as relative errors, clearly slower. In addition to this, renormalisation constants need to be computed in the DSE formalism. This requires extra integrations that, even though they do not increase evaluation time much due to the numerical integration, increases the number of parameters to converge and raises the evaluation time to reach convergence.

One of the interesting feaures of the FRG is the relatively low amount of external grid momentum points necessary to achieve convergence. Furthermore, the simpler the approximations are, the shorter they take to convergence. For instance, calculations within the QM model in the LPA truncation use to take shorter than half a dozen of seconds. Nevertheless, with the same number of grid points and reasonably comparable approximations DSE calculations reach convergence faster.

The amount of parameters involved changes greatly in both of the methods. This is naturally dependent on the truncation used, but in our best approximation, we have a number of the order of 10 different momentum independent parameters, together with the momentum dependent quantities: a great number of objects have their own flow equations. On the other hand, in the DSE only momentum dependent quantities are used and the number of parameters involved is proportional to the number of grid points.

There are now two important aspects that work differently in both methods: initial conditions and renormalisation conditions. In the FRG every parameter involved has to be given a value for the initial condition which, for simplicity, is set to be the same for every momentum-dependent

variable. This is employed similarly in the DSE approach. Nevertheless, the effect caused is completely different. In the DSE, different initial conditions may lead to the exactly same solution of the system, provided that the same renormalisation condition is chosen. This shows that the final solution is independent of the initial conditions but on the renormalisation conditions. On the other hand, the initial conditions in the FRG play a crucial role, since they indirectly fix the values of the full solution at the infrared. In other words, they determine implicitly the renormalisation conditions. Furthermore, there exist sets of initial conditions that make the system impossible to converge. This is performed in the DSE formalism by choosing a particular renormalisation scale μ and choosing values of the correlators to be satisfied in that scale. This fixes the values of the renormalisation constants.

Both methods have their own pros and cons regarding numerics. Initial conditions play a greater role in the FRG, but in practise a convenient set of conditions stabilises numerics and obtains the solution of the flows sometimes faster than the DSE. On the other hand, the DSE formalism provides the solutions of the equations in a much more simpler way, and the generalisation to complex-valued quantities is straightforward with minimal changes. Provided that equivalent approximations are used in both methods, the evaluation time required is expected to be of the same order of magnitude. Different kinds of tools are required in both of the methods and they are all analysed in the Appendix B.

Chapter 5

Summary and conclusions

The Functional Renormalisation Group provides an alternative approach in the continuum to the Dyson-Schwinger/Bethe-Salpeter equations formalism to determine the Green's functions of quantum field theories. Hence, it grants access to properties of bound states of quarks and gluons in QCD and QCD-like theories. As a continuum functional method truncations and approximations are required to determine the Green's functions self-consistently. By construction, a different set of truncations and approximations can be used in the FRG that shall lead to compatible results obtained within the DSE-BSE formalism.

In this thesis, we first analysed the viability of the Functional Renormalisation Group as a method to derive Green's functions in a low-energy QCD model: the Quark-Meson model. This system reflects intrinsic properties of QCD such as dynamical chiral symmetry breaking and includes quark and meson fields as degrees of freedom instead of gauge bosons. We used the flexibility of the FRG to solve the system in different truncations, setting the infrared values to be similar. The solutions we obtained show that even though the overall behaviour of the system is maintained, significant changes occurred. The inclusion of the running wave function renormalisations redefined the renormalised parameters and changed the values of the initial conditions. In our best approximation, we implemented the dynamical hadronisation technique, allowing to formally cancel the quark four-point function in every scale by redefining our 1PI correlators.

Using the results obtained in our most complete approximation including the dynamical hadronisation technique, we succeeded in extracting properties of pions and the sigma meson such as pole masses, decay widths and spectral functions. In contrast to the usual procedure performed within the DSE-BSE approach, instead of calculating directly Green's function in the complex plane, analytic continuation via extrapolation of Euclidean data was used. The continuation using the Padé approximant proved to be adequate to extract pole masses and decay widths, but not entirely optimal for a quantitative calculation of spectral functions as small numerical noise modifies the results completely. Future studies willing to extract properties of bound states shall aim to perform analytical continuation via direct calculation with modified regulator approaches such as the ones implemented in [101, 102].

In the second part of the thesis we compared different aspects of the FRG and the DSE-BSE formalisms. Formally the FRG equations are the differential version of the DSEs and the full effective actions are equivalent. Furthermore, a connection between the FRG and BSE can be established, relating the approximations used in both methods. The main difference found between the methods is the renormalisation procedure that, due to the way it is constructed, the one in the FRG is intrinsically different and working in the same scheme is a non-trivial task.

We analysed the implementation of both functional methods in different low-energy energy systems: the NJL model, the Gross-Neveu model and the Quark-Meson model. In the former model we could find an exact agreement between the methods, as the usual DSE approach corresponds to the FRG one with small couplings. In the Gross-Neveu model, we used previously known correlators, working only with the quark mass function. In this case we could see that, diagrammatically, the DSE approach is more laborious due to the two-loop diagrams, included implicitly in the FRG in the momentum dependent four-point function. In this case, we succeeded in finding a set of conditions such that the quark mass function behaves qualitatively in a similar way with minor quantitative differences. Lastly, a comparison between the FRG and DSE results was attempted, in an approximation in which the same correlator is neglected in both approaches. Despite the correlators behaving similarly, the difference between numerical results prove that the approximations are not equivalent and further DSEs are required. In this model, however, we succeeded in extracting interesting relations within the FRG that are not obtainable in the DSE approach which may lead, in a more complete approximation, to important statements involving gauge dependence and confinement.

Finally, we analysed the numerics involved within the computations. Even though the FRG requires solving differential equations in addition to the integral ones, the one-loop-only diagram terms greatly simplify the complexity of the functional equations involved. Furthermore, the presence of the regulator in the FRG stabilises numerics in a way that the parameters evolve smoothly, making it easy and intuitive to keep track of the quantities and set the initial parameters accordingly. The evaluation time required is strongly dependent on the truncation. In the FRG, calculations used to take from a few seconds to several hours depending on the desired number of points and precision. Nevertheless, using an optimised code, stable calculations took usually no more than half an hour to be completed. In contrast, DSE calculations with the same number of points and precision usually took at least twice the time. This fact does not necessarily mean that FRG is computationally more adequate. A proper comparison of the evaluation time needs to be performed in systems with compatible approximations and, in the ones analysed, the evaluation time in both methods is similar. We expect that in full QCD calculations with comparable approximations take approximately the same evaluation time.

The FRG results are indeed compatible with the DSE ones, yielding similar results but yet approached differently. Both methods shall be complementary: numerical difficulties involved in the FRG approach may be inexistent in some DSE formalism and vice-versa. Nevertheless, a complete comparison between methods should be performed in a full QCD system including complex-valued quantities with compatible approximations.

Appendix A

Conventions

A.1 Space-time conventions

Unless specified explicitly, this work uses mostly equations defined in Euclidean space-time. The metric used is expressed in its matrix representation as:

$$\delta^{\mu\nu} = \begin{pmatrix} \mathbb{I}_{3\times3} & 0 \\ 0 & 1 \end{pmatrix} \tag{A.1}$$

where $\mathbb{I}_{3\times3}$ represents the space components and time always in the 4th term of the diagonal. Scalar products are then defined as:

$$p \cdot q = \sum_{\mu,\nu=1}^{4} p_\mu q_\nu \delta^{\mu\nu} = \sum_{\mu=1}^{4} p_\mu q_\mu \qquad\qquad \not{p} = p \cdot \gamma = \sum_{\mu=1}^{4} p_\mu \gamma_\mu \tag{A.2}$$

Dirac matrices γ are defined so that the identity $\{\gamma^\mu, \gamma^\nu\} = 2\delta^{\mu\nu}$ is satisfied. Furthermore, they fulfill the relations:

$$(\gamma^\mu)^\dagger = \gamma^\mu \qquad\qquad \gamma_5 = -\gamma_1\gamma_2\gamma_3\gamma_4 \qquad\qquad (\gamma_5)^\dagger = \gamma_5 \tag{A.3}$$

In general, the explicit matrix expression of the gamma matrices is not needed, since they are in general traced out. Nevertheless, for numerical cross-checking, Dirac matrices were used in their standard Euclidean representation:

$$\gamma_{1,2,3} = \begin{pmatrix} 0 & -i\sigma_{1,2,3} \\ i\sigma_{1,2,3} & 0 \end{pmatrix} \qquad \gamma_4 = \begin{pmatrix} \mathbb{I}_{2\times2} & 0 \\ 0 & -\mathbb{I}_{2\times2} \end{pmatrix} \qquad \gamma_5 = \begin{pmatrix} 0 & \mathbb{I}_{2\times2} \\ \mathbb{I}_{2\times2} & 0 \end{pmatrix} \tag{A.4}$$

A.2 Index and field conventions

The general choice of indices is the following:

- *Colour indices*: Uppercase latin letters $A, B, C, ...$ running from 1 to N_c from $SU(3)_C$.
- *Flavour indices*: Lowercase latin letters $a, b, c, ...$ running from 1 to N_f from $SU(2)_f$.
- *Lorentz indices*: Lowercase greek letters $\mu, \nu, \rho, ...$ running from 1 to $d = 4$.
- *Dirac indices*: Lowercase greek letters $\alpha, \beta, \gamma, ...$ running from 1 to 4.
- *Adjoint Flavour indices*: Lowercase latin letters $z, y, x, ...$ from 1 to $N_f^2 - 1$ from $SU(2)_f$.
- *Numbered indices*: Set of all the previous indices encoded into a numbered index $a_1, a_2...$, refering to the indices of a field.
- *Field indices*: Lowercase latin letters in bold $\boldsymbol{a}, \boldsymbol{b}, ...$ They contain information regarding the bosonic or fermionic nature of the fields and sources. They are extended to $\boldsymbol{a} = a_1...a_n$ for the case of superfields, and they satisfy the property $\Phi^{\boldsymbol{a}} J^{\boldsymbol{a}} = \Phi^{\boldsymbol{a}} J^{\boldsymbol{b}} (-1)^{\boldsymbol{ab}}$, where:

$$(-1)^{\boldsymbol{ab}} = \begin{cases} -1 & \text{odd number of fermionic indices of } \boldsymbol{a} \text{ and } \boldsymbol{b} \\ +1 & \text{even number of fermionic indices of } \boldsymbol{a} \text{ and } \boldsymbol{b} \end{cases} \tag{A.5}$$

The general choice of bosonic and fermionic fields is:

$$\text{Bosons}: \quad \phi, \sigma, \vec{\pi}, A_\mu, ... \tag{A.6}$$
$$\text{Fermions}: \quad \psi, \bar{\psi}, q, \bar{q}, ... \tag{A.7}$$

Unless specified, fields without arguments are always in position space. The source terms for the general nPI path integral for general bosonic fields ϕ follows:

$$S_{ST}[\phi, J, K, L, ...] = \int_x \phi^{a_1} J^{a_1} + \phi^{a_1}\phi^{b_1} K^{a_1 b_1} + \phi^{a_1}\phi^{b_1}\phi^{c_1} L^{a_1 b_1 c_1} + ... \tag{A.8}$$

The expression is simplified under the definition of the super field Φ and supersource term $\mathcal{J}$ as:

$$\Phi = (\phi, \phi\phi, \phi\phi\phi, ...) \tag{A.9}$$
$$\mathcal{J} = (J, K, L, ...) \tag{A.10}$$

so that the whole expression is reduced to

$$S_{ST}[\Phi, \mathcal{J}] = \int_x \Phi^{\boldsymbol{a}} \mathcal{J}^{\boldsymbol{a}}. \tag{A.11}$$

This expression includes also proper negative sign for fermionic field contributions.

A.3 Numerical conventions

Scalar derivatives:

$$\frac{\partial}{\partial t} \equiv \partial_t \qquad \partial_t = k\partial_k \qquad \partial_t R_k \equiv \dot{R}_k \tag{A.12}$$

Functional derivatives, vertex functions and tensor structures:

$$\frac{\delta}{\delta J} F[J] \equiv \delta_J F[J] \qquad \frac{\delta^n \Gamma[\Phi]}{\delta\phi^{\boldsymbol{a}}\ldots\delta\psi^{\boldsymbol{b}}} \equiv \Gamma^{(n)}_{\boldsymbol{\phi}\ldots\boldsymbol{\psi}}\, T^{\boldsymbol{a}\ldots\boldsymbol{b}} \tag{A.13}$$

$$\delta_\phi \left(\Gamma^{(2)}_{\boldsymbol{ab}}\right)^{-1} = -\left(\Gamma^{(2)}_{\boldsymbol{ac}}\right)^{-1} \Gamma^{(3)}_{\boldsymbol{c\phi d}} \left(\Gamma^{(2)}_{\boldsymbol{db}}\right)^{-1} \tag{A.14}$$

Propagators in usual parametrisation:

$$\left(\Gamma^{(2)}_{\boldsymbol{\phi\phi}}\right)^{-1} \equiv G^\phi = \left(Z_\phi p^2 + m_\phi^2\right)^{-1}, \tag{A.15}$$

$$\left(\Gamma^{(2)}_{\boldsymbol{\psi\bar{\psi}}}\right)^{-1} \equiv, G^\psi \left(-i\not{p}A(p) + B(p)\right) \qquad G^\psi = \left(A(p)^2 p^2 + B(p)^2\right)^{-1}. \tag{A.16}$$

Regularised propagators:

$$G_k \equiv \left(\Gamma^{(2)}_k + R_k\right)^{-1}. \tag{A.17}$$

Regulator and propagator matrices (see Appendix C):

$$\dot{R}_k = \begin{pmatrix} \dot{R}_k^\phi & 0 & 0 \\ 0 & 0 & -\dot{R}_k^\psi \\ 0 & \dot{R}_k^\psi & 0 \end{pmatrix} \qquad G_k = \begin{pmatrix} G_k^\phi & 0 & 0 \\ 0 & 0 & -G_k^\psi \\ 0 & G_k^\psi & 0 \end{pmatrix} \tag{A.18}$$

Space-time and momentum integrals are expressed in a compact form, the latter using hyperspherical coordinates:

$$\int_x \equiv \int d^4x \qquad p^\mu = \sqrt{p^2} \begin{pmatrix} \sqrt{1-z^2}\sqrt{1-y^2}\sin\phi \\ \sqrt{1-z^2}\sqrt{1-y^2}\cos\phi \\ y\sqrt{1-z^2} \\ z \end{pmatrix} \tag{A.19}$$

$$\int_p \equiv \int \frac{d^4p}{(2\pi)^4} = \frac{1}{2}\frac{1}{(2\pi)^4} \int_0^\infty dp^2 p^2 \int_{-1}^1 dz\sqrt{1-z^2} \int_{-1}^1 dy \int_0^{2\pi} d\phi \tag{A.20}$$

A.4 Diagrammatic conventions

Functional methods allow a diagrammatic description of their correlator equations, which makes the behaviour of the n-point functions more intuitive and easier to treat. Systems in momentum space require consistent conventions that, as long are they are kept along the calculation, can be chosen freely. This work, and both in the FRG and DSE approach, uses only the convention in which all the momentum lines add up to zero. This is achieved by consider the Grassman fields $\bar{\psi}$ and ψ to Fourier-transform in the same way. This means that, given the superfield $\Phi = (\phi, \bar{\psi}, \psi)$ and being ϕ any kind of bosonic field, the result of a Fourier-transform works as:

$$\Phi(x) = \int_p \Phi(p) e^{-ip\cdot x} \tag{A.21}$$

Under this definition, the sum of the fields momenta of every term in the effective action adds up to 0. Explicitly, this means:

$$\text{2-Field terms:} \qquad \int_p \Phi(p)\Phi(-p) \tag{A.22}$$

$$\text{3-Field terms:} \qquad \int_p \int_q \Phi(p)\Phi(q)\Phi(-q-p) \tag{A.23}$$

$$\text{4-Field terms:} \qquad \int_p \int_q \int_r \Phi(p)\Phi(q)\Phi(r)\Phi(-p-q-r) \tag{A.24}$$

$$\vdots$$

For terms with 3 fields or more, any other combination of momenta is allowed by the Fourier transform, as long as it is consistent with the addition to zero. By changing the dependence of such fields properly, terms within functional equations include more convenient momentum dependent terms, which can reduce significantly the amount of computational time and increases accuracy, when interpolation needs to be performed.

Diagrammatically, ingoing and outgoing momenta are chosen such that when all the lines are ingoing, the sum of the momenta is zero. Below is shown the example of the quark propagator in both approaches, choosing the sign of the momenta according to the counter-clockwise loop direction:

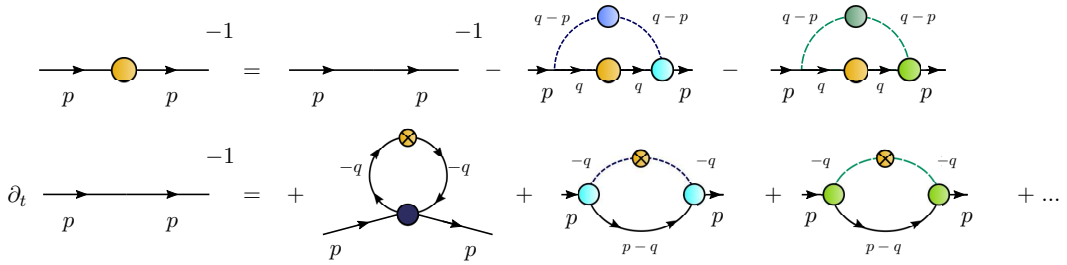

Figure A.1: Explicit momentum dependence in Dyson-Schwinger and FRG equations for the quark propagator.

A.4.1 DSE-BSE diagrams

Diagrams in both DSE and BSE approaches share the same conventions. Since the main objects that appear in the equations are dressed and undressed correlators and, in the case of the BSEs, also the Bethe-Salpeter amplitudes and interaction kernel, the diagrammatic convention taken follows:

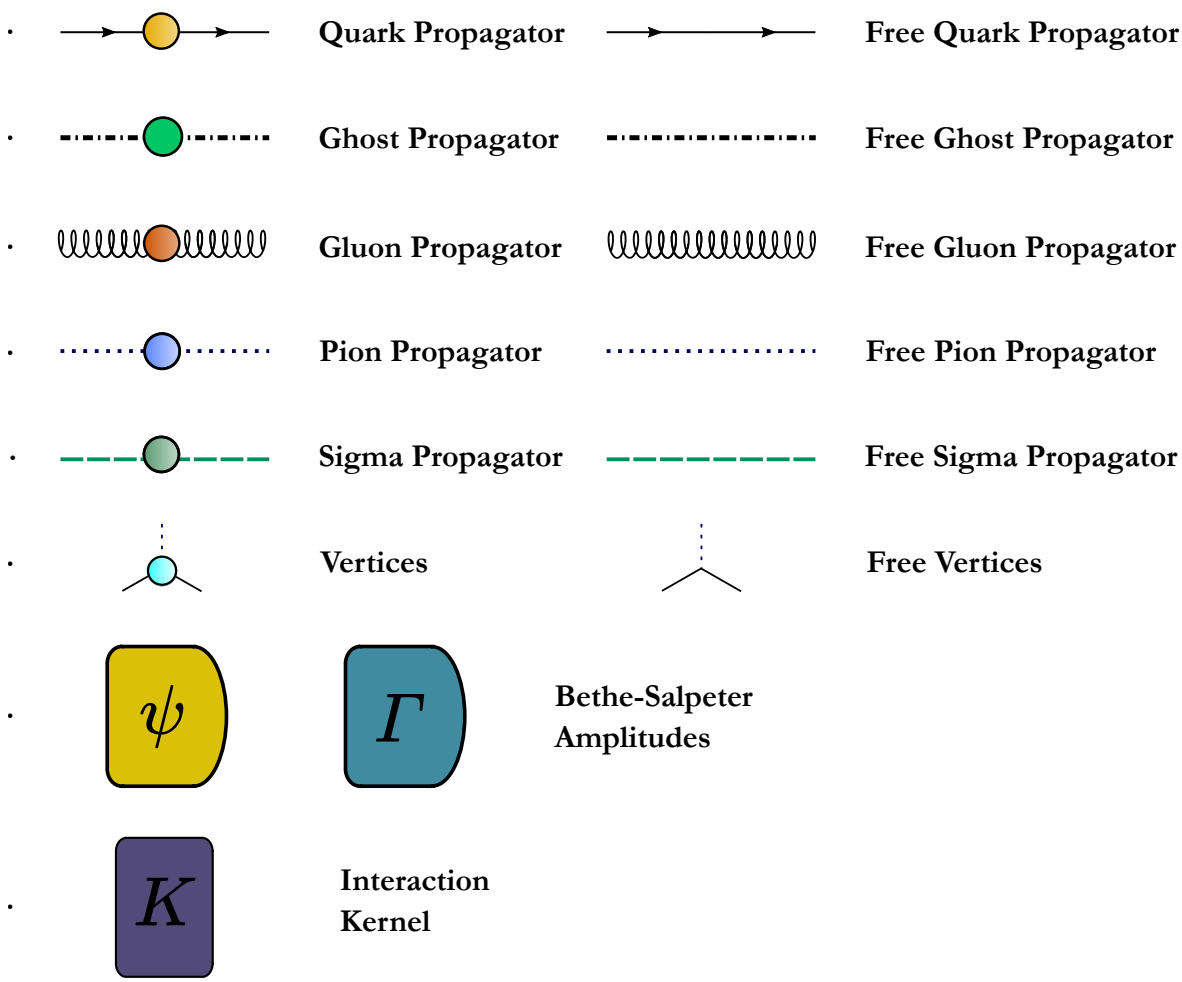

Figure A.2: Objects appearing in the DSE-BSE diagrams in this work.

Colours of the dressings (circles) as well as the form of the correlator lines are kept consistent along the diagrams of this work. The vertices appearing depend on the colour and shape of the field lines involved and, when they are dressed, also on the colour of the dressing circle. The Bethe-Salpeter amplitudes are differentiated according to the bound-state equations that involve dressed Green's functions (ψ) or amputated Green's function (Γ).

A.4.2 FRG diagrams

Wetterich's flow equation parameters are directly related to the effective and not the bare action. As a consequence, every propagator and n-point vertex appearing in a diagram will be a full or dressed object. Hence, instead of indicating the dressings of the propagators diagrammatically, only bare lines are drawn. Using this notation, regulators are drawn on top of the propagators letting a more compact, clear identification of the flow equation, being the objects in this work:

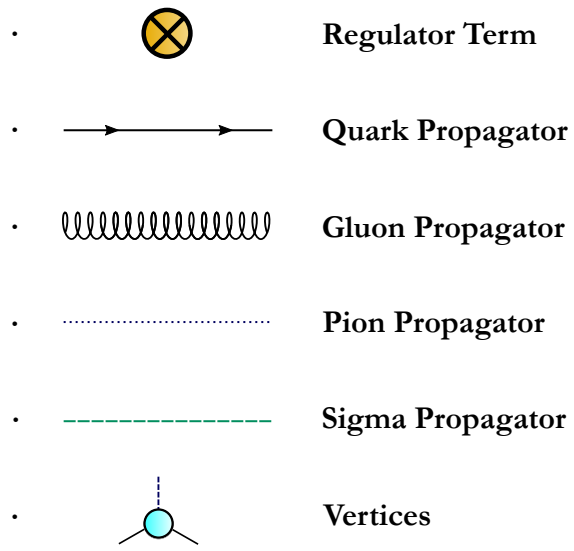

Figure A.3: Objects appearing in the FRG diagrams in this work.

Here one must keep in mind that the regulator term corresponds to $\partial_t R_k$, independently from its bosonic or fermionic nature.

Several flow equations include contributions from a large number of diagrams which are equivalent to the others, with the exception of the regulator position. In order to avoid redundancy and to write the diagrams more compactly, the term $+perm$ is defined:

- *+perm*: Permutation of the regulator position of every previous diagram, independently of its bosonic/fermionic behaviour. Unless specified otherwise, every diagram included in the permutation keeps the same factor and sign as in the original terms.

Appendix B

Identities and numerical tools

B.1 Analytic continuation

Properties of bound states are obtained from the expression of the momentum dependent Green's function in Minkowski space. Some of these properties are pole masses, decay widths or spectral functions. The functional methods are built in Euclidean space and therefore one needs to perform an analytic continuation.

There are several ways to analytically continue the obtained Green's functions into real-time momenta. The direct calculation of such objects is obtainable in both functional methods, but they require rewriting of the equations and are, in general not trivial. The usual approach, which uses the Euclidean correlators as initial input, is the extrapolation using the Padé approximant. The approximant of order (m,n) is generally defined as:

$$R^{(m,n)}(x) = \frac{\sum_{i=0}^{m} c_i x^i}{1 + \sum_{j=1}^{n} d_j x^j}. \tag{B.1}$$

The approximant is simply a quotient of polynomials and encodes every property of a function, including zeros and poles. The usual procedure is the following:

1. Select the function to perform the analytic continuation and the arguments. As an example, the propagator of the pion G_π in function of the momentum square p^2.
2. Identify the argument x with the argument of the function to continue. In the current example, $x = \bar{p}^2$, where $\bar{p}^2$ is a dimensionless momentum square, so that every coefficient c_i and d_j is also dimensionless.
3. Choose orders (m, n) of the approximant, taking into consideration that the higher the order, the more coefficients are needed.

4. Fit the parameters c_i and d_j using the method of the least squares.

5. Work only with the fitted approximant. Poles are generally found by setting

$$1 + \sum_{j=1}^{n} d_j x^j = 0 \tag{B.2}$$

and solving for x. Special treatment is only required when also the numerator cancels at the same x point. In such case, a study of the limits around x is needed.

By virtue of the fundamental theorem of the algebra, the polynomial in the denominator has n poles, most of them artificial. The fit and comparison of approximants of different orders shall clarify which poles are spurious and which of them are physical. On the other hand, higher order approximants provide a better description of the object in real-time momenta, therefore one should keep both positive and negative aspects of this method into consideration.

B.2 Modified Padé (RVM) method

A slightly modified Padé approximant has been recently used to perform analytic continuation with very successful results. This method, commonly known as the RVM method [94], is based on the Schlessinger point method and uses a nested function to apply the continuation:

$$C(x) = \cfrac{z_0}{1 + \cfrac{z_1(x-x_1)}{1+\cfrac{z_2(x-x_2)}{\ddots \\ \cfrac{}{z_M(x-x_M)}}}}, \tag{B.3}$$

where z_i are the coefficients to be found and x_i are the numerical data points. Notice that this approximant is equivalent to the previously defined Padé approximant of order $(M-1, M)$, being $M-1$ the number of data points. The great advantage of this method is the calculation of coefficients which is computed exactly. The procedure is the following:

1. Select the function to apply the analytic continuation on.

2. Identify the function and the arguments.

3. Insert data points for x_i, with $i = 1, ...M-1$ to determine the coefficients in the form:

$$z_0 = C(x_1), \qquad z_1 = \frac{z_0 - C(x_2)}{C(x_2)(x_2 - x_1)} \qquad ... \tag{B.4}$$

4. Work with the new function $C(x)$.

This method allows us to properly find poles and to obtain spectral functions but, in comparison to the usual Padé method, strongly depends on the number of data points used.

B.3 Bosonisation and the Hubbard-Stratonovich transformation

Bosonisation is the technique based on the Hubbard-Stratonovich transformation that allows the inclusion of macroscopic degrees of freedom in low-energy QCD effective systems. As shown in chapter 3, the effective model for low-energy QCD includes the fermionic kinetic term and four-Fermi interaction. Therefore, the NJL model is a convenient starting point, defined in a uniquely fermionic action S_F:

$$S_F[\bar{\psi},\psi] = \int_x -\bar{\psi}\partial\!\!\!/\psi - \lambda\left[(\bar{\psi}\psi)^2 + (\bar{\psi}i\gamma_5\psi)^2\right]. \tag{B.5}$$

This system includes a $U(1)\times U(1)$ invariant four-Fermi interaction, since chiral symmetry plays a crucial role in QCD. By identifying $\lambda = \frac{h^2}{2m^2}$, the action can be rewritten as:

$$S_F[\bar{\psi},\psi] = \int_x -\bar{\psi}\partial\!\!\!/\psi + \frac{1}{2m^2}\left(O_1O_1 + O_5O_5\right). \tag{B.6}$$

By having defined the operators:

$$O_1 = -i\left(h\bar{\psi}\psi\right) \qquad\qquad O_5 = -i\left(h\bar{\psi}i\gamma_5\psi\right), \tag{B.7}$$

where the imaginary numbers i are introduced to compensate the negative sign of the four-Fermi interaction. The operator terms of the fermionic action (B.6) are quadratic and can be transformed using the Hubbard-Stratonovich (HS) transformation. The HS transformation can be easily derived from the Fourier transformation of the exponential term of a Gaussian distribution and follows:

$$\exp\left(-\frac{ax^2}{2}\right) = N\int dy\exp\left(-\frac{y^2}{2a} - ixy\right). \tag{B.8}$$

where a is a real constant, N is a normalization constant and y is the new variable introduced via transformation. In QFT the variables are no longer real numbers but fields and operators. Therefore, the analogous HS transformation for fields follows:

$$\exp\left(-\int_x\frac{a\chi^2}{2}\right) = \mathcal{N}\int\mathcal{D}\phi\,\exp\left(\int_x\left\{-\frac{\phi^2}{2a} - i\chi\phi\right\}\right). \tag{B.9}$$

The x and y from the classical expression of the transformation are now replaced by the fields χ and ϕ, and the integral on the right hand side becomes a field measure. This expression is directly relatable to the Euclidean path-integral formulation. Hence, the HS transformation shall be implemented within the path-integral formalism.

The path integral of the purely fermionic system becomes, under the HS transformation:

$$\begin{aligned}\mathcal{N}\int \mathcal{D}\bar{\psi}\mathcal{D}\psi\; e^{-S_F} &= \mathcal{N}\int \mathcal{D}\bar{\psi}\mathcal{D}\psi\; e^{-\int_x -\bar{\psi}\partial\!\!\!/\psi+\frac{1}{2m^2}[O_1O_1+O_5O_5]}\\ &= \mathcal{N}\int \mathcal{D}\bar{\psi}\mathcal{D}\psi\; e^{-\int_x -\bar{\psi}\partial\!\!\!/\psi}\\ &\quad\times \mathcal{N}_1\int \mathcal{D}\phi_1 e^{-\int_x \frac{m^2\phi_1^2}{2}+i\phi_1O_1}\mathcal{N}_5\int \mathcal{D}\phi_5 e^{-\int_x \frac{m^2\phi_5^2}{2}+i\phi_5O_5}\\ &= \mathcal{N}'\int \mathcal{D}\bar{\psi}\mathcal{D}\psi\mathcal{D}\phi_1\mathcal{D}\phi_5\; e^{-\int_x -\bar{\psi}\partial\!\!\!/\psi+\frac{m^2\phi_1^2}{2}+i\phi_1O_1+\frac{m^2\phi_5^2}{2}+i\phi_5O_5},\end{aligned} \tag{B.10}$$

where we identified χ as O_1, O_5 and ϕ as ϕ_1 and ϕ_5 respectively and all the normalization constants are absorbed in $\mathcal{N}'$. Notice that the terms $\phi_i O_i$ are Yukawa interactions. Furthermore, due to the properties associated to their quantum numbers, ϕ_1 and ϕ_5 are identified as the σ and π fields of the system respectively. The new action, namely S_{FB} with now both fermionic and bosonic degrees of freedom, follows the expression:

$$S_{FB}[\psi,\bar{\psi},\sigma,\pi] = \int_x \bar{\psi}i\partial\!\!\!/\psi + \frac{1}{2}m^2\left(\sigma^2+\pi^2\right) + h\bar{\psi}\left(\sigma+i\gamma_5\pi\right)\psi. \tag{B.11}$$

The HS transformation reduced the four-Fermi interaction into a Yukawa interaction with coupling h by introducing these new boson terms. There are however some subtleties that need to be mentioned. First of all, the introduced boson fields are not dynamic, as they have no kinetic term. As a consequence, one should not consider these fields as physical but as tools for computation. Secondly, one can not freely turn the mass of the new bosons to 0 since it affects the four-Fermi and Yukawa couplings. This has an important consequence when dealing with the chiral limit, where the mass of the pions should be 0. Hence, the chiral symmetry should be treated carefully in this kind of system.

Up to this point, the system was only half-bosonised, since fermions are still present in the system. To complete the bosonisation procedure, one needs to integrate out fermionic degrees of freedom [26], yielding a purely bosonic action S_B:

$$S_B[\sigma,\pi] = \int_x m^2\phi^*\phi + \ln\left\{\det\left[i\partial\!\!\!/ + h\left(\sigma+i\gamma_5\pi\right)\right]\right\}. \tag{B.12}$$

In this work, only the steps until half-bosonisation are used, since both microscopic and macroscopic degrees of freedom of QCD are required in the systems. A generalisation to $U(2)\times U(2)$ symmetric systems is easily obtained by including further terms into the four-Fermi interaction and introducing more mesonic fields. The procedure is, however, analogous to the $U(1)\times U(1)$ shown above.

B.4 Numerical Integration

The functional equations treated in this work include integrals. None of them can be solved analytically, and therefore a numerical approach is required. In this work, we used Gauss-Legendre and Gauss-Chebyshev quadratures. The definition and treatment of the quadratures can be found in textbooks, see for example [117], and therefore will be omitted. Nevertheless, we used particular sets of mappings depending on the nature of the integrals that are relevant.

For some angular integrals is enough to use an evenly-spaced grid of points or a proportional mapping to x, for instance, $\theta = \pi(x+1)$, which would correspond to the integral of $\theta \in (0, 2\pi)$. However, as this work deals with functional methods and momentum dependent objects, most of the desired information belongs in the low-energy regime. Therefore is preferably suggested to create a grid of points for momentum integrals such that most of numerical points used belong to the low-energy regime. There are several possible mappings and, the ones used in this work, are classified according to the proper and improper nature of the integral.

- Proper integrals $\int_a^b dq^2$:

$$\text{Logarithmic distribution:} \qquad q^2 = \sqrt{ab}\left(\sqrt{\frac{b}{a}}\right)^x, \qquad \frac{dq^2}{dx} = \frac{q^2}{2}\log\left(\frac{b}{a}\right). \tag{B.13}$$

- Improper integrals $\int_0^\infty dq^2$:

$$\text{Tangent:} \qquad q^2 = \tan\left(\frac{\pi}{4}(x+1)\right), \qquad \frac{dq^2}{dx} = \frac{\pi}{4}\left(\cos\left(\frac{\pi}{4}(x+1)\right)\right)^{-2}. \tag{B.14}$$

$$\text{Pole function:} \qquad q^2 = \left(\frac{1+x}{1-x}\right)^m, \qquad \frac{dq^2}{dx} = \frac{2m}{1-x^2}\, q^2 \quad , \; m = 1, 2, \ldots \tag{B.15}$$

Proper integrals appear in most of the functional equations to be solved, as infrared and ultraviolet cutoffs limit the interval of the integral. For the case of improper integrals, it is suggested to check the range of q^2. In particular for the pole function, a large number of integration points is needed to reach very high momenta for $m = 1$, so the choice of m depend on the number of points use and efficiency of the integration routine. For a complete set of quadrature rules, see also [117–119].

It is convenient to minimise the numerical errors along the integration. Therefore, adaptive routines based on the Gauss-Kronrod quadrature formula were also used.

B.5 Multidimensional Interpolation and extrapolation

The generalisation of the one-dimensional interpolation is required within the functional methods when full momentum dependence of three and higher order n-point functions is introduced into the system and consequently into the equations. For instance, the Yukawa coupling in the quark meson model can be expressed according to :

$$h(p,q) = \tilde{h}(p^2, q^2, z_{pq}). \tag{B.16}$$

Unless the momentum dependent Yukawa coupling is parametrised to be a one-argument dependent function like previously done in chapter 3, the function depends generally on, at least, three arguments. In this work, two different multidimensional methods have been applied: the multicubic spline and the polynomial factorisation.

- *Multicubic spline*: This method is the direct generalisation of the one-dimensional cubic spline. The idea is to create multiple sets of grid points according to the arguments of the function to interpolate, and to perform a large number of one-dimensional cubic splines until the function is interpolated at the desired point. The case of the bicubic spline provides an intuitive insight of how this kind of interpolation works.

  Let $f(x,y)$ be a two-dimensional function to interpolate at the point (x_a, y_a). Choosing N for the number of x_i grid points and M for y_j, one creates a $N \times M$ two-dimensional array according to the values $f(x_i, y_1)$, $f(x_i, y_2)$, ... In matrix terms, this would correspond to the $N \times M$ matrix:

$$\begin{pmatrix} f(x_1,y_1) & f(x_2,y_1) & \dots & f(x_N,y_1) \\ f(x_1,y_2) & f(x_2,y_2) & \dots & f(x_N,y_2) \\ \vdots & \vdots & & \vdots \\ f(x_1,y_M) & f(x_2,y_M) & \dots & f(x_N,y_M) \end{pmatrix}. \tag{B.17}$$

  Once the array is built, the following steps are followed:

  1. Perform one-dimensional cubic spline interpolation for the $f(x_i, y_j)$ values at the point (x_a, y_j), corresponding to the rows of the matrix (B.17)
  2. With the M interpolated values, create a one-dimensional array and perform cubic spline interpolation.
  3. Interpolate finally at the point corresponding to y_a.

  Using this procedure, $M+1$ one-dimensional interpolations are performed, achieving a considerably accurate value for the interpolated value. This method is particularly convenient to use, since the interpolation is smooth in both directions. However, the computational time greatly increases when higher dimensions are involved since more interpolations are required and coefficients need to be calculated at integration time.

- *Polynomial expansion*: This method describes a one-dimensional function as a sum of polynomial. Choosing particularly the Chebyshev's polynomials of first kind $T_n(x)$, any one dimensional function is described as:

$$f(x) = \sum_{i=0}^{n} c_i T_i(x), \tag{B.18}$$

where n is the order of the expansion, c_i are real coefficients and $x \in [-1, 1]$. For multidimensional functions, this translates into promoting the coefficients to argument dependent objects. In two dimensions, this would correspond to the case:

$$f(x, y) = \sum_{i=0}^{n} c_i(x) T_i(y). \tag{B.19}$$

In order to understand how it works, some understanding ot the first kind Chebyshev's polynomials is needed. They are defined under the recurrence relation:

$$T_n(x) = 2xT_{n-1}(x) - T_{n-2}(x), \qquad n = 2, 3, ... \tag{B.20}$$

with $T_0(x) = \frac{1}{\sqrt{2}}$ and $T_1(x) = x$. They satisfy the orthogonality relation:

$$\sum_{k=0}^{m-1} T_i(x_k) T_j(x_k) = a_{ij}. \tag{B.21}$$

where x_k are the nodes of the polynomial $T_m(x)$. They follow the expression $x_k = \cos\left(\pi\left(\frac{k+\frac{1}{2}}{m}\right)\right)$ with $k = 0, ..., m-1$, and the coefficient a_{ij} satisfies:

$$a_{ij} = \begin{cases} 0 & i \neq j \\ \frac{m}{2} & i = j \end{cases} \tag{B.22}$$

for i and j running from 0 to $m-1$. Under this condition, it is easy to check that the coefficient $c_i(x)$ satisfies the relation:

$$c_i(x) = \frac{2}{m_y} \sum_{k=0}^{m_y-1} f(x, y_k) T_i(y_k), \tag{B.23}$$

where the subindex in m_y simply indicates which variable is expanded. The function $f(x, y_k)$ is now a one parameter function and allows also a polynomial decomposition. By repeating the same procedure but now with momentum independent coefficients c_i' instead, the $f(x, y_k)$ function becomes:

$$f(x, y_k) = \sum_{j=0}^{n} c_j' T_j(x). \tag{B.24}$$

With the now variable independent coefficient c'_j:

$$c'_j = \frac{2}{m_x} \sum_{l=0}^{m_x-1} f(x_l, y_k) T_j(x_l). \tag{B.25}$$

By finally combining everything together into one expression, the original function to interpolate $f(x, y)$ becomes:

$$f(x,y) = \left(\frac{2}{m_x}\right)\left(\frac{2}{m_y}\right) \sum_{i=0}^{n}\sum_{j=0}^{n}\sum_{k=0}^{m_y-1}\sum_{l=0}^{m_x-1} f(x_l, y_k) T_j(x_l) T_i(y_k) T_j(x) T_i(y). \tag{B.26}$$

The expression (B.26) looks troublesome, but in terms of computation it offers many advantages. First of all, the terms of the function $f(x_l, y_k)$ do not require any interpolation if the grid points coincide. Furthermore, the expression in this form is evaluated at Chebyshev's polynomials, which are explicitly known. Particularly, the ones evaluated at the nodes are computed before any iteration or any scale-step, and the ones to compute at the point to interpolate are quickly evaluated at running time. In terms of computation, it is much faster than the multidimensional cubic interpolation, but it requires higher order of the expansion to be precise, and it does not provide the same level of smoothness. In the calculations used in this work, an order of the expansion $n = 10$ is enough for a stable behaviour. The generalisation to higher dimension functions is straightforward.

Both methods are used accordingly to the precision required in every system. In functional methods, and in particular in the most complete approximations of the quark-meson model, the use of the multicubic spline provides a better behaviour and fast convergence in terms of $k-$steps, but is noticeably more computational time demanding. On the other hand, the polynomial expansions make global computation faster, but some accuracy is lost.

In this work, both methods were used, trying to achieve a middle point between smooth interpolation with accurate results and efficiency of the code. This was achieved in three point functions $\tilde{h}(p^2, q^2, z_{pq})$ by performing the polynomial expansion to the angular components z_{pq} and bicubic spline for momentum variables, or two polynomial expansions in q^2 and z_{pq} and cubic spline for p^2. Numerical results in both approaches are similar in accuracy, but the two-variable polynomial expansion is clearly faster.

B.5.1 Interpolation in the complex plane

Direct calculations in the complex plane allow to obtain observables without using any extrapolation method. The approach is treated within the FRG since recently and the application in the DSE-BSE is well established. The need for these calculations in the BSE can be easily seen in the Rainbow-Ladder truncation where, in the pion pole $P^2 = -M^2$, the quark propagator momentum is required to be complex in the form:

$$p_{1,2}^2 = \tilde{q}^2 - \frac{M^2}{4} \pm iMz_{pq}\sqrt{\tilde{q}^2}, \tag{B.27}$$

which is the form of a parabola in the complex plane centred at $p_{1,2}^2 = \frac{M^2}{4}$ and $z_{pq} = 0$. The DSE of the quark propagator needs to be solved for complex momentum and therefore complex interpolation is eventually needed [21]. For an easier treatment of this problem, the complex momentum parabola is expressed following the expression:

$$x = ay^2 + c, \tag{B.28}$$

which is conveniently rewritten in terms of a parameter t as:

$$x = t^2 + c, \qquad \frac{dx}{dt} = 2t, \tag{B.29}$$

$$y = \pm\frac{z_{pq}t}{\sqrt{a}}, \qquad \frac{dy}{dt} = \pm\frac{z_{pq}}{\sqrt{a}}. \tag{B.30}$$

The parametrisation and the expression(B.27) are directly related with $a = \frac{1}{m_\pi^2}$, $c = \frac{M^2}{4}$, $t = \tilde{q}^2 \in (0, \Lambda_{UV}^2)$, being x and y the real and imaginary part of $p_{1,2}^2$ respectively. The parabola was parametrised in terms of t so that the integration uses t as integration variable. As a last remark, z_{pq} was left explicit in the parametrisation, but in order to interpolate it can be considered $z_{pq} = 1$ as this value is associated to the largest parabola. Lastly, the integration of t is bounded by an ultraviolet cutoff Λ_{UV}. Consequently, it is interesting to close the parabola at $x = \Lambda_{UV}^2 + C$ so that the properties of complex analysis can be used. In particular, Cauchy's integral formula for a complex number z_0 following:

$$f(z_0) = \frac{1}{2\pi i}\oint_C \frac{f(z)}{z - z_0}dz, \tag{B.31}$$

is a perfect candidate to interpolate in the complex plane. There exist, however, two ways of implementing this formula and both of them require special care. The first method consists in using the Cauchy's integral formula directly from the values of the parabola at $z = \pm 1$, and the second one is the so-called shell-method, which performs the integration using different parabolas.

- *Direct application of Cauchy's integral formula*: This is the most direct of complex interpolation. Since Cauchy's integral formula includes integrals, the initial step is to solve Cauchy's formula splitting the closed-path integral into parts:

$$\oint_C \frac{f(z)}{z - z_0} dz = \sum_{j=1}^{4} \int_{C_j} \frac{f(z)}{z - z_0} dz, \tag{B.32}$$

where the paths C_1, C_2, C_3 and C_4 correspond to the negative and positive sections of the parabola with $z_{pq} = -1$ (C_1) and $z_{pq} = +1$ (C_4), and to the negative and positive parts of the vertical line (C_2 and C_3 respectively), as shown in figure B.1. The next step is giving values to the function $f(z)$ as a grid. The grid needs to correspond to the points right on top of the path C_j. Given a function $f(z)$, a grid of N points $f(z_1), ..., f(z_N)$ is built corresponding to the parabola points $z_1, ...z_N$. Once this is applied, the next step is to rewrite $z = x + iy$ and $dz = dx + idy$ in terms of the integration variable t so that quadrature rules are possible.

	x	dx	y	dy	$z = x + iy$	$dz = dx + idy$
C_1	$t^2 + c$	$2t$	$-\frac{t}{\sqrt{a}}$	$\frac{1}{\sqrt{a}}$	$t^2 + c - i\frac{t}{\sqrt{a}}$	$2t - \frac{i}{\sqrt{a}}$
C_2	Λ_{UV}^2	0	$-t$	-1	$\Lambda_{UV}^2 - it$	$-i$
C_3	Λ_{UV}^2	0	t	1	$\Lambda_{UV}^2 + it$	i
C_4	$t^2 + c$	$2t$	$\frac{t}{\sqrt{a}}$	$\frac{1}{\sqrt{a}}$	$t^2 + c + i\frac{t}{\sqrt{a}}$	$2t + \frac{i}{\sqrt{a}}$

Table B.1: Table of parameters involved in the integrals in function of the integration variable t.

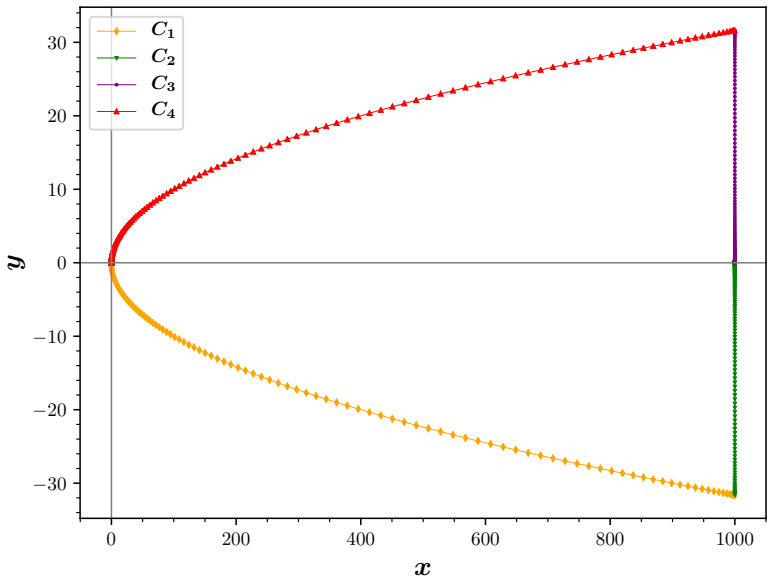

Figure B.1: Close path of the parametrised parabola in terms of x and y. Path C_1 starts at the point $x = \left(-\frac{m_\pi^2}{4}, 0\right)$ and runs counter-clockwise through C_2, C_3 and C_4 until the initial point.

Under the parametrisations tabulated in table B.1, every line integral is solved using:

$$\begin{aligned} f(z_0) &= \frac{1}{2\pi i}\oint_C \frac{f(z)}{z-z_0}dz = \frac{1}{2\pi i}\sum_{j=1}^{4}\int_{C_j}\frac{f(z(t))}{z(t)-z_0}dz(t) \\ &= \frac{1}{2\pi i}\sum_{j=1}^{4}\int_0^{\Lambda_{UV}^2}\left(\frac{f(z(t))}{z(t)-z_0}\frac{dz(t)}{dt}\right)_{C_j}dt = \sum_{j=1}^{4}\int_0^{\Lambda_{UV}^2}\tilde{f}_j(t)dt, \end{aligned} \tag{B.33}$$

where $\tilde{f}_j(t) = \frac{1}{2\pi i}\left(\frac{f(z(t))}{z(t)-z_0}\frac{dz(t)}{dt}\right)_{C_j}$. Every remaining integral is now solved using a standard Gaussian quadrature routine. There are a few remarks to be mentioned in this routine:

- The grid points are necessarily sorted according to the direction of the closed path.
- It is recommended to have more grid points in the lower section of x for better behaving interpolation.
- The points outside the contour cannot be calculated using this method. The values of the function at these points are set to zero by default.
- The interpolation of the points close to the parabola may lead to singularities given by $z - z_0$ in the denominator, therefore the interpolating points should not correspond to these values to avoid numerical misbehaviour.
- To improve behaviour given by these troublesome points, the following identity given by complex analysis can be used:

$$2\pi i = \oint_C \frac{1}{z-z_0}dz. \tag{B.34}$$

  By including this integral instead of the $2\pi i$, the interpolated function becomes a ratio of quadratures. Since they include the same denominator, the singularity terms cancel each other solving, in principle, numerical issues.

Once these steps are performed, the interpolation is generalised for one dimensional complex functions. This method is also useful to check the values of the functions when the variable is real. In the DSE calculations, the Euclidean real momentum differed from the interpolated values by 1%. The method is very simple to implement and is very fast, but the precision of the calculations is very strongly dependent on the number of points and, even in the best of the cases, the interpolated results of the real axis still differ. For this reason, more precise methods like the shell-method were created.

- *Shell method*: This method is based on the idea of not building the parabola corresponding to $z_{pq} = \pm 1$, but extrapolating the real axis result to small parabolas until the parabola used in the previous method is reached [120]. This requires a grid of N quadrature points for the M parabolas created.

  Since the main difference between the real axis and complex plane approaches is the presence of the mass of the pion, one can define:

$$\tilde{M}^2 = M^2 z_m, \tag{B.35}$$

  where $z_m \in [0, 1]$, in order to distinguish the parabolas. It is easy to see that the momentum of the quark propagator is purely real when $z_m = 0$, and it becomes a parabola when $z_m \neq 0$. Under this definition, z_m is slowly increased to obtain different parabolas with the same number points as shown in Figure B.2.

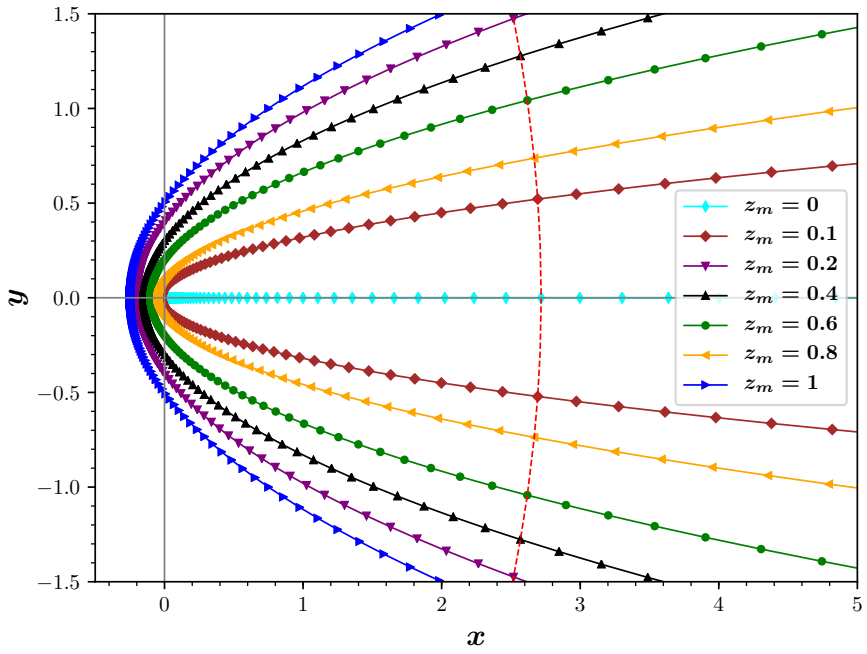

Figure B.2: Pictorial representation of the shell method interpolation, showing several parabolas in terms of z_m. The red, dashed line indicates the same point when parametrised by t in the different parabolas.

For every point $z(t) = (x(t), y(t))$ defined in the real axis, an extrapolation using Cauchy-Riemann equations is performed to obtain the value of the function at the same t, but now on the parabola. From the function $f(z) = f(x, y) = u(x, y) + iv(x, y)$:

$$u_x\left(x(t_0), y(t_0)\right) = \; v_y\left(x(t_0), y(t_0)\right), \tag{B.36}$$
$$u_y\left(x(t_0), y(t_0)\right) = -\, v_x\left(x(t_0), y(t_0)\right). \tag{B.37}$$

where $u_x = \frac{\partial u}{\partial x}$ and analogously for the rest of derivatives. This requires also:

$$f'(z(t_0)) = v_y\left(x(t_0), y(t_0)\right) - iu_y\left(x(t_0), y(t_0)\right). \tag{B.38}$$

The numerical values of the derivatives are obtained by using the usual definition of partial differentiation. The values of the function in the next shell are obtained by using an ordinary differential equation solver. This procedure is iterated until the largest parabola is reached, keeping the values of all the points of every parabola as a two-dimensional grid.

Once the iterations are finished, the values of a function at any point within the largest parabola can be obtained by applying a two-dimensional interpolation routine in the (t^2, z_m) space. This procedure is slightly slower than the first approach mentioned, which uses Cauchy's integral formula, but the precision of the interpolation becomes considerably better.

Appendix C

Explicit Functional Equations and Expressions

This appendix shows the explicit expressions of the flow equations and regulators within the FRG and explicit vertex functions within the DSE formalism. In addition, the derivations of several quantities relevant in functional calculations depending on the choice of regulator are shown.

C.1 Matrix Derivation of Flow Equations

Wetterich's flow equation in its most compact form allows a derivation of the beta functions of the parameters. The propagator and regulator matrices defined in Appendix A and the matrix of the n-point function with $n \geq 2$, which are all obtained from the $\Gamma_k^{(2)}$ matrix which reads in our convention:

$$\Gamma_k^{(2)} = \begin{pmatrix} \Gamma^{(2)}_{k,\phi\phi} & \Gamma^{(2)}_{k,\phi\psi} & \Gamma^{(2)}_{k,\phi\bar{\psi}} \\ \Gamma^{(2)}_{k,\psi\phi} & \Gamma^{(2)}_{k,\psi\psi} & \Gamma^{(2)}_{k,\psi\bar{\psi}} \\ \Gamma^{(2)}_{k,\bar{\psi}\phi} & \Gamma^{(2)}_{k,\bar{\psi}\psi} & \Gamma^{(2)}_{k,\bar{\psi}\bar{\psi}} \end{pmatrix}. \tag{C.1}$$

Here the fermion two-point functions have been taken such that $\Gamma^{(2)}_{k,\psi\bar{\psi}} G_k^{\psi} = 1$ and, by virtue of Fermi statistics, $\Gamma^{(2)}_{k,\psi\bar{\psi}} = -\Gamma^{(2)}_{k,\bar{\psi}\psi}$. The flows of the n-point functions are obtained by applying n-field derivatives at both sides of Wetterich's flow equation and by using the property described in (A.14). In order to provide an example, we compute the flow of the quark 2-point function of a general system step by step. From Wetterich's flow equation, the flow of the 1-point function satisfies:

$$\delta_{\bar{\psi}} \dot{\Gamma}_k = \frac{1}{2} \left(\delta_{\bar{\psi}} G_k \right) \dot{R}_k = -\frac{1}{2} G_k \left(\delta_{\bar{\psi}} \Gamma_k^{(2)} \right) G_k \dot{R}_k. \tag{C.2}$$

On the right hand side of the expression the trace over every possible index and matrix elements is implied in order to facilitate the reading of the expression. Furthermore, it is convenient to use $\left(\delta_{\bar{\psi}}\Gamma_k^{(2)}\right) \equiv \Gamma_{k,\bar{\psi}}^{(3)}$ to indicate 3-point functions and, in an analogous way, higher order n-point functions. Using the same properties on the matrix terms derived, one obtains the flow of the quark two-point function following the expression:

$$\begin{aligned}\delta_\psi\delta_{\bar{\psi}}\dot{\Gamma}_k = &+\frac{1}{2}\,G_k\,\Gamma_{k,\psi}^{(3)}\,G_k\,\Gamma_{k,\bar{\psi}}^{(3)}\,G_k\,\dot{R}_k - \frac{1}{2}\,G_k\,\Gamma_{k,\bar{\psi}}^{(3)}\,G_k\,\Gamma_{k,\psi}^{(3)}\,G_k\,\dot{R}_k \\ &- \frac{1}{2}\,G_k\,\Gamma_{k,\psi\bar{\psi}}^{(4)}\,G_k\,\dot{R}_k.\end{aligned} \tag{C.3}$$

Here every term on the right hand side is also traced over all indices. First of all, the relative minus sign between the first two terms appears during the application of the Grassmann-derivative chain rule due to the anti-commuting behaviour of Fermi derivatives, i.e. $\delta_\psi\delta_{\bar{\psi}} = -\delta_{\bar{\psi}}\delta_\psi$. Secondly, even if in general systems some of the two-point function terms are zero, for instance $\Gamma_{k,\psi\psi}^{(2)}$, the terms in expression (C.1) must be kept non-zero until the very end of the derivation as they are used to obtain higher order n-point functions. Otherwise, some contributions may be omitted and the derivation of the flow equation is incorrect. Furthermore, the terms $G_k\dot{R}_kG_k$ always appear together and, from the way the matrices are defined, they always keep the same bosonic or fermionic nature without any field mixing and, consequently, this term is usually interpreted as a propagator that includes the regulator term $\dot{R}_k$. Thus we define $\overline{G}_k = G_k\dot{R}_kG_k$. Under this interpretation, it is clear that the first two terms in (C.3) correspond to one-loop terms composed of a propagator G_k and $\overline{G}_k$ between two 3-point functions, and the last term corresponds to a tadpole diagram consisting of a 4-point function and $\overline{G}_k$.

Once the expression of the flow is obtained, the terms can be replaced by the explicit matrix terms, Nevertheless, the left hand side of the expression, in our example $\delta_\psi\delta_{\bar{\psi}}\dot{\Gamma}_k$, is not equivalent to the flow of the two-point function. In general, this expression depends on the tensor structures of the systems. For instance, the two-field derivative on the effective action of a fermionic system may lead to, at least, a flow with two terms:

$$\delta_{\psi_j}\delta_{\bar{\psi}_i}\dot{\Gamma}_k = \left(i\not{p}\dot{Z}_{k,\psi} + \dot{m}_k\right)\delta^{ij}. \tag{C.4}$$

In order to obtain the flow of every tensor structure one must project both sides of the flow equation and normalise accordingly, so that the left hand side of the flow equation leaves only $\dot{Z}_{k,\psi}$ or $\dot{m}_k$. Only then, the right hand side of the flow equation can be properly traced and yield an equation solvable, in general, numerically.

C.2 Regulators

The regulators play a capital role within the FRG not only formally, but also computationally. In this section different choices of regulators are discussed, both in terms of convenience and applicability. The regulators defined in the FRG that lead to Wetterich's flow equation are the ones quadratic in the fields. Due to the different dimensions of the bosonic and fermionic fields, boson regulators need to be treated differently than fermionic ones. In four dimensions, the scalar and pseudoscalar fields involved in the theory have dimension of energy. Consequently, the regulator term R_k^B in $\int_p \Phi R_k^B \Phi$ must be quadratic with the energy. Hence, it is convenient to rewrite the bosonic regulator term as:

$$R_k^B(p^2) = p^2 r_k^B(p^2), \tag{C.5}$$

where r_k^B is the bosonic dimensionless shape function that dictates the behaviour of the regulator. Similarly performed for fermions, the fermionic regulator term must have units of mass. There exist several ways of defining the fermion regulator term covariantly. For instance:

$$R_k^F(p) = i\not{p}\, r_k^F(p^2) \qquad \text{or} \tag{C.6}$$

$$R_k^F(p) = \sqrt{p^2}\, r_k^F(p^2). \tag{C.7}$$

Both of the alternatives correspond to the different tensor structures of the quark two-point function. Both of the options are applicable, only the flow equations derived become different. In this work only regulators of the form (C.6) have been used. Even though it is convenient to work with the same bosonic and fermionic regulator shape functions, they do not necessarily need to be the same. The terms proportional to p^2 in the denominators of the regularised boson propagators follow $(1+r_k^B)$, whereas it is $(1+r_k^F)^2$ for fermions. Up to their tensor structures, both propagators behave equivalently under the choice:

$$r_k^F(p^2) = -1 + \sqrt{1 + r_k^B(p^2)} \tag{C.8}$$

This choice was used along every calculation shown in this work.

Before analysing the different kinds of regulators studied along this work or, equivalently, the different shape functions used, we need to consider also the possibility of having dressed regulators. This would lead to:

$$R_k^B(p^2) = Z_{k,\phi}\, p^2 r_k^B(p^2), \qquad R_k^F(p) = Z_{k,\psi}\, i\not{p}\, r_k^F(p^2). \tag{C.9}$$

This choice may simplify the expressions of some flow and may be convenient for numerical stabilisation. Nevertheless, the flow of the regulator gets additional terms that need to be treated carefully.

C.2.1 Shape functions

As long as the regulator term satisfies the properties described in (2.56), any shape function can be used. Depending on the choice, flow equations can be easily treated analytically or momentum dependence can be better included. In this work, two kinds of regulator shape functions were used: the optimised regulator and the exponential regulator.

- *Optimised regulator*: This regulator is also known as Litim's regulator [121]. In a very simple expression, it cancels identically every loop-momentum contribution larger than the scale k. Furthermore, it converts the momentum-dependent inverse propagators into momentum-independent quantities. Its explicit form for bosonic regulators follows:

$$r_k^B(p^2) = \left(\frac{k^2}{p^2} - 1\right) \theta(k^2 - p^2). \tag{C.10}$$

  Due to the slight difference between the definitions of bosonic and fermionic regulators, the optimised regulator is defined differently in the case of fermions. Therefore, it follows:

$$r_k^F(p^2) = \left(\sqrt{\frac{k^2}{p^2}} - 1\right) \theta(k^2 - p^2). \tag{C.11}$$

  Under this choice, the approximations that include terms that are proportional to $p^2(1 + r_k^B)$ or to $p^2(1 + r_k^F)^2$ become k^2, thus greatly simplifying the momentum dependence of the integrand. Particularly, approximations with propagators with no further momentum dependence allow us to remove these terms from the momentum integral, simplifying the treatment of the integrand. Furthermore, the theta function defines the upper integration limit in k^2 and the momentum integral becomes finite. Several examples of calculation of flows with this regulator can be found in [121]. In this work, the optimised regulator was used to qualitatively analyse the general behaviour of the systems.

- *Exponential regulator*: This regulator does not behave so sharply as the optimised regulator and higher loop-momentum contributions become simply smaller. This regulator is suitable for numerical simulations and for the inclusion of momentum dependence into the system. Its general form follows the expression:

$$r_k(x) = \frac{x^{m-1}}{e^{x^m} - 1}, \tag{C.12}$$

  with $x = \frac{p^2}{k^2}$ and m being an integer. The numerical computations performed show that in the analysed systems the exponential regulators with $m = 2$ reach convergence faster and calculations behave smoothly. Furthermore, it is necessary to include external momenta P in the one-loop diagram contributions. In practice, quantities may involve momentum contribution up to $(2P)^2$, and this regulator can properly include it by limiting the loop-momentum integral within the interval $p^2 \in (0, (2.5k)^2)$. Hence, this exponential is the one used in every calculation in this work.

C.2.2 Dressed regulators and anomalous dimensions

Even though calculations shall lead to the same results, practical computations with dressed regulators become slightly more complex due to the additional scale-dependent term. For simplicity, we show it explicitly for bosonic regulators defined in this section as:

$$R_k(p^2) = p^2\, Z_k\, r_k(p^2). \tag{C.13}$$

In Wetterich's flow equation, the term $\partial_t R_k$ acts differently due to the chain rule. It can be easily shown that:

$$\partial_t R_k(p^2) = p^2\, Z_k\, \partial_t r_k(p^2) - p^2\, Z_k\, r_k(p^2)\eta, \tag{C.14}$$

where η is the anomalous dimension defined as:

$$\eta = -\frac{\partial_t Z_k}{Z_k}. \tag{C.15}$$

Similarly, the same behaviour for $\partial_t R_k$ follows for the fermion regulators, with the only change of $i\not{p}$ instead of p^2 in (C.14). In order to solve the system self-consistently, the anomalous dimension or, equivalently, the flow of Z_k needs to be found. In the following lines we show how this is performed within the Quark-Meson model calculations, which include pions, sigma meson and quarks as degrees of freedom.

In general, the flow of Z_k, obtained from the parametrisation of the bosonic and fermionic 2-point function, can be split in terms proportional to $\partial_t Z_{k,\pi}$, $\partial_t Z_{k,\sigma}$, $\partial_t Z_{k,\psi}$ and terms proportional to the flow of the shape functions $\partial_t r_k^i$, which we will call $\dot{R}_{k,0}$ as would match the expression of the undressed regulator. Since there is no mixing between the derivative terms, the system can be written in a matrix notation:

$$\begin{pmatrix} \dot{Z}_{k,\pi} \\ \dot{Z}_{k,\sigma} \\ \dot{Z}_{k,\psi} \end{pmatrix} = \begin{pmatrix} \cdots & \cdots & \cdots \\ \cdots & \cdots & \cdots \\ \cdots & \cdots & \cdots \end{pmatrix}_{3\times 3} \begin{pmatrix} \dot{Z}_{k,\pi} \\ \dot{Z}_{k,\sigma} \\ \dot{Z}_{k,\psi} \end{pmatrix} + \begin{pmatrix} \dot{R}^{\pi}_{k,0} \\ \dot{R}^{\sigma}_{k,0} \\ \dot{R}^{\psi}_{k,0} \end{pmatrix}. \tag{C.16}$$

The system becomes a matrix-vector system of the form $\vec{a} = M\vec{a} + \vec{b}$, where M is a 3×3 matrix the elements of which correspond to the momentum integral of the flow. The system is trivially solved with $\vec{a} = (\mathbb{I} - M)^{-1}\vec{b}$.

Since every flow equation depends on the anomalous dimension or $\dot{Z}_{k,i}$, this operation must be applied in every RG-step before the calculation of the flow of the other quantities is performed. This increases the computational time but, in the case where the dressed regulator is proportional to a momentum dependent Z_k, the additional evaluation time is negligible.

In some other calculations not displayed in this work, the dressed, momentum dependent regulators were used in the form:

$$R_k(p^2) = p^2\, Z_k(p^2)\, r_k(p^2) \tag{C.17}$$

This choice is convenient since, in momentum dependent systems, it significantly reduces the final expression of the flow equation. In this case, $\partial_t R_k$ becomes:

$$\partial_t R_k(p^2) = p^2\, Z_k(p^2)\, \partial_t r_k(p^2) + p^2\, r_k(p^2) \partial_t Z_k(p^2), \tag{C.18}$$

Here we do not include the anomalous dimension η since it becomes momentum dependent and its meaning would become ambiguous. Under this choice, we can write the general flow in a matrix notation:

$$\begin{pmatrix} \dot{Z}_{k,\pi}(p_1) \\ \vdots \\ Z_{k,\pi}(p_N) \\ \dot{Z}_{k,\sigma}(p_1) \\ \vdots \\ Z_{k,\sigma}(p_N) \\ \dot{Z}_{k,\psi}(p_1) \\ \vdots \\ Z_{k,\psi}(p_N) \end{pmatrix} = \begin{pmatrix} \dots & \dots & \dots & \dots & \dots \\ & & \vdots & & \\ \dots & \dots & \dots & \dots & \dots \\ \dots & \dots & \dots & \dots & \dots \\ & & \vdots & & \\ \dots & \dots & \dots & \dots & \dots \\ \dots & \dots & \dots & \dots & \dots \\ & & \vdots & & \\ \dots & \dots & \dots & \dots & \dots \end{pmatrix}_{3N\times 3N} \begin{pmatrix} \dot{Z}_{k,\pi}(p_1) \\ \vdots \\ Z_{k,\pi}(p_N) \\ \dot{Z}_{k,\sigma}(p_1) \\ \vdots \\ Z_{k,\sigma}(p_N) \\ \dot{Z}_{k,\psi}(p_1) \\ \vdots \\ Z_{k,\psi}(p_N) \end{pmatrix} + \begin{pmatrix} \dot{R}^{\pi}_{k,0}(p_1) \\ \vdots \\ \dot{R}^{\pi}_{k,0}(p_N) \\ \dot{R}^{\sigma}_{k,0}(p_1) \\ \vdots \\ \dot{R}^{\sigma}_{k,0}(p_N) \\ \dot{R}^{\psi}_{k,0}(p_1) \\ \vdots \\ \dot{R}^{\psi}_{k,0}(p_N) \end{pmatrix} \tag{C.19}$$

Here N is the choice of quadrature points of the momentum integral which, for simplicity, is taken to be the same for the three types of flows. As equation (C.19) suggests, obtaining the flow of $Z_{k,i}(p^2)$ is much more laborious. In order to do it, we derive the expression of the flow of every momentum dependent $Z_{k,i}$ and split it in terms of every $\dot{Z}_{k,i}(p_j)$ and $R_{k,0}(p_j)$. Naturally, this has two important consequences. The splitting can only be done if the grid of the external momentum quantities is exactly the same as the one inside the momentum integral. This can be easily achieved by choosing a particular set of quadrature points for the momentum integral and using it also for the external momenta.

C.3 Functional Renormalisation Group Flow equations

The conventions in the FRG differ from the DSE formalism mainly in the definition of renormalised and unrenormalised parameters, in addition to the presence of scale dependent objects and regulators. The general conventions used along all the FRG calculations follow:

- Scale-dependent Quark correlator and propagator in Landau gauge:

$$\Gamma^{(2)}_{\boldsymbol{k},\boldsymbol{\psi}\bar{\boldsymbol{\psi}}}\left(p^2\right) = i\not{p} Z_{k,\psi}\left(p^2\right) + M_k\left(p^2\right), \tag{C.20}$$

$$\left(\Gamma^{(2)}_{k,\boldsymbol{\psi}\bar{\boldsymbol{\psi}}}\left(p^2\right)\right)^{-1} = \left(-i\not{p} Z_{k,\psi}\left(p^2\right) + M_k\left(p^2\right)\right) G^{\psi}_k\left(p^2\right), \tag{C.21}$$

  where $G^{\psi}_k\left(p^2\right) = \left(Z^2_{k,\psi}\left(p^2\right)p^2 + M^2_k\left(p^2\right)\right)^{-1}$.

- Meson correlators:

$$\begin{aligned}\Gamma^{(2)}_{\boldsymbol{k},\boldsymbol{\sigma}\bar{\boldsymbol{\sigma}}}\left(p^2\right) &= \left(G^{\sigma}_k(p^2)\right)^{-1} = Z_{k,\sigma}\left(p^2\right)p^2 + m^2_{k,\sigma},\\ \Gamma^{(2)}_{\boldsymbol{k},\boldsymbol{\pi}\bar{\boldsymbol{\pi}}}\left(p^2\right) &= \left(G^{\pi}_k(p^2)\right)^{-1} = Z_{k,\pi}\left(p^2\right)p^2 + m^2_{k,\pi}.\end{aligned} \tag{C.22}$$

- Yukawa running coupling as 3-point function:

$$h_k(q,p) = \left(\frac{\delta^3\Gamma_k}{\delta\sigma\left(-q\right)\delta\psi\left(-p+\frac{q}{2}\right)\delta\bar{\psi}\left(p+\frac{q}{2}\right)}\right)^{\boldsymbol{abc}} P^{\boldsymbol{cba}}_{\pi\psi\bar{\psi}} \tag{C.23}$$

- 4-Point functions:

$$\lambda_k(r,q,p) = \left(\frac{\delta^4\Gamma_k}{\delta\psi\left(-p-q-r\right)\delta\bar{\psi}\left(r\right)\delta\psi\left(q\right)\delta\bar{\psi}\left(p\right)}\right)^{\boldsymbol{abcd}} P^{\boldsymbol{dcba}}_{4\psi} \tag{C.24}$$

The functions $P^{\boldsymbol{cba}}_{\pi\psi\bar{\psi}}$ and $P^{\boldsymbol{dcba}}_{4\psi}$ are used to project the expressions left after performing the field derivatives by closing all the open indices and tracing. There are P functions for every flow and heir parametrisation will be explicitly described in every case.

C.3.1 The NJL model

The effective action associated to the NJL model follows the expression shown in (4.20) . In our best truncation, the scale-dependent quantities are $Z_{k,\psi}$ and m_k related to the quark propagator and running four-Fermi coupling λ_k. The diagrammatic form of the flow equations is shown in Figure 4.4.

Before writing down the explicit behaviour of the quantities in terms of the scale, we need to parametrise the momentum dependent four-point function. In our FRG calculations, we use constant coupling as $\lambda_k(p,q,r) = \lambda$ and momentum-averaged vertex as:

$$\lambda_k(p_1,p_2,p_3,p_4) = \lambda_k\left(\left(\frac{p_1-p_2+p_3-p_4}{4}\right)^2\right). \tag{C.25}$$

The flow equations are derived from the n-Fermi derivative of the effective action and are projected using the parameters:

$$P_Z^{\boldsymbol{ba}} = \frac{-i\not{p}^{\boldsymbol{ba}}}{4N_cN_fp^2}, \qquad P_m^{\boldsymbol{ba}} = \frac{\delta^{\boldsymbol{ba}}}{4N_cN_f}, \qquad P_\lambda^{\boldsymbol{dcba}} = \frac{\delta^{\boldsymbol{dc}}\delta^{\boldsymbol{ba}}}{(4N_cN_f-1)4N_c}, \tag{C.26}$$

where the deltas indicate colour, flavour and Dirac indices. The parameter $\not{p}^{\boldsymbol{ba}}$ is short for $\not{p}^{\beta\alpha}\delta_c^{BA}\delta_f^{ba}$. The flow equations read:

$$\partial_k Z_{k,\psi}(p^2) = \frac{2}{2N_fp^2}\int_q (q\cdot p)\left(G_k^\psi(q^2)\right)^2\left(q^2(Z_{k,\psi}(q^2)+r_k^F(q))^2 - m_k^2(p^2)\right) \partial_k r_k^F(q^2)\lambda_k\left(\frac{p+q}{2}\right), \tag{C.27}$$

$$\partial_k m_k(p^2) = \frac{4}{2N_f}\left(4N_cN_f-1\right)\int_q \left(G_k^\psi(q^2)\right)^2 m_k(p^2)\left(q^2(Z_{k,\psi}(q^2)+r_k^F(q))\right) \partial_k r_k^F(q^2)\lambda_k\left(\frac{p+q}{2}\right). \tag{C.28}$$

We omit the explicit form of the flow of the four-Fermi coupling due to its length and non-trivial momentum dependence.

C.3.2 The Gross-Neveu model

The Gross-Neveu model used in this work follows the same structure as in the NJL but in $d = 2$ dimensions. Consequently, since, diagrammatically, the flow equations follow Figure 4.4, the main differences between the equations in both models are expected to be numerical factors.

In the performed calculations, a constant four-point function or a particular ansatz was used, therefore no flow equation for λ_k was needed. Nevertheless, its derivation is straightforward and can be easily obtained using DoFun and FormTracer.

For simplicity, we define the 2-dimensional momentum integral:

$$\int_{\tilde{q}} \equiv \int \frac{d^2q}{(2\pi)^2}. \tag{C.29}$$

Using the same definition for correlators and projecting using:

$$P_Z^{\boldsymbol{ba}} = \frac{-i\not{p}^{\boldsymbol{ba}}}{2N_cN_fp^2}, \qquad P_m^{\boldsymbol{ba}} = \frac{\delta^{\boldsymbol{ba}}}{2N_cN_f}, \qquad P_\lambda^{\boldsymbol{dcba}} = \frac{\delta^{\boldsymbol{dc}}\delta^{\boldsymbol{ba}}}{(2N_cN_f-1)2N_c}, \tag{C.30}$$

the flow equations for the scale-dependent quantities are derived:

$$\begin{aligned}\partial_k Z_{k,\psi}(p^2) = \frac{2}{2N_fp^2}\int_{\tilde{q}}(q\cdot p)\,\left(G_k^\psi(q^2)\right)^2\left(q^2(Z_{k,\psi}(q^2)+r_k^F(q))^2 - m_k^2(p^2)\right) \\ \partial_k r_k^F(q^2)\lambda_k\left(\frac{p+q}{2}\right),\end{aligned} \tag{C.31}$$

$$\begin{aligned}\partial_k m_k(p^2) = \frac{4}{2N_f}\left(2N_cN_f-1\right)\int_{\tilde{q}}\left(G_k^\psi(q^2)\right)^2 m_k(p^2)\left(q^2(Z_{k,\psi}(q^2)+r_k^F(q))\right) \\ \partial_k r_k^F(q^2)\lambda_k\left(\frac{p+q}{2}\right).\end{aligned} \tag{C.32}$$

Once again, the flow of the four-point function is omitted due its length and complexity. Notice that the differences between these flow equations and the ones obtained in the NJL model differ only in constant factors.

C.3.3 The Quark-Meson model

The effective action used in the Quark-Meson model follows expression (3.9) and includes the four-point function since its flow is necessary in order to apply the dynamical hadronisation technique appropriately. In this work, the flow equations are solved for unrenormalised parameters, see Chapter 3.

The expressions in this section are derived in a way that they fit in all of the employed approximations used, but the parameters involved require to be adjusted to the system (e.g. momentum dependent Yukawa $h_k(p, q)$ is interpreted as h in the LPA).

The coupled set of flow equations for the unrenormalised parameters in the Quark-Meson model is displayed in Figure C.1.

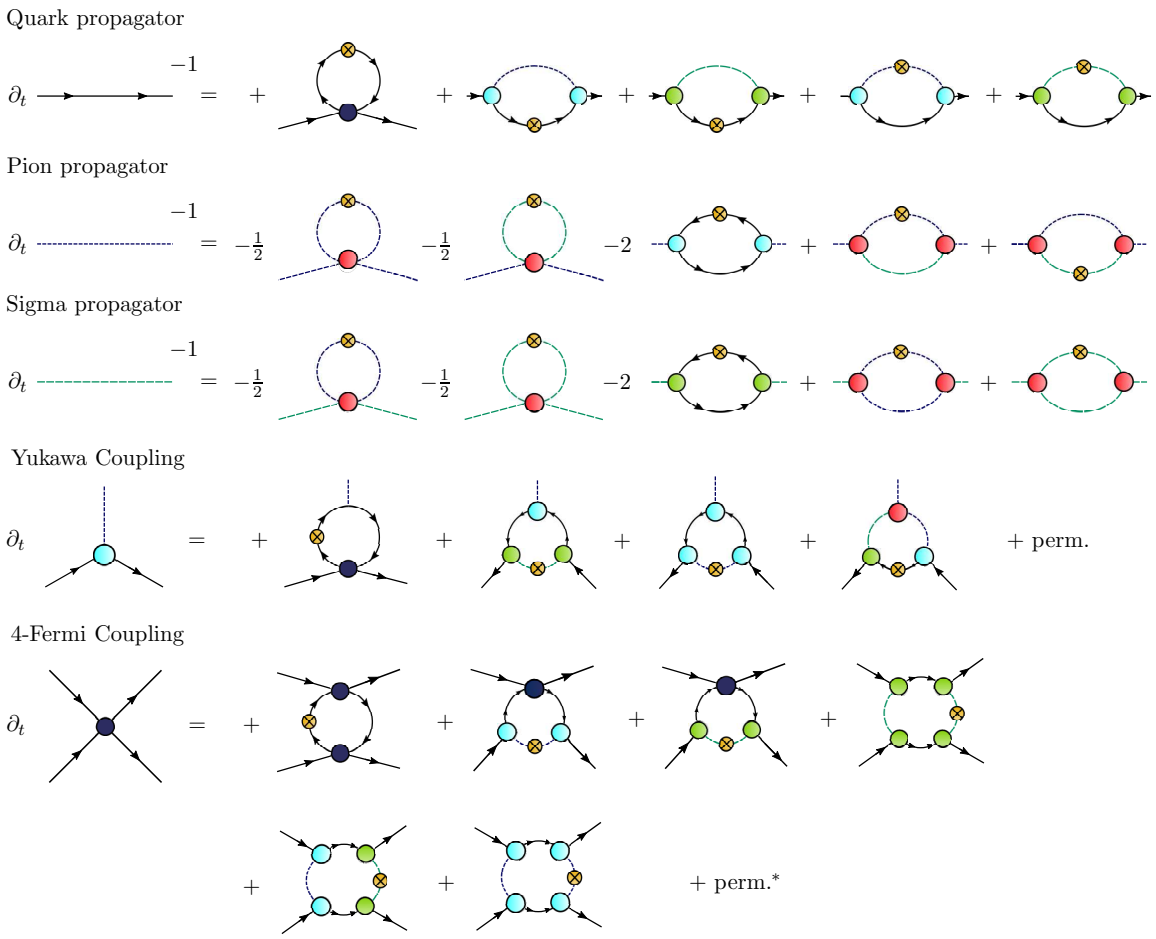

Figure C.1: Diagrammatic flow equations for the Quark-Meson model. Red dressings relate the multi-meson couplings obtained from the local potential. The perm* term indicates not only permutation of the previous diagrams, but also modification of the sign depending on the fermion channels of the 4-Fermi interaction.

The scale-dependent parameters involved in the system include not only the ones shown in Figure C.1, but also the ones obtained directly from the local potential. Since higher-order functions are included in every higher approximation, the most convenient starting point is the derivation of the potential flows.

In the LPA, the flow of the potential $V[\rho]$ with $\rho = \frac{1}{2}(\sigma^2 + \vec{\pi}^2)$ is obtained from Wetterich's flow equation and satisfies:

$$\begin{aligned}\partial_t V_k[\rho] &= \frac{1}{2}\mathrm{Tr}\left[G_k \dot{R}_k\right] \\ &= \int_q q^2 \left(\frac{1}{2}\left(N_f^2 - 1\right) G_k^\pi \, \dot{r}_k^B + \frac{1}{2} G_k^\sigma \, \dot{r}_k^B - 4 N_c N_f \left(Z_{k,\psi} + r_k^F\right) G_k^\psi \, \dot{r}_k^F\right), \end{aligned} \tag{C.33}$$

where the global q^2 appears from the regulators expressed in their shape-function form and every G_k^i, $Z_{k,\psi}$ and r_k^i depend on q^2, omitted for simplicity. The term $(Z_{k,\psi} + r_k^F)$ appears due to our choice of undressed regulator. Once the left hand side of the expression is expanded according to (3.14), the expression yields flow equations for every term of the potential $V_k^{(n)}$.

Since the mass terms of every propagator are defined according to some relation with ρ, the procedure to obtain the flow equations is the following: n-field derivatives in function of ρ are applied on both sides of the equations, and then everything is evaluated at the expansion point $\rho = \rho_{exp}$. In other words:

$$\partial_t V_k^{(n)} = \delta_\rho^n \partial_t V_k[\rho]|_{\rho_{exp}}, \tag{C.34}$$

leading to a more complicated equation due to the relation:

$$\delta_\rho G_k^i = -G_k^i \, \delta_\rho m_{k,i}^2[\rho] \, G_k^i, \tag{C.35}$$

with the mass relations:

$$m_{k,\pi}^2[\rho] = V'[\rho], \tag{C.36}$$

$$m_{k,\sigma}^2[\rho] = V'[\rho] + 2\rho V''[\rho], \tag{C.37}$$

$$m_{k,\psi}^2[\rho] = \frac{h_k^2}{N_f}\rho. \tag{C.38}$$

In higher approximations, the Yukawa coupling needs to be accordingly defined with its momentum dependence, but the derivation is equivalent.

Taking into consideration that now every quantity is evaluated at $\rho = \rho_{exp}$, the flow equations of the potential terms are the following:

$$\partial_t V_k^{(0)} = \int_q q^2 \left(\frac{1}{2} \left(N_f^2 - 1\right) G_k^\pi \, \dot{r}_k^B + \frac{1}{2} G_k^\sigma \, \dot{r}_k^B - 4 N_c N_f \left(Z_{k,\psi} + r_k^F\right) G_k^\psi \, \dot{r}_k^F \right), \tag{C.39}$$

$$\begin{aligned} \partial_t V_k^{(1)} = \int_q q^2 \Bigg(& -\frac{1}{2}(N_f^2 - 1) V_k^{(2)} \left(G_k^\pi\right)^2 \dot{r}_k^B - \frac{1}{2} \left(3 V_k^{(2)} + 2\rho_{exp} V_k^{(3)}\right) \left(G_k^\sigma\right)^2 \dot{r}_k^B \\ & + 4 N_c N_f \left(\frac{h_k^2}{N_f}\right) \left(Z_{k,\psi} + r_k^F\right) \left(G_k^\psi\right)^2 \dot{r}_k^F \Bigg), \end{aligned} \tag{C.40}$$

$$\begin{aligned} \partial_t V_k^{(2)} = \int_q q^2 \Bigg(& \frac{1}{2}(N_f^2 - 1) \left(G_k^\pi\right)^2 \dot{r}_k^B \left(2 G_k^\pi - V_k^{(3)}\right) \\ & + \frac{1}{2} \left(G_k^\sigma\right)^2 \dot{r}_k^B \left(-5 V_k^{(3)} + 2 G_k^\sigma \left(3 V_k^{(2)} + 2\rho_{exp} V_k^{(3)}\right)^2 - 2\rho_{exp} V_k^{(4)}\right) \\ & - 8 N_c N_f \left(\frac{h_k^2}{N_f}\right)^2 \left(Z_{k,\psi} + r_k^F\right) \left(G_k^\psi\right)^3 \dot{r}_k^F \Bigg), \end{aligned} \tag{C.41}$$

$$\begin{aligned} \partial_t V_k^{(3)} = \int_q q^2 \Bigg(& -\frac{1}{2}(N_f^2 - 1) \left(G_k^\pi\right)^2 \dot{r}_k^B \left(6 \left(G_k^\pi\right)^2 \left(V_k^{(2)}\right)^3 - 6 G_k^\pi V_k^{(2)} V_k^{(3)} - V_k^{(4)}\right) \\ & - \frac{1}{2} \left(G_k^\sigma\right)^2 \dot{r}_k^B \Big(6 \left(G_k^\sigma\right)^2 \left(3 V_k^{(2)} + 2\rho_{exp} V_k^{(3)}\right)^3 + 7 V_k^{(4)} \\ & - 6 G_k^\sigma \left(3 V_k^{(2)} + 2\rho_{exp} V_k^{(3)}\right) \left(5 V_k^{(3)} + 2 \rho_{exp} V_k^{(4)}\right) + 2\rho_{exp} V_k^{(5)}\Big) \\ & + 24 N_c N_f \left(\frac{h_k^2}{N_f}\right)^3 \left(Z_{k,\psi} + r_k^F\right) \left(G_k^\psi\right)^4 \dot{r}_k^F \Bigg), \end{aligned} \tag{C.42}$$

$$\vdots$$

Flow equations for higher potential terms are neglected due to their complexity. The expressions shown suffice to prove that they are derived applying ρ-derivatives.

In practice, in our calculations $V_k^{(0)}$ played no active role, and therefore its presence could be neglected. Nevertheless, its expression is shown for further calculations. Particularly interesting is the expression (C.40), since by construction it must be equivalent to the flow of $\partial_t \Gamma_{k,\pi}^{(2)}$ at zero momentum.

The remaining scale-dependent quantities of interest are the Yukawa h_k, the bosonic two-point functions, the wave-function renormalisation of the quark $Z_{k,\psi}$ and the four-Fermi coupling λ_k. As described in Chapter 3, the Yukawa coupling is obtained from the mass function of the quark propagator following the expression (3.15). Hence, we will start from the quantities derivable from two-field derivatives in the form:

$$\partial_t \Gamma_k^{(2),\boldsymbol{ab}}(p^2) = \frac{\delta^2 \partial_t \Gamma_k}{\delta \Phi^{\boldsymbol{b}}(p) \delta \Phi^{\boldsymbol{a}}(-p)}. \tag{C.43}$$

Once the two-field derivatives in Wetterich's flow equation are applied, the resulting expressions are projected according to the inner indices of the fields in a way that yield the flows of the quantities previously mentioned. The projections are performed according to the following expressions:

$$\begin{aligned} P_\sigma &= 1, & P_\pi^{yz} &= \frac{\delta_{adj}^{yz}}{N_f^2 - 1}, \\ P_Z^{\boldsymbol{ba}} &= \frac{-i\not{p}^{\boldsymbol{ba}}}{4 N_f N_c \, p^2}, & P_m^{ba} &= \frac{\delta^{\boldsymbol{ba}}}{4 N_c N_f} \frac{\sqrt{2 N_f}}{\langle \sigma \rangle}. \end{aligned} \tag{C.44}$$

Here $\langle \sigma \rangle$ stands for $\langle \sigma \rangle = \sqrt{2\rho_{exp}}$. In order to simplify notation, the momentum dependent quantities which depend on the integration variable alone, e.g. $G_k^i(q)$ or $r_k^i(q)$ will be written without argument. For the Yukawa coupling case, this will be applied in the case $h_k(0,q) \equiv h_k$. As a last remark, the expression is reformulated in a way that the regulator terms $\dot{r}_k^i$ do not depend on the external momenta, simplifying thus computational time and facilitating the use of modified regulators. Under these conventions, the resulting flow equations are:

$$\begin{aligned} \partial_t \Gamma^{(2)}_{k,\boldsymbol{\pi\pi}}(p^2) = \int_q \Bigg(& -\frac{1}{2}(N_f^2 - 1) \left(G_k^\pi\right)^2 V_k^{(2)} \dot{r}_k^B - \frac{1}{2} \left(G_k^\sigma\right)^2 \left(V_k^{(2)} + 2\rho_{exp} V_k^{(3)} \right) \dot{r}_k^B \\ & + 2 (V_k^{(2)})^2 \dot{r}_k^B \left(\left(G_k^\pi\right)^2 G_k^\sigma(p-q) + \left(G_k^\sigma\right)^2 G_k^\pi(p+q) \right) \Bigg) q^2 \\ & + 4 N_f N_c \left(\frac{h_k(p, -q - \frac{p}{2}) h_k(-p, -q - \frac{p}{2})}{N_f} \right) \left(G_k^\psi \right)^2 G_k^\psi(p+q) \dot{r}_k^F \\ & \Big((Z_{k,\psi}(p+q) + r_k^F(p+q))(q^2 (Z_{k,\psi} + r_k^F)^2 - \frac{h_k}{N_f} \rho_{exp})(q^2 + (q \cdot p)) \\ & + 2 q^2 (Z_{k,\psi} + r_k^F) \rho_{exp} \frac{h_k h_k(0, q+p)}{N_f} \Big), \end{aligned} \tag{C.45}$$

$$
\begin{aligned}
\partial_t \Gamma^{(2)}_{k,\boldsymbol{\sigma}\boldsymbol{\sigma}}(p^2) = \int_q \Bigg(& -\frac{1}{2}(N_f^2-1)\left(G_k^{\pi}\right)^2 \left(V_k^{(2)} + 2\rho_{exp} V_k^{(3)}\right) \dot{r}_k^B \\
& -\frac{1}{2}\left(G_k^{\sigma}\right)^2 \left(3V_k^{(2)} + 4\rho_{exp}(3V_k^{(3)} + \rho_{exp} V_k^{(4)})\right) \dot{r}_k^B \\
& + 2(N_f^2-1)(V_k^{(2)})^2 \dot{r}_k^B \left(G_k^{\pi}\right)^2 G_k^{\pi}(p-q) \\
& + 2\left(G_k^{\pi}\right)^2 G_k^{\sigma}(p-q)\dot{r}_k^B \rho_{exp}(3V_k^{(2)} + 2\rho_{exp} V_k^{(3)})^2 \Bigg) q^2 \\
& + 4N_f N_c \left(\frac{h_k(p,-q-\frac{p}{2})h_k(-p,-q-\frac{p}{2})}{N_f}\right) \left(G_k^{\psi}\right)^2 G_k^{\psi}(p+q)\dot{r}_k^F \\
& \Big((Z_{k,\psi}(p+q) + r_k^F(p+q))(q^2(Z_{k,\psi}+r_k^F)^2 - \frac{h_k}{N_f}\rho_{exp})(q^2 + (q\cdot p)) \\
& - 2q^2(Z_{k,\psi}+r_k^F)\rho_{exp}\frac{h_k h_k(0,q+p)}{N_f}\Big),
\end{aligned}
\tag{C.46}
$$

$$
\begin{aligned}
\partial_t Z_{k,\psi}(p^2) = \frac{1}{p^2}\int_q q^2 \Bigg(& -\frac{1}{2}\left((-1+N_f^2)\left(G_k^{\pi}\right)^2 + \left(G_k^{\sigma}\right)^2\right) G_k^{\psi}(p-q) \\
& (Z_{k,\psi}(p-q) + r_k^F(p-q))(p^2 - q\cdot p)\left(\frac{h_k(-q,p-\frac{q}{2})h_k(q,p-\frac{q}{2})}{N_f}\right)\dot{r}_k^B \Bigg) \\
& -\frac{1}{2}\left((-1+N_f^2)G_k^{\pi}(p+q) + G_k^{\sigma}(p+q)\right)\left(G_k^{\psi}\right)^2 (q\cdot p)\dot{r}_k^F \\
& (-q^2(Z_{k,\psi}+r_k^F)^2 + h_k^2\rho_{exp})\left(\frac{h_k(p+q,\frac{(q-p)}{2})h_k(p+q,\frac{(p-q)}{2})}{N_f}\right),
\end{aligned}
\tag{C.47}
$$

$$
\begin{aligned}
\partial_t h_k(p^2) = \frac{1}{p^2}\int_q q^2 \Bigg(& -\frac{1}{2}\left(\left(G_k^{\pi}\right)^2(-1+N_f^2) - \left(G_k^{\sigma}\right)^2\right) G_k^{\psi}(p-q) \\
& \left(\frac{h_k(-q,p-\frac{q}{2})h_k(q,p-\frac{q}{2})}{N_f}\right)\dot{r}_k^B \Bigg) \\
& -\left(G_k^{\psi}\right)^2\left(G_k^{\pi}(p+q)(-1+N_f^2) - G_k^{\sigma}(p+q)\right) h_k(Z_{k,\psi}+r_k^F) \\
& \left(\frac{h_k(p+q,\frac{(q-p)}{2})h_k(p+q,\frac{(p-q)}{2})}{N_f}\right)\dot{r}_k^F.
\end{aligned}
\tag{C.48}
$$

The last expression required is the flow equation of the four-Fermi coupling λ_k, which is also momentum dependent. The explicit form of this expression is omitted from this work due to its length and complexity. Nevertheless, its calculation is necessary in order to implement dynamical hadronisation correctly.

The expression (C.48) is derived from the quark two-point function, but its form is equivalent to the one derived from the quark-pion three-point function. Nevertheless, it is more convenient in the used form due to the smaller number of diagrams. It is important to emphasise that, in similar calculations within the Quark-Meson model, this expression must agree only with the quark-pion three-point function but not with $h_{k,\sigma}$. Other approximations allow the three point function to be not only momentum dependent, but also field dependent as $h_k[\rho](p)$. Since the field derivatives of σ satisfy:

$$\frac{\delta}{\delta\sigma} = \frac{\delta\rho}{\delta\sigma}\frac{\delta}{\delta\rho} = \sigma\frac{\delta}{\delta\rho} \tag{C.49}$$

and, when evaluated at their mean value, $\langle\sigma\rangle$ is the only field different from 0, the quark-sigma three-point function may carry additional contributions to the quark-pion one.

From the definition of the pion two-point function, it is clear that $\partial_t\Gamma^{(2)}_{k,\pi}(p^2 = 0) = \partial_t m^2_{k,\pi}$. Since the pion mass obtained from the curvature of the potential is defined as $m^2_{k,\pi} = V^{(1)}_k$, the flow of the two-point function at zero momentum must agree with the flow $\partial_t V^{(1)}_k$. This fact provides a consistency check to guarantee that the form of flow equations is correct. The wave function renormalisations of the mesons, i.e. $Z_{k,\pi}(p^2)$ and $Z_{k,\sigma}(p^2)$ are obtained from the expressions derived above and the relation described in (3.31).

C.4 Dyson-Schwinger Equations

The general conventions used in the DSE formalism are the following:

- Quark correlator and propagator in Landau gauge (cf. equations (C.20) and (C.21) for the respective FRG conventions):

$$\Gamma^{(2)}_{\boldsymbol{\psi\bar{\psi}}}(p) = i\not{p}A(p^2) + B(p^2), \qquad M(p^2) \equiv \frac{B(p^2)}{A(p^2)}, \tag{C.50}$$

$$\left(\Gamma^{(2)}_{\boldsymbol{\psi\bar{\psi}}}(p)\right)^{-1} = \left(-i\not{p}A(p^2) + B(p^2)\right) G^{\psi}(p^2), \tag{C.51}$$

  with $G^{\psi}(p^2) = \left(A^2(p^2)p^2 + B^2(p^2)\right)^{-1}$.

- Meson correlator and propagator:

$$\left(\Gamma^{(2)}_{\boldsymbol{\sigma\sigma}}(p^2)\right)^{-1} = G^{\sigma}(p^2) \qquad \left(\Gamma^{(2)}_{\boldsymbol{\pi\pi}}(p^2)\right)^{-1} = G^{\pi}(p^2)\,\delta^{zy}_{adj} \tag{C.52}$$

- 3-Point functions:

$$\Gamma^{(3)}_{\boldsymbol{\sigma\psi\bar{\psi}}}(q,p) = \left(\frac{\delta^3\Gamma}{\delta\sigma\,(-q)\,\delta\psi\left(-p+\frac{q}{2}\right)\delta\bar{\psi}\left(p+\frac{q}{2}\right)}\right)^{\boldsymbol{abc}} P^{\boldsymbol{cba}}_{\sigma} \equiv H_{\sigma}(q,p) \tag{C.53}$$

$$\Gamma^{(3)}_{\boldsymbol{\pi\psi\bar{\psi}}}(q,p) = \left(\frac{\delta^3\Gamma}{\delta\pi\,(-q)\,\delta\psi\left(-p+\frac{q}{2}\right)\delta\bar{\psi}\left(p+\frac{q}{2}\right)}\right)^{\boldsymbol{abc}} P^{\boldsymbol{cba}}_{\pi} \equiv H_{\pi}(q,p) \tag{C.54}$$

$$\Gamma^{(3)}_{\boldsymbol{\sigma\sigma\sigma}}(q,p) = \left(\frac{\delta^3\Gamma}{\delta\sigma\,(-q)\,\delta\sigma\left(-p+\frac{q}{2}\right)\delta\sigma\left(p+\frac{q}{2}\right)}\right)^{\boldsymbol{abc}} P^{\boldsymbol{cba}}_{3\sigma} \equiv G_{3\sigma}(q,p) \tag{C.55}$$

$$\Gamma^{(3)}_{\boldsymbol{\pi\pi\sigma}}(q,p) = \left(\frac{\delta^3\Gamma}{\delta\pi\,(-q)\,\delta\pi\left(-p+\frac{q}{2}\right)\delta\sigma\left(p+\frac{q}{2}\right)}\right)^{\boldsymbol{abc}} P^{\boldsymbol{cba}}_{\sigma 2\pi} \equiv G_{\sigma 2\pi}(q,p) \tag{C.56}$$

- 4-Point functions:

$$\Gamma^{(4)}_{\boldsymbol{\psi\bar{\psi}\psi\bar{\psi}}}(r,q,p) = \left(\frac{\delta^4\Gamma}{\delta\psi\,(-p-q-r)\,\delta\bar{\psi}\,(r)\,\delta\psi\,(q)\,\delta\bar{\psi}\,(p)}\right)^{\boldsymbol{abcd}} P^{\boldsymbol{dcba}}_{4\psi} \tag{C.57}$$

C.4.1 Rainbow-Ladder QCD

In this section, the explicit derivation of the quark DSE in the Rainbow-Ladder truncation is shown. This system has been well-known for the last decades, see for example [65, 66]. Since it provides a good example on how a DSE can be obtained and solved, we will show the mathematical treatment in detail.

The quark propagator DSE involves the dressed quark two-point function (1), the free fermionic two-point function (2) and the quark-gluon loop Σ (3). In this calculation, the propagators are written in Landau gauge. The expression to be solved is $S^{-1} = S_0^{-1} - \Sigma$ and, including every index explicitly, the three terms look as following:

$$1- \qquad (S^{-1})^{AB}_{ab}(p) = A(p^2)\left(i\not{p}_{ab} + M(p^2)\cdot\mathbb{I}_{ab}\right)\delta^{AB}, \tag{C.58}$$

$$2- \qquad (S_0^{-1})^{AB}_{ab}(p) = Z_2\left(i\not{p}_{ab} + Z_m m\cdot\mathbb{I}_{ab}\right)\delta^{AB}, \tag{C.59}$$

$$3- \qquad \Sigma = \sum_{C,D}^{N_c}\sum_{r,s}^{N_c^2-1}\int_q \left(-igZ_{1f}\gamma^\mu_{ac}t^{AC}_r\right) S^{CD}_{cd}(q)\left(-ig\Gamma^\nu_{db}t^{DB}_s\right) D^{rs}_{\mu\nu}(k). \tag{C.60}$$

Here k denotes the relative momentum $k = p - q$ and q is the loop integration variable. Both of the momenta can be used as integration variables. Note that every object is extracted from the renormalised QCD Lagrangian using the Feynman rules. The full quark propagator follows:

$$S(p)^{AB}_{ab} = G^\psi(p^2)\left(-A(p^2)i\not{p}_{ab} + B(p^2)\cdot\mathbb{I}_{ab}\right)\delta^{AB}. \tag{C.61}$$

Here $B(p^2)$ satisfies $B(p^2) \equiv A(p^2)M(p^2)$, where $M(p^2)$ is the mass function. The full, dressed gluon propagator in Landau Gauge follows the expression:

$$D^{rs}_{\mu\nu}(k) = \frac{Z(k^2)}{k^2}\left(\delta_{\mu\nu} - \frac{k_\mu k_\nu}{k^2}\right)\delta^{rs}, \tag{C.62}$$

being $Z(k^2)$ the gluon dressing. The only term whose expression is still left is the full quark-gluon vertex. Since the Rainbow-Ladder truncation reduces the vertex to its free version, the explicit momentum dependence is omitted. The Rainbow-Ladder truncation is applied and, effectively, the system is rewritten according to the relation:

$$Z_{1f}g^2\frac{Z(k^2)}{k^2}\Gamma^\mu_{db} \qquad \longrightarrow \qquad Z_2^2 4\pi\frac{\alpha(k^2)}{k^2}\gamma^\mu_{db}. \tag{C.63}$$

The term $\alpha(k^2)$ encodes the non-perturbative information of both gluon and quark-gluon vertex and will be modelled.

A successful parametrisation of this term is given by Maris-Tandy [65]. It is split into ultraviolet and infrared terms:

$$\alpha(k^2) = \alpha_{IR}(k^2) + \alpha_{UV}(k^2), \tag{C.64}$$

with the explicit forms:

$$\alpha_{IR}(k^2) = \pi\eta^7 \left(\frac{k^2}{\Lambda^2}\right) e^{-\eta^2\left(\frac{k^2}{\Lambda^2}\right)}, \tag{C.65}$$

$$\alpha_{UV}(k^2) = \frac{2\pi\gamma_m \left(1 - \exp\left(-\frac{k^2}{\Lambda_0^2}\right)\right)}{\log\left(e^2 - 1 + \left(1 + \frac{k^2}{\Lambda_{QCD}^2}\right)^2\right)}. \tag{C.66}$$

Here the parameters η and Λ used are, respectively, 1.8 and 0.72 GeV. The other parameters are $\Lambda_0 = 1$ GeV, $\Lambda_{QCD} = 0.234$ GeV and $\gamma_m = \frac{12}{11N_c - 2N_f}$, which in the present calculations are $N_c = 3$ and $N_f = 2$. Back to the loop term of the general quark DSE equation, now with the gluon propagator and quark-gluon vertex in its free formulation, the remaining objects that can be refined are the colour terms. Gathering every colour contribution and using the properties of $SU(3)$, the following expression is satisfied:

$$\sum_{r,s}^{N_c^2-1} \sum_{C,D}^{N_c} t_r^{AC} t_s^{DB} \delta^{rs} \delta^{CD} \quad = \quad \sum_{r}^{N_c^2-1} \sum_{C}^{N_c} t_r^{AC} t_r^{CB} \quad = \quad \frac{N_c^2 - 1}{2N_c} \delta^{AB} \quad \xrightarrow{N_c=3} \quad \frac{4}{3}\delta^{AB}, \tag{C.67}$$

leaving the δ^{AB} in both sides of the DSE, which can be trivially projected out. Lastly, the three terms of the quark DSE are projected to obtain equations related to $A(p^2)$ and $B(p^2)$. The equation are projected using $P_A^{ba} = \frac{-i\not{p}^{ba}}{4p^2}$ and $P_B^{ba} = \frac{\delta^{ba}}{4}$ and the final equations yield:

$$A(p^2) = Z_2 + \frac{4}{3} Z_2^2 \int_q \frac{4\pi\alpha(k^2)}{k^2 p^2} A(q^2) G^{\psi}(q^2) \left(3(p \cdot q) - \frac{2p^2q^2 - 2(p \cdot q)^2}{k^2}\right), \tag{C.68}$$

$$B(p^2) = Z_2 Z_m m_q + Z_2^2 \int_q \frac{16\pi\alpha(k^2)}{k^2} B(q^2) G^{\psi}(q^2). \tag{C.69}$$

The system is based on these two equations and can be solved iteratively. There are some remarks to mention in order to solve the equations consistently.

- *Simplification of the integral*: Lorentz invariance lets the system to be solved using any reference frame. Particularly interesting is the rest frame, where $p^2 = \sqrt{p^2}(0,0,0,1)$. In such case, the scalar product with q becomes simply $p \cdot q = \sqrt{p^2}\sqrt{q^2}z$. The other angular variables y and ϕ are trivially integrated, leaving the remaining integrals:

$$\int_q \frac{d^4p}{(2\pi)^4} = \frac{1}{(2\pi)^3}\int_0^\infty dp^2 p^2 \int_{-1}^{1} dz\sqrt{1-z^2}. \tag{C.70}$$

- *Cutoff integration*: although the momentum integral is supposed to go from zero up to infinity, in practice an infrared and ultraviolet cutoff are needed. The usual choice is the logarithmic distribution quadrature with $b = 10^5$ GeV^2 and $a = 10^{-5}$ GeV^2.

- *Regulated propagators*: Even though it is not necessary for renormalised integrals, the use of regulators may facilitate convergence. Hence, regulators may be used as numerical tools. The regulators we used in this work are based on the Pauli-Villars regulator:

$$R^{PV}\left(p^2\right) = \left(1 + \frac{p^2}{\mu^2}\right)^{-1}, \tag{C.71}$$

where μ is the renormalisation scale, point beyond of which the contributions become suppressed. In the usual calculations, the regulator is introduced as $R^{PV}(k^2)$ indicating that the gluon propagator is the one regularised. Conveniently, it is usually introduced into the Maris-Tandy coupling $\alpha(k^2) \to \hat{\alpha}(k^2) = \alpha(k^2)R^{PV}(k^2)$.

- *Selection of renormalisation conditions*: before trying to solve the system iteratively, the specification of the renormalisation conditions is required. This determines in the end the numerical value of Z_2 and Z_m. In the calculation performed in this work, the renormalisation scale is chosen to be $\mu = 19$ GeV and, in this scale, $A(\mu^2) = 1$ and $B(\mu^2) = m_q$. Consequently, Z_2 and Z_m are determined by solving:

$$Z_2^2\Sigma_A(\mu^2) + Z_2 - 1 = 0, \tag{C.72}$$

$$Z_m = \begin{cases} \frac{m_q - Z_2^2\Sigma_B(\mu^2)}{Z_2 m_q} & m_q \neq 0 \\ 0 & m_q = 0 \end{cases}, \tag{C.73}$$

where $\Sigma_{A,B}$ represent the loop terms of the equations for $A(p^2)$ and $B(p^2)$, respectively. Notice that Z_m plays no role in the chiral limit when $m_q = 0$, therefore it is manually set to 0 to avoid any numerical difficulty.

- *Iteration*: the system is solved iteratively. The values of A and B are given an initial value, namely $A(p^2) = 1$ and $B(p^2) = 1$ GeV, and by applying interpolation the system is solved to obtain A and B at the renormalisation scale and, once Z_2 and Z_m are found, it is done for the rest of p^2. With the new values of A and B, the procedure is iterated to find new renormalisation constants and new dressings. The system is iterated until the values of the dressing no longer change in comparison to the ones in the previous iteration for every p^2 up to certain relative error (e.g. 10^{-5}). The final renormalisation constants with the mentioned conditions are $Z_2 = 0.96$ and $Z_m = 0.79$.

The next step to solve the full Rainbow-Ladder DSE-BSE system is to compute the dressings $A(p_{1,2}^2)$ and $B(p_{1,2}^2)$ for complex momentum following the parabola:

$$p_{1,2}^2 = \tilde{q}^2 - \frac{M^2}{4} \pm izM\sqrt{\tilde{q}^2}, \tag{C.74}$$

where $\tilde{q}^2$ is real and is used as the BSE integration variable. The steps required to solve the complex-valued dressing equations are explained in Appendix B. There are only a few remarks to be made:

- *Real renormalisation constants*: since they correspond to the same system as the real Euclidean momentum case, the converged values of the renormalisation constants Z_2 and Z_m are maintained, thus performing the iteration only in every $p_{1,2}^2$ as explained in the appendix.
- *Gluon momenta as integration variable*: Since both the regulator and the Maris-Tandy coupling depend on k^2, it is recommended to use it as integration variable and therefore keep it real.
- *Cross-check*: Once the system has converged, a result cross-check can be performed by projecting the values into the real axis using Cauchy's integral formula. The previous results with real momenta shall be recovered.

Up to this point, the dressings $A(p^2)$ and $B(p^2)$ are considered calculated with any of the methods offered in Appendix B, and is also considered to be complex valued. The next steps explain how to include the results obtained in the complex DSEs in order to solve the homogeneous and inhomogeneous Bethe-Salpeter equations. The starting point is the integral expression of the homogeneous BSE in the Rainbow-Ladder truncation, following:

$$\Gamma(q,\, P) = \int_q \gamma^\mu S(p_1)\Gamma(\tilde{q}, P)S(p_2)\gamma^\nu D_{\mu\nu}(k), \tag{C.75}$$

where $S(p_i)$ is now complex valued and $D^{\mu\nu}(k) = \frac{1}{k^2}\left(g^{\mu\nu} - \frac{k^\mu k^\nu}{k^2}\right)$ is the known free gluon propagator. Now the Bethe-Salpeter amplitues are expressed in a tensorial expansion:

$$\Gamma(q,P) = \sum_{i=0}^{3} f^i(q^2, P^2, q\cdot P)\tau^i, \tag{C.76}$$

where the τ encodes the tensor structure in a basis of four elements, the ones that a pseudoscalar meson can have. The basis τ and the conjugate basis $\bar{\tau}$ are defined as:

$$\tau = \gamma_5\{\ \mathbb{I}\ ,\ \hat{q}\!\!\!/_T\ ,\ \hat{P}\!\!\!/\ ,\ i\hat{q}\!\!\!/_T\hat{P}\!\!\!/\ \}, \tag{C.77}$$

$$\bar{\tau} = \{\ \mathbb{I}\ ,\ \hat{q}\!\!\!/_T\ ,\ \hat{P}\!\!\!/\ ,\ i\hat{q}\!\!\!/_T\hat{P}\!\!\!/\ \}\gamma_5. \tag{C.78}$$

The relative transverse momentum $q_T = q^2 - \frac{q\cdot P}{P^2}$ and total momentum P are expressed in their unitary form. Under this definition, the orthogonality condition of the basis terms becomes:

$$\frac{1}{4}\mathrm{Tr}\left[\tau^i \bar{\tau}^j\right] = \delta^{ij}. \tag{C.79}$$

Using this identity, expression (C.76) is traced according to every term of the basis, yielding:

$$f_q^{(0)} = X_{00}\, f_{\tilde{q}}^{(0)} + X_{01}\, f_{\tilde{q}}^{(1)} + X_{02}\, f_{\tilde{q}}^{(2)} + X_{03}\, f_{\tilde{q}}^{(3)}, \tag{C.80}$$
$$f_q^{(1)} = X_{10}\, f_{\tilde{q}}^{(0)} + X_{11}\, f_{\tilde{q}}^{(1)} + X_{12}\, f_{\tilde{q}}^{(2)} + X_{13}\, f_{\tilde{q}}^{(3)}, \tag{C.81}$$
$$f_q^{(2)} = X_{20}\, f_{\tilde{q}}^{(0)} + X_{21}\, f_{\tilde{q}}^{(1)} + X_{22}\, f_{\tilde{q}}^{(2)} + X_{23}\, f_{\tilde{q}}^{(3)}, \tag{C.82}$$
$$f_q^{(3)} = X_{30}\, f_{\tilde{q}}^{(0)} + X_{31}\, f_{\tilde{q}}^{(1)} + X_{32}\, f_{\tilde{q}}^{(2)} + X_{33}\, f_{\tilde{q}}^{(3)}. \tag{C.83}$$

Here the terms $f_q^{(i)} \equiv f^{(i)}(q^2, P^2, z)$ and $X_{ij} f_{\tilde{q}}^{(j)} \equiv \int_{\tilde{q}} X_{ij} f^{(j)}(\tilde{q}^2, P^2, \tilde{z})$, with $z = \frac{(q\cdot P)}{\sqrt{q^2 P^2}}$ and $\tilde{z} = \frac{(\tilde{q}\cdot P)}{\sqrt{\tilde{q}^2 P^2}}$, were used for simplicity. The terms X_{ij} depend on every internal $(\tilde{q}, \tilde{z})$ and external (q, z) variable and the total momentum P. The explicit expressions of X_{ij} are omitted due to their length. The way the equations (C.80) to (C.83) are written suggests a reformulation into matrix-vector. In order to achieve that, one must choose a grid of N_q elements for q^2 and N_z elements for z. Then, the vector $\vec{f_q}$ is built with $4N_qN_z$ components following:

$$\vec{f_q} = \begin{pmatrix} f^{(0)}(q_1, z_1) \\ \vdots \\ f^{(0)}(q_1, z_{N_z}) \\ f^{(0)}(q_2, z_1) \\ \vdots \\ f^{(0)}(q_{N_q}, z_{N_z}) \\ f^{(1)}(q_1, z_1) \\ \vdots \\ \vdots \\ f^{(3)}(q_{N_q}, z_{N_z}) \end{pmatrix}. \tag{C.84}$$

Notice that the parameter P was not included in the parametrisation of the vector. The reason: the procedure starting from this point is done for a particular P^2, and it is used as an external input variable. Analogously, the vector $\vec{f_{\tilde{q}}}$ is constructed. It is crucial, however, that the vector $\vec{f_{\tilde{q}}}$ shares the same components as $\vec{f_q}$, i.e., the same grid is used. In such case, both vectors are equivalent and a square matrix $4N_qN_z \times 4N_qN_z$ can be generated, so that:

$$\vec{f_q} = X\vec{f_{\tilde{q}}}. \tag{C.85}$$

The matrix is then built following:

$$X = \begin{pmatrix} X_{00}(q_1, z_1, \tilde{q}_1, \tilde{z}_1) & \dots & X_{00}(q_1, z_1, \tilde{q}_1, \tilde{z}_{N_z}) & \dots & \dots & X_{03}(q_1, z_1, \tilde{q}_{N_q}, \tilde{z}_{N_z}) \\ \vdots & & \vdots & & & \vdots \\ X_{10}(q_1, z_1, \tilde{q}_1, \tilde{z}_1) & \dots & X_{10}(q_1, z_1, \tilde{q}_1, \tilde{z}_{N_z}) & \dots & \dots & X_{13}(q_1, z_1, \tilde{q}_{N_q}, \tilde{z}_{N_z}) \\ \vdots & & \vdots & & & \vdots \\ X_{20}(q_1, z_1, \tilde{q}_1, \tilde{z}_1) & \dots & X_{20}(q_1, z_1, \tilde{q}_1, \tilde{z}_{N_z}) & \dots & \dots & X_{23}(q_1, z_1, \tilde{q}_{N_q}, \tilde{z}_{N_z}) \\ \vdots & & \vdots & & & \vdots \\ X_{30}(q_1, z_1, \tilde{q}_1, \tilde{z}_1) & \dots & X_{30}(q_1, z_1, \tilde{q}_1, \tilde{z}_{N_z}) & \dots & \dots & X_{33}(q_1, z_1, \tilde{q}_{N_q}, \tilde{z}_{N_z}) \end{pmatrix}. \tag{C.86}$$

Notice that equations (C.80) to (C.83) are recovered where X_{ij} are expressed in their quadrature form. This means that every term of the matrix must include every quadrature weight and jacobian (in case of change of variable). The larger the matrix is, the more precise the quadrature is but the computational time increases very fast. The matrix needs to be constructed and then we use a routine to obtain both eigenvalues and eigenvectors of the system. In the present calculations, Eigen for C++ was used. The value of P^2 for which the largest eigenvalue of the matrix X is $\lambda = 1$ corresponds to the on-shell value $P^2 = -M^2$ and the eigenvector is the solution of the BSE.

As mentioned in Chapter 2, an equation of interest is the inhomogeneous Bethe-Salpeter equation. It is defined, in the case of the pseudoscalar pion, as:

$$\Gamma = \Gamma_0 + KG_0\Gamma, \tag{C.87}$$

where Γ_0 is expanded according to the basis:

$$\tau_{inh} = \gamma_5 \left\{\mathbb{I}, 0, 0, 0\right\}, \tag{C.88}$$

which is expressed, after tracing the equations out, in the form of a vector:

$$\Gamma_0 \to Z_2 \begin{pmatrix} 1 \\ \vdots \\ 1 \\ 0 \\ \vdots \\ 0 \end{pmatrix} \equiv \vec{f}_0, \tag{C.89}$$

in which the non-zero values are associated to the $f^{(0)}$ terms. The solution is obtained by rewriting Γ in terms of $f^{(i)}$ and $KG_0\Gamma$ as $X\vec{f}$. Under this notation, the following relation is clear:

$$\vec{f} = (1 - X)^{-1}\vec{f}_0, \tag{C.90}$$

which solves the inhomogeneous BSE. The solution of this equation provides insight involving the position of the pole, which needs to agree with the point where the eigenvalue of X is $\lambda = 1$, as shown in Figure 2.6.

C.4.2 The NJL - QM model (1)

It is instructive to understand how DSEs change before and after the application of the Hubbard-Stratonovich transformation. For this purpose, we will analyse the transformation of the NJL when it has a $U(2)_L \times U(2)_R$ symmetric four-Fermi interaction. The Euclidean NJL model follows the bare action:

$$\begin{aligned} S[\bar{\psi},\psi] = \int_x & -\bar{\psi}\left(\not{\partial} - m_q\right)\psi \\ & - \lambda\left(\frac{\left(\bar{\psi}\psi\right)^2}{2N_f} + \left(\bar{\psi}i\gamma_5\tau^z\psi\right)^2 + \frac{\left(\bar{\psi}i\gamma_5\psi\right)^2}{2N_f} + \left(\bar{\psi}\tau^z\psi\right)^2\right), \end{aligned} \tag{C.91}$$

where $N_f = 2$ is the flavour number and τ^z are the generators of $SU(2)$, following $\tau^z = \frac{\sigma^z}{2}$ being σ^z the Pauli matrices. The summation of colour, flavour and Dirac indices is implied. The choice of the terms in the 4-Fermi interaction correspond to the basis terms for the $S-P$ channels, see [73].

In the NJL in the usual approach, only the quark propagator DSE is present - and therefore the $A(p)$ and $B(p)$ dressings-, since the two-loop term of the DSE is neglected. Projecting the quark DSE using the expressions:

$$P_A^{\boldsymbol{ba}} = \frac{-i\not{p}^{\boldsymbol{ba}}}{4N_cN_fp^2}, \qquad P_B^{\boldsymbol{ba}} = \frac{\delta^{\boldsymbol{ba}}}{4N_cN_f}, \tag{C.92}$$

where $\not{p}^{\boldsymbol{ba}}$ is short for $\not{p}^{\beta\alpha}\delta_c^{BA}\delta_f^{ba}$. Parametrizing the free 2-point function as:

$$\Gamma^{(2)}_{0,\psi\bar{\psi}}(p) = Z_2(i\not{p} + Z_m m_q). \tag{C.93}$$

The DSEs for the quark propagator dressings follow:

$$A(p^2) = Z_2 + \frac{2N_f\lambda}{p^2}\int_q G^\psi(q^2)A(q^2)(q\cdot p) = Z_2, \tag{C.94}$$

$$B(p^2) = Z_2Z_m m_q + 4N_c\lambda\int_q G^\psi(q^2)B(q^2). \tag{C.95}$$

Notice that $A(p^2)$ and $B(p^2)$ are momentum independent. Hence, one can safely set the values $A(p^2) = Z_2 = 1$ and $B(p^2) = M(p^2) = M$.

The expression for M is solved easily. Setting, for simplicity, $Z_m = 1$, the implicit expression becomes:

$$M = m_q + 4N_c\lambda \int \frac{d^4q}{(2\pi)^4} \frac{M}{q^2 + M^2}. \tag{C.96}$$

The integral is quadratically divergent and the only possible approach is the use of a cutoff Λ. It is not only introduced in the momentum integral, but also in the four-Fermi coupling as $\lambda = \frac{\tilde{c}}{\Lambda^2}$. By setting the numerical constants coming from the flavour and colour terms, 2π terms from the Fourier transform and angular integration within a constant c defined as:

$$c = \tilde{c} \left(\frac{4N_c}{(2\pi)^4} \frac{1}{2} \int d\Omega \right), \tag{C.97}$$

the DSE for M becomes with a sharp cutoff a compact equation:

$$M = m_q + \frac{c}{\Lambda^2} M \int_0^{\Lambda^2} dq^2 \frac{q^2}{q^2 + M^2}. \tag{C.98}$$

In any NJL model with distinct symmetries the DSE will be equivalent as the one obtained. The only difference will come from numerical factors which are encoded within the c constant differently. By defining $a = \left(\frac{M}{\Lambda}\right)^2$, the solution for M reads:

$$M = m_q + cM \left(1 - a \ln \left(1 + \frac{1}{a} \right) \right), \tag{C.99}$$

where, even in the chiral limit, there exists a critical value of c in which M is generated. The corresponding plot related to the solution of this equation is found in Figure 4.3.

At this point, we would like to analyse the behaviour of the system after performing the Hubbard-Stratonovich transformation. Due to the different terms of the four-point interaction, several new fields are introduced. The bare action of the system becomes:

$$\begin{aligned} S[\psi, \bar{\psi}, \sigma, \vec{\pi}, \eta, \vec{a}] = & \int_x -\bar{\psi} \left(\not{\partial} - m_q \right) \psi + \frac{1}{2} m^2 \left(\sigma^2 + \vec{\pi}^2 + \eta^2 + \vec{a}^2 \right) \\ & + h\bar{\psi} \left(\frac{\sigma}{\sqrt{2N_f}} + i\gamma_5 \vec{\tau}\vec{\pi} + \frac{i\gamma_5 \eta}{\sqrt{2N_f}} + \vec{\tau}\vec{a} \right) \psi, \end{aligned} \tag{C.100}$$

where $\vec{\pi}$ and η are identified as pseudoscalars, whereas σ and $\vec{a}$ are scalar fields.

In this case, η and $\vec{a}$ propagators and vertices (defined equivalently as G^{π} and H_{π}) also contribute into the system. The Dyson-Schwinger equation of the quark propagator in this system, projecting equivalently as defined in (C.92) follows:

$$A(p^2) = Z_2 + \frac{h}{2N_f p^2}\int_q \Bigg((N_f^2-1)\left(G^{\pi}(p-q)\tilde{H}_{\pi}(p,q) + G^{\vec{a}}(p-q)\tilde{H}_{\vec{a}}(p,q)\right) \tag{C.101}$$
$$+ G^{\sigma}(p-q)\tilde{H}_{\sigma}(p,q) + G^{\eta}(p-q)\tilde{H}_{\eta}(p,q)\Bigg) G^{\psi}(q)A(q^2)(q\cdot p),$$

$$B(p^2) = Z_2 Z_m m_q + \frac{h}{2N_f}\int_q \Bigg((N_f^2-1)\left(G^{\pi}(p-q)\tilde{H}_{\pi}(p,q) - G^{\vec{a}}(p-q)\tilde{H}_{\vec{a}}(p,q)\right) \tag{C.102}$$
$$- G^{\sigma}(p-q)\tilde{H}_{\sigma}(p,q) + G^{\eta}(p-q)\tilde{H}_{\eta}(p,q)\Bigg) G^{\psi}(q)B(q^2),$$

where h is the tree level Yukawa coupling. The arguments of the propagators are understood to be squared, but the explicit expression is omitted for simplicity. In a similar way, the dressed three-point functions arguments have been compacted for simplicity. Their explicit dependence follows $\tilde{H}_i(p,q) = H_i(q-p, p+q)$. Under the assumption that all the dressed bosonic correlators are free, i.e, $H_i = h_i = h$ and $G_i = \frac{1}{m^2}$, the expression (C.101) and (C.102) become:

$$A(p^2) = Z_2 + \frac{N_f}{p^2}\frac{h^2}{m^2}\int_q G^{\psi}(q)A(q^2)(q\cdot p) = Z_2, \tag{C.103}$$

$$B(p^2) = Z_2 Z_m m_q. \tag{C.104}$$

Even though the loop integral of the $A(p^2)$ dressing DSE is zero, it is clear that identifying $\lambda = \frac{h^2}{2m^2}$, equation (C.103) becomes exactly equivalent to (C.94), as expected from the HS transformation. Moreover, the mass term is not only momentum independent, but also the contributions given by the loop terms cancel completely. In this case, the DSE is not recovered. This fact emphasises the importance of the dressed boson correlators in the system.

When the system is bosonised, meson correlators also get their own DSE and become, in general, momentum dependent. Therefore, it is expected that the quark propagator also gets momentum dependent mass term. Additionally, calculations have shown that η and $\vec{a}$ can be neglected, since they are massive enough to cancel the propagators, leaving the half-bosonised action as the one used in the previous chapters.

C.4.3 The NJL - QM model (2)

Since in practice heavy mesons can be neglected, it is interesting to analyse how DSE behave not only cancelling heavy meson propagators, but also not including them from the very beginning. Hence, in this section the starting point is the bare action:

$$S[\bar{\psi},\psi] = \int_x -\bar{\psi}\left(\not{\partial} - m_q\right)\psi - \lambda\left(\frac{\left(\bar{\psi}\psi\right)^2}{2N_f} + \left(\bar{\psi}i\gamma_5\tau^z\psi\right)^2\right). \tag{C.105}$$

Summation over colour, flavour and Dirac indices is implied. Under this choice, the terms in the 4-Fermi interaction still correspond to the $S-P$ channels, but now a half-bosonisation will only include σ and $\vec{\pi}$ mesons. Using the same projections as in (C.92) and the same tree level parametrisations, the DSEs for the quark propagator dressings become:

$$A(p^2) = Z_2 + \frac{N_f\lambda}{p^2}\int_q G^{\psi}(q)A(q^2)(q\cdot p), \tag{C.106}$$

$$B(p^2) = Z_2 Z_m m_q + \left(\frac{N_f^2 + 4N_cN_f - 2}{N_f}\right)\lambda\int_q G^{\psi}(q)B(q^2). \tag{C.107}$$

In this case, the loop term of the $A(p^2)$ equation, related to the tadpole loop diagram, is half the one obtained in the previous case, showing explicitly that the two different $S-P$ contribute the same in this equation. Nevertheless, this contribution cancels in both systems. On the other hand, the DSE for $B(p^2)$ is still momentum independent, although the loop term is multiplied by a different factor.

Once the bare action is half-bosonised using the Hubbard-Stratonovich transformation, the resulting bare action follows:

$$S[\psi,\bar{\psi},\sigma,\vec{\pi}] = \int_x -\bar{\psi}\left(\not{\partial} - m_q\right)\psi + \frac{1}{2}m^2\left(\sigma^2+\vec{\pi}^2\right) + h\bar{\psi}\left(\frac{\sigma}{\sqrt{2N_f}} + i\gamma_5\vec{\tau}\vec{\pi}\right)\psi, \tag{C.108}$$

where colour, flavour and Dirac indices are summed over. Note that now the meson fields are the ones related to the sigma meson and the pions.

The Dyson-Schwinger equation of the quark propagator in this system, projecting as in expression (C.92), follows:

$$A(p^2) = Z_2 + \frac{h}{N_f p^2}\int_q \Bigg((N_f^2-1)G^\pi(p-q)H_\pi(q-p,p+q) + G^\sigma(p-q)H_\sigma(q-p,p+q)\Bigg) G^\psi(q)A(q^2)(q\cdot p), \tag{C.109}$$

$$B(p) = Z_2 Z_m m_q + \frac{h}{2N_f}\int_q \Bigg((N_f^2-1)G^\pi(p-q)H_\pi(q-p,p+q) - G^\sigma(p-q)H_\sigma(q-p,p+q)\Bigg) G^\psi(q)B(q^2). \tag{C.110}$$

Under the assumption that all the dressed bosonic correlators are free, i.e, $H_i = h$ and $G_i = \frac{1}{m^2}$, the expressions (C.109) and (C.110) become:

$$A(p^2) = Z_2 + \frac{N_f}{p^2}\frac{h^2}{2m^2}\int_q G^\psi(q)A(q^2)(q\cdot p) = Z_2, \tag{C.111}$$

$$B(p^2) = Z_2 Z_m m_q + \left(\frac{N_f^2-2}{N_f}\right)\frac{h^2}{2m^2}\int_q G^\psi(q)B(q^2). \tag{C.112}$$

By identifying $\lambda = \frac{h^2}{2m^2}$, the equation (C.111) becomes exactly equivalent to (C.106). The mass term, although still momentum independent, does no longer cancel its contributions. The solution will match qualitatively with the one obtained from the previous NJL model DSE, but the numerical factor multiplying the integral (the parameter c within the NJL solution) will not be the same. In such case, the relation between the half-bosonised NJL model does not agree with the NJL.

The DSEs are solved self-consistently using the DSEs of the meson correlators and three-point functions. The mesonic full propagators are obtained projecting over the terms:

$$P_\sigma = 1, \qquad P_\pi^{\boldsymbol{ab}} = \frac{\delta^{zy}_{adj}}{N_f^2-1}. \tag{C.113}$$

With them, the DSE for the mesonic correlators are:

$$\Gamma^{(2)}_{\boldsymbol{\sigma\sigma}}(p^2) = \Gamma^{(2)}_{0,\boldsymbol{\sigma\sigma}}(p^2) + \int_q 2N_c\, h_\sigma\, H_\sigma(p+q,p-q)\Big(B(q)B(p-q) + A(q)A(p-q)(-q^2+q\cdot p)\Big) G^\psi(q)G^\psi(p-q), \tag{C.114}$$

$$\Gamma^{(2)}_{\boldsymbol{\pi\pi}}(p^2) = \Gamma^{(2)}_{0,\boldsymbol{\pi\pi}}(p^2) + \int_q 2N_c\, h_\pi\, H_\pi(p+q,p-q)\Big(-B(q)B(p-q) + A(q)A(p-q)(-q^2+q\cdot p)\Big) G^\psi(q)G^\psi(p-q), \tag{C.115}$$

where $\Gamma^{(2)}_{0,\boldsymbol{\pi\pi}}(p^2)$ and $\Gamma^{(2)}_{0,\boldsymbol{\sigma\sigma}}(p^2)$ are respectively the inverse tree-level propagators of the sigma and pion fields. The arguments of all the dressings and propagators are written without the square for simplicity. The flow equations of the three-point functions involved in the system are omitted due their length and complexity.

C.4.4 The Gross-Neveu model

The NJL model described in the previous section was solved within reasonable truncations, but two-loop diagrams were neglected from the very beginning. Since the theory is non-renormalisable, a cutoff implementation -breaking translational symmetry- is necessary and two-loop integrals cannot be solved without the use of particular regulators. This is not the case in lower dimensions, where the theory becomes renormalisable. In particular, in the 2-dimensional case, the system becomes perturbatively renormalisable and all the diagrams from the DSE are solvable. Under this consideration the simplest truncation already yields momentum dependent quark dressings, and several properties regarding bosonisation in DSE can be analysed.

The bare action of the system is defined within a two-dimensional framework:

$$S[\bar\psi,\psi] = \int d^2x \left(-\bar\psi\left(\not\partial - m_q\right)\psi + \frac{\lambda}{2N_f}\left(\bar\psi\psi\right)^2 \right). \tag{C.116}$$

From this action, the DSEs are obtained under the usual parametrisation. There exist in this case an infinite set of DSE involving $2n$ point functions, therefore the most reasonable truncation is neglecting the diagrams involving the 6-point function, yielding a self-consistent system of equation as shown in figure 4.5 involving only the quark propagator dressings and the full four-point function.

The full four-point function includes, due to momentum conservation, three independent arguments: $\Gamma^{(4)}_{\psi\bar{\psi}\psi\bar{\psi}}(p,q,r)$. For simplicity and in order to still consider momentum dependence into the 4-point function, the latter is redefined in the t-channel as:

$$\Gamma^{(4)}_{\psi\bar{\psi}\psi\bar{\psi}}(p,-p,p) \equiv \Gamma^{(4)}_{\psi\bar{\psi}\psi\bar{\psi}}(p^2). \tag{C.117}$$

The DSEs involving two-loop diagrams include a very wide set of indices and momenta. In order to reduce notation, the following conventions are used in this case:

$$\begin{aligned}
&A(q^2) \equiv A_q, && A(r^2) \equiv A_r, && A((p+q+r)^2) \equiv A_{pqr},\\
&B(q^2) \equiv B_q, && B(r^2) \equiv B_r, && B((p+q+r)^2) \equiv B_{pqr},\\
&G^{\psi}(q^2) \equiv G^{\psi}_q, && G^{\psi}(r^2) \equiv G^{\psi}_r, && G^{\psi}((p+q+r)^2) \equiv G^{\psi}_{pqr}.
\end{aligned} \tag{C.118}$$

At this point, the expressions for the quark propagator dressings are projected according to:

$$P_A^{\boldsymbol{ba}} = \frac{-i\not{p}^{\boldsymbol{ba}}}{2N_c N_f p^2}, \qquad P_B^{\boldsymbol{ba}} = \frac{\delta^{\boldsymbol{ba}}}{2N_c N_f}, \tag{C.119}$$

where $\not{p}^{\boldsymbol{ba}}$ includes also flavour and colour Kronecker deltas. The resulting expressions read:

$$A(p^2) = Z_2 - \frac{c_2\lambda}{p^2}\int_q\int_r \Sigma_A^{(2)}(p,q,r), \tag{C.120}$$

$$B(p^2) = Z_2 Z_m m_q + c_1\lambda\int_q B_q G^{\psi}_q + c_2\lambda\int_q\int_r \Sigma_B^{(2)}(p,q,r). \tag{C.121}$$

Here the constants c_1 and c_2 are defined from the flavour and colour indices and renormalisation constants as:

$$c_1 \equiv Z_\lambda\left(\frac{-1+2N_cN_f}{N_f}\right), \qquad c_2 = \frac{Z_\lambda}{N_f^2}. \tag{C.122}$$

The explicit expressions of the two-loop terms $\Sigma_A^{(2)}$ and $\Sigma_B^{(2)}$ follow:

$$\begin{aligned}\Sigma_A^{(2)}(p,q,r) = G_q^{\psi} G_r^{\psi} G_{pqr}^{\psi}(-B_{pqr}((-1+N_cN_f)A_qB_r(p\cdot q)+A_rB_q(p\cdot r))+\\ A_{pqr}((-1+N_cN_f)B_qB_r(p\cdot(p+q+r))+\\ A_qA_r((-1+N_cN_f)p^2(q\cdot r)+(p\cdot r)(q^2+N_cN_f(q\cdot r))+\\ (p\cdot q)(N_cN_f(p\cdot r)+\\ (-1+N_cN_f)(r^2+2(q\cdot r))))))\Gamma^{(4)}_{\psi\bar{\psi}\psi\bar{\psi}}\left(\left(\frac{p+r}{2}\right)^2\right),\end{aligned} \tag{C.123}$$

$$\begin{aligned}\Sigma_B^{(2)}(p,q,r) = G_q^{\psi} G_r^{\psi} G_{pqr}^{\psi}(B_r((1-2N_cN_f)B_qB_{pqr}+\\ A_qA_{pqr}(q\cdot(p+q+r)))+(-1+N_cN_f)A_r(-A_qB_{pqr}(q\cdot r)+\\ A_{pqr}B_q(r\cdot(p+q+r))))\Gamma^{(4)}_{\psi\bar{\psi}\psi\bar{\psi}}\left(\left(\frac{p+r}{2}\right)^2\right).\end{aligned} \tag{C.124}$$

The DSE for the 4-point vertex is obtained by projecting the expression with:

$$P_{4\psi}^{\boldsymbol{dcba}} = \frac{\delta^{\boldsymbol{dc}}\delta^{\boldsymbol{ba}}}{(2N_cN_f-1)2N_c}. \tag{C.125}$$

Consequently, the associated DSE follows:

$$\Gamma^{(4)}_{\psi\bar{\psi}\psi\bar{\psi}}(p^2) = Z_\lambda\lambda\left(1+\Sigma_\lambda^{(1,2)}(p^2)\right), \tag{C.126}$$

where $\Sigma_\lambda^{(1,2)}(p^2)$ includes the contributions of one- and two-loop diagrams. The explicit expression of this term is omitted due to its length and complexity.

In the calculations used in $d=2$ dimensions, the momenta in two loop terms need to be properly defined. Our momentum vectors are generally expressed in polar coordinates. We choose for simplicity the reference frame where the quark is at rest, and therefore:

$$p=\sqrt{p^2}\begin{pmatrix}0\\1\end{pmatrix}, \qquad q=\sqrt{q^2}\begin{pmatrix}\sqrt{1-z_q^2}\\ z_q\end{pmatrix}, \qquad r=\sqrt{r^2}\begin{pmatrix}\sqrt{1-z_r^2}\\ z_r\end{pmatrix}. \tag{C.127}$$

Under these parametrisations, the expressions of the DSEs are well defined. Finally, for completeness, the 2-dimensional momentum integral reads:

$$\int\frac{d^2q}{(2\pi)^2} = \frac{1}{(2\pi)^2}\frac{\pi}{2}\int_0^\infty dq^2\int_{-1}^1 dz_q. \tag{C.128}$$

Appendix D

Computation

Sophisticated numerical tools are required to perform the DSE-BSE and FRG calculations numerically. The implementation of these tools was performed using different kinds of software, packages and programming codes. In this appendix, the general structure of the files used to the derive and solve functional equations is described.

The general structure of the codes is the same for both DSE-BSE and FRG methods. It consists of two main parts: the derivation of the functional equations and the numerical solution given by the expressions.

- *Derivation of functional equations*: the flow equations and Dyson-Schwinger equations are generated using Mathematica [122] and the packages DoFun [123] and FormTracer [124]. The user introduces the number and type of fields involved in the system, together with their respective indices and arguments. Afterwards, the action of the system is introduced. Then, once the correlators and vertices are parametrised, the functions DoDSE and DoRGE yield the respective Dyson-Schwinger and flow equations. Such functions also yield the diagrammatic form of the expressions shown in this work. The resulting expressions need to be accordingly projected and traced using the FormTrace function. Finally, the traced expression is exported to an external file that is read by the functional equation solving code.

  The Bethe-Salpeter equations cannot be derived from DoFun since they depend explicitly on the parametrisation of the interaction kernel. Nevertheless, if the form of the involved entities is known, the objects and BSA are written with explicit indices and basis expansion and traced out. The remaining expressions, related to the matrix X in (C.86), are exported for the use of the equation-solving routine.

- *Equation-solving routine - DSE*: this part of the code is written in C++. The system reads the global variables placed in a file and generates the momentum grid and quadrature points and weights. The system reads the file including the expression of the DSEs and solves the integral for external momentum p^2 which initially is the renormalisation scale μ^2, allowing to compute the values of the renormalisations constants Z_i and, afterwards, the solution of the DSEs. Then, this system is iterated until the relative error between every value of the solution in the momentum grid and their value in the previous iteration is lower than a

certain amount. During the calculation, cubic-splines are used for the interpolations. The quadrature procedure is, in some cases, parallelised using OpenMP [125]. In the complex-momentum case, the variables are complex-valued and a closed-curve is generated with the momentum grid points. In this case, the renormalisation constants obtained in the real-axis are used and the iteration is performed on the values of the complex curve. The solutions of the DSE are finally saved in external files.

- *Equation-solving routine - BSE*: working similarly as its DSE counterpart, this routine generates not only a momentum grid for the quadrature, but also the matrix elements. The code reads the solutions obtained in the DSE routine and sets the splines to determine the matrix elements involved in the BSE. Using the Eigen package [126], the matrix can be inverted and eigenvalues and eigenvectors are easily extracted. Such values, as well as the solution of the inhomogeneous BSE, are saved in an external file.

- *Equation-solving routine - FRG*: written also in C++, this routine is more laborious than the two previous ones. First of all, the code reads the initial values that are necessary for the integration, but also the initial conditions for the differential equation solving using the Boost package. In the calculations performed, we use a Runge-Kutta routine with an adaptive stepper, letting the system reach apparent convergence using fewer steps. Before calling the Boost package function, the user needs to determine which parameters evolve during the differential equation solving and set their values in their initial conditions. During each of the integration steps, two functions are necessary:

  - Momentum integration: the function sets the conditions for the momentum integration and calls an adaptive quadrature function provided by the Cubature package. This function reads the flow equation in the external files and solves the integral equations adaptively, minimising the number of evaluations and numerical error. The function returns the solutions that are used as input values for the differential equation solving routine. Parallelisation using OpenMP is implemented within the adaptive quadrature routine.
  - Output function: in every step of the Runge-Kutta solving, the code is allowed to print, both on terminal and in external files, the values of the running parameters at every step. This function is useful to control scale-dependent quantities. It is convenient, however, to save not only scale-dependent values but also their momentum dependence, giving the user a complete control of the values in every step on the integration. Nevertheless, this practice causes greater data files and longer evaluation time due to the required output steps.

  Once the system has converged, momentum dependent parameters in the infrared are saved as final solutions of the flow equations.

The commented codes, necessary files and executables will be available in the GitHub repository https://github.com/jordiparislopez/PhdThesis early 2019.

Bibliography

[1] M. Gell-Mann, "A Schematic Model of Baryons and Mesons", *Phys. Lett.* 8, 214 (1964).

[2] C. Patrignani, *et al.*, "Review of Particle Physics", *Chin. Phys.* C40, 100001 (2016).

[3] B. C. Odom, D. Hanneke, B. D'Urso, G. Gabrielse, "New Measurement of the Electron Magnetic Moment Using a One-Electron Quantum Cyclotron", *Phys. Rev. Lett.* 97, 030801 (2006). [Erratum: Phys. Rev. Lett.99,039902(2007)].

[4] L. Ya. Glozman, D. O. Riska, "The Spectrum of the nucleons and the strange hyperons and chiral dynamics", *Phys. Rept.* 268, 263 (1996), arXiv:hep-ph/9505422 [hep-ph].

[5] L. Ya. Glozman, W. Plessas, K. Varga, R. F. Wagenbrunn, "Unified description of light and strange baryon spectra", *Phys. Rev.* D58, 094030 (1998), arXiv:hep-ph/9706507 [hep-ph].

[6] S. Scherer, "Introduction to chiral perturbation theory", *Adv. Nucl. Phys.* 27, 277 (2003), arXiv:hep-ph/0210398 [hep-ph]. [,277(2002)].

[7] S. Scherer, "Chiral Perturbation Theory: Introduction and Recent Results in the One-Nucleon Sector", *Prog. Part. Nucl. Phys.* 64, 1 (2010), arXiv:0908.3425 [hep-ph].

[8] J. Smit, "Introduction to quantum fields on a lattice: A robust mate", *Cambridge Lect. Notes Phys.* 15, 1 (2002).

[9] T. DeGrand, C. E. Detar, *Lattice methods for quantum chromodynamics* (2006).

[10] C. Gattringer, C. B. Lang, "Quantum chromodynamics on the lattice", *Lect. Notes Phys.* 788, 1 (2010).

[11] F. J. Dyson, "The S matrix in quantum electrodynamics", *Phys. Rev.* 75, 1736 (1949).

[12] J. S. Schwinger, "On the Green's functions of quantized fields. 1.", *Proc. Nat. Acad. Sci.* 37, 452 (1951).

[13] C. Wetterich, "Exact evolution equation for the effective potential", *Phys. Lett. B* 301, *90* (1993).

[14] R. Alkofer, L. von Smekal, "The Infrared behavior of QCD Green's functions: Confinement dynamical symmetry breaking, and hadrons as relativistic bound states", *Phys. Rept.* 353, 281 (2001).

[15] A. Bashir, *et al.*, "Collective perspective on advances in Dyson-Schwinger Equation QCD", *Commun.Theor.Phys.* 58, 79 (2012), arXiv:1201.3366 [nucl-th].

[16] C. D. Roberts, A. G. Williams, "Dyson-Schwinger equations and their application to hadronic physics", *Prog. Part. Nucl. Phys.* 33, 477 (1994), arXiv:hep-ph/9403224 [hep-ph].

[17] P. Maris, C. D. Roberts, "Dyson-Schwinger equations: A Tool for hadron physics", *Int. J. Mod. Phys.* E12, 297 (2003), arXiv:nucl-th/0301049 [nucl-th].

[18] A. Holl, C. D. Roberts, S. V. Wright, *20th Annual Hampton University Graduate Studies Program (HUGS 2005) Newport News, Virginia, May 31-June 17, 2005* (2006).

[19] C. S. Fischer, "Infrared properties of QCD from Dyson-Schwinger equations", *J. Phys.* G32, R253 (2006), arXiv:hep-ph/0605173 [hep-ph].

[20] G. Eichmann, H. Sanchis-Alepuz, R. Williams, R. Alkofer, C. S. Fischer, "Baryons as relativistic three-quark bound states", *Prog. Part. Nucl. Phys.* 91, 1 (2016), arXiv:1606.09602 [hep-ph].

[21] H. Sanchis-Alepuz, R. Williams, "Recent developments in bound-state calculations using the Dyson–Schwinger and Bethe–Salpeter equations", *Comput. Phys. Commun.* 232, 1 (2018), arXiv:1710.04903 [hep-ph].

[22] K. G. Wilson, "Renormalization group and critical phenomena. 1. Renormalization group and the Kadanoff scaling picture", *Phys. Rev.* B4, 3174 (1971).

[23] K. G. Wilson, "The Renormalization Group: Critical Phenomena and the Kondo Problem", *Rev. Mod. Phys.* 47, 773 (1975).

[24] J. Berges, N. Tetradis, C. Wetterich, "Non-perturbative renormalization flow in quantum field theory and statistical physics", *Phys. Rept.* 363, 223 (2002), arXiv:hep-ph/0005122.

[25] J. M. Pawlowski, "Aspects of the functional renormalisation group", *Annals Phys.* 322, 2831 (2007), arXiv:hep-th/0512261 [hep-th].

[26] H. Gies, "Introduction to the functional RG and applications to gauge theories", *Lect.Notes Phys.* 852, 287 (2012), arXiv:hep-ph/0611146 [hep-ph].

[27] B.-J. Schaefer, J. Wambach, "Renormalization group approach towards the QCD phase diagram", *Phys.Part.Nucl.* 39, 1025 (2008), arXiv:hep-ph/0611191 [hep-ph].

[28] J. Braun, "Fermion Interactions and Universal Behavior in Strongly Interacting Theories", *J.Phys.* G39, 033001 (2012), arXiv:1108.4449 [hep-ph].

[29] U. Ellwanger, "FLow equations for N point functions and bound states", *Z. Phys.* C62, 503 (1994), arXiv:hep-ph/9308260 [hep-ph]. [,206(1993)].

[30] R. Alkofer, L. von Smekal, "The Infrared behavior of QCD propagators in Landau gauge", *Nucl. Phys.* A680, 133 (2000), arXiv:hep-ph/0004141 [hep-ph].

[31] R. Alkofer, C. S. Fischer, H. Sanchis-Alepuz, "Electromagnetic transition form factors of baryons in a relativistic Faddeev approach", *EPJ Web Conf.* 181, 01013 (2018), arXiv:1802.09775 [hep-ph].

[32] A. S. Miramontes, H. Sanchis-Alepuz, "Decay mechanisms in bound state interaction kernels", *arXiv:1805.03572 [hep-ph]* (2018), arXiv:1805.03572 [hep-ph].

[33] E. Weil, G. Eichmann, C. S. Fischer, R. Williams, "Electromagnetic decays of the neutral pion investigated in the Dyson-Schwinger formalism", *J. Phys. Conf. Ser.* 1024, 012032 (2018), arXiv:1710.08169 [hep-ph].

[34] M. E. Carrington, "The effect of a Chern-Simons term on dynamical gap generation in graphene" (2019), arXiv:1901.03757 [cond-mat.other].

[35] E. Salpeter, H. Bethe, "A Relativistic equation for bound state problems", *Phys.Rev.* 84, 1232 (1951).

[36] M. Blank, A. Krassnigg, "Matrix algorithms for solving (in)homogeneous bound state equations", *Comput. Phys. Commun.* 182, 1391 (2011), arXiv:1009.1535 [hep-ph].

[37] M. Blank, "Properties of quarks and mesons in the Dyson-Schwinger/Bethe-Salpeter approach", Ph.D. thesis, Graz U. (2011).

[38] S.-x. Qin, L. Chang, Y.-x. Liu, C. D. Roberts, D. J. Wilson, "Investigation of rainbow-ladder truncation for excited and exotic mesons", *Phys. Rev.* C85, 035202 (2012), arXiv:1109.3459 [nucl-th].

[39] C. S. Fischer, S. Kubrak, R. Williams, "Mass spectra and Regge trajectories of light mesons in the Bethe-Salpeter approach", *Eur. Phys. J.* A50, 126 (2014), arXiv:1406.4370 [hep-ph].

[40] C. S. Fischer, S. Kubrak, R. Williams, "Spectra of heavy mesons in the Bethe-Salpeter approach", *Eur. Phys. J.* A51, 10 (2015), arXiv:1409.5076 [hep-ph].

[41] D. J. Gross, "The role of symmetry in fundamental physics", *Proceedings of the National Academy of Sciences* 93, 14256 (1996), *Preprint:* https://www.pnas.org/content/93/25/14256.full.pdf.

[42] S. Weinberg, *The Quantum theory of fields. Vol. 1: Foundations* (Cambridge University Press, 2005).

[43] S. Weinberg, *The quantum theory of fields. Vol. 2: Modern applications* (Cambridge University Press, 2013).

[44] P. H. Frampton, *Gauge Field Theories: Third Revised and Improved Edition* (2008).

[45] J. Goldstone, "Field Theories with Superconductor Solutions", *Nuovo Cim.* 19, 154 (1961).

[46] J. Goldstone, A. Salam, S. Weinberg, "Broken Symmetries", *Phys. Rev.* 127, 965 (1962).

[47] J. C. Ward, "An Identity in Quantum Electrodynamics", *Phys. Rev.* 78, 182 (1950).

[48] Y. Takahashi, "On the generalized Ward identity", *Nuovo Cim.* 6, 371 (1957).

[49] R. Contant, M. Q. Huber, C. S. Fischer, C. A. Welzbacher, R. Williams, "On the quark-gluon vertex at non-vanishing temperature", *Acta Phys. Polon. Supp.* 11, 483 (2018), arXiv:1805.05885 [hep-ph].

[50] M. Q. Huber, "Correlation functions of three-dimensional Yang-Mills theory from Dyson-Schwinger equations", *Phys. Rev.* D93, 085033 (2016), arXiv:1602.02038 [hep-th].

[51] R. Williams, C. S. Fischer, W. Heupel, "Light mesons in QCD and unquenching effects from the 3PI effective action", *Phys. Rev.* D93, 034026 (2016), arXiv:1512.00455 [hep-ph].

[52] M. Gell-Mann, *Murray Gell-Mann: Selected Papers* (World Scientific, 2010), pp. 81–127.

[53] D. J. Gross, F. Wilczek, "Ultraviolet behavior of non-abelian gauge theories", *Physical Review Letters* 30, 1343 (1973).

[54] K. G. Wilson, "Confinement of quarks", *Physical Review D* 10, 2445 (1974).

[55] M. Gell-Mann, R. J. Oakes, B. Renner, *Murray Gell-Mann: Selected Papers* (World Scientific, 2010), pp. 160–164.

[56] V. P. Nair, *Quantum field theory: A modern perspective* (Springer Science & Business Media, 2005).

[57] V. N. Gribov, "Quantization of non-abelian gauge theories", *Nuclear Physics B* 139, 1 (1978).

[58] N. Vandersickel, D. Zwanziger, "The Gribov problem and QCD dynamics", *Phys. Rept.* 520, 175 (2012), arXiv:1202.1491 [hep-th].

[59] L. D. Faddeev, V. N. Popov, "Feynman Diagrams for the Yang-Mills Field", *Phys. Lett.* B25, 29 (1967). [,325(1967)].

[60] C. Becchi, A. Rouet, R. Stora, "The abelian higgs kibble model, unitarity of the s-operator", *Physics Letters B* 52, 344 (1974).

[61] C. Becchi, A. Rouet, R. Stora, "Renormalization of the abelian higgs-kibble model", *Communications in Mathematical Physics* 42, 127 (1975).

[62] C. Becchi, A. Rouet, R. Stora, "Renormalization of gauge theories", *Annals of Physics* 98, 287 (1976).

[63] P. Maris, P. C. Tandy, "QCD modeling of hadron physics", *Nucl. Phys. Proc. Suppl.* 161, 136 (2006), arXiv:nucl-th/0511017 [nucl-th]. [,136(2005)].

[64] P. Maris, "Hadron Physics and the Dyson-Schwinger Equations of QCD", *AIP Conf. Proc.* 892, 65 (2007), arXiv:nucl-th/0611057 [nucl-th]. [,65(2006)].

[65] P. Maris, P. C. Tandy, "Bethe-Salpeter study of vector meson masses and decay constants", *Phys. Rev.* C60, 055214 (1999), arXiv:nucl-th/9905056 [nucl-th].

[66] P. Maris, C. D. Roberts, "Pi- and K meson Bethe-Salpeter amplitudes", *Phys. Rev.* C56, 3369 (1997), arXiv:nucl-th/9708029 [nucl-th].

[67] R. Williams, "The quark-gluon vertex in Landau gauge bound-state studies", *Eur. Phys. J.* A51, 57 (2015), arXiv:1404.2545 [hep-ph].

[68] M. S. Bhagwat, P. Maris, "Vector meson form factors and their quark-mass dependence", *Phys. Rev.* C77, 025203 (2008), arXiv:nucl-th/0612069 [nucl-th].

[69] K. G. Wilson, J. B. Kogut, "The Renormalization group and the epsilon expansion", *Phys. Rept.* 12, 75 (1974).

[70] T. Appelquist, J. Carazzone, "Infrared Singularities and Massive Fields", *Phys. Rev.* D11, 2856 (1975).

[71] D. F. Litim, J. M. Pawlowski, "Completeness and consistency of renormalisation group flows", *Phys. Rev.* D66, 025030 (2002), arXiv:hep-th/0202188 [hep-th].

[72] N. Defenu, A. Codello, "Scaling solutions in the derivative expansion", *Phys. Rev.* D98, 016013 (2018), arXiv:1711.01809 [hep-th].

[73] M. Mitter, J. M. Pawlowski, N. Strodthoff, "Chiral symmetry breaking in continuum QCD", *Phys.Rev.* D91, 054035 (2015), arXiv:1411.7978 [hep-ph].

[74] J. Hubbard, "Calculation of partition functions", *Phys. Rev. Lett.* 3, 77 (1959).

[75] D. Ebert, H. Reinhardt, M. K. Volkov, "Effective hadron theory of QCD", *Prog. Part. Nucl. Phys.* 33, 1 (1994).

[76] H. Gies, C. Wetterich, "Renormalization flow of bound states", *Phys.Rev.* D65, 065001 (2002), arXiv:hep-th/0107221 [hep-th].

[77] S. Floerchinger, C. Wetterich, "Exact flow equation for composite operators", *Phys.Lett.* B680, 371 (2009), arXiv:0905.0915 [hep-th].

[78] S. Floerchinger, "Exact Flow Equation for Bound States", *Eur. Phys. J.* C69, 119 (2010), arXiv:1001.4497 [hep-th].

[79] R. Alkofer, *et al.*, "Bound state properties from the Functional Renormalisation Group" (2018), arXiv:1810.07955 [hep-ph].

[80] A. K. Cyrol, M. Mitter, J. M. Pawlowski, N. Strodthoff, "Nonperturbative quark, gluon, and meson correlators of unquenched QCD", *Phys. Rev.* D97, 054006 (2018), arXiv:1706.06326 [hep-ph].

[81] J. Braun, L. Fister, J. M. Pawlowski, F. Rennecke, "From Quarks and Gluons to Hadrons: Chiral Symmetry Breaking in Dynamical QCD", *Phys. Rev.* D94, 034016 (2016), arXiv:1412.1045 [hep-ph].

[82] fQCD Collaboration, J. Braun, L. Corell, A. K. Cyrol, W.-J. Fu, M. Leonhardt, M. Mitter, J. M. Pawlowski, M. Pospiech, F. Rennecke, C. Scheider, N. Wink.

[83] A. K. Cyrol, L. Fister, M. Mitter, J. M. Pawlowski, N. Strodthoff, "Landau gauge Yang-Mills correlation functions", *Phys. Rev.* D94, 054005 (2016), arXiv:1605.01856 [hep-ph].

[84] A. Sternbeck, E. M. Ilgenfritz, M. Muller-Preussker, A. Schiller, I. L. Bogolubsky, "Lattice study of the infrared behavior of QCD Green's functions in Landau gauge", *PoS* LAT2006, 076 (2006), arXiv:hep-lat/0610053 [hep-lat].

[85] R. Alkofer, H. Reinhardt, "Chiral quark dynamics", *Lect. Notes Phys. Monogr.* 33, 1 (1995).

[86] Y. Nambu, G. Jona-Lasinio, "Dynamical model of elementary particles based on an analogy with superconductivity. i", *Phys. Rev.* 122, 345 (1961).

[87] Y. Nambu, G. Jona-Lasinio, "Dynamical model of elementary particles based on an analogy with superconductivity. ii", *Phys. Rev.* 124, 246 (1961).

[88] D. U. Jungnickel, C. Wetterich, "Effective action for the chiral quark-meson model", *Phys. Rev.* D53, 5142 (1996), arXiv:hep-ph/9505267 [hep-ph].

[89] J. Eser, F. Divotgey, M. Mitter, D. H. Rischke, "Low-energy limit of the $O(4)$ quark-meson model from the functional renormalization group approach", *Phys. Rev.* D98, 014024 (2018), arXiv:1804.01787 [hep-ph].

[90] J. M. Pawlowski, F. Rennecke, "Higher order quark-mesonic scattering processes and the phase structure of QCD", *Phys. Rev.* D90, 076002 (2014), arXiv:1403.1179 [hep-ph].

[91] F. Rennecke, B.-J. Schaefer, "Fluctuation-induced modifications of the phase structure in (2+1)-flavor QCD", *Phys. Rev.* D96, 016009 (2017), arXiv:1610.08748 [hep-ph].

[92] J. Braun, M. Leonhardt, M. Pospiech, "Fierz-complete NJL model study: Fixed points and phase structure at finite temperature and density", *Phys. Rev.* D96, 076003 (2017), arXiv:1705.00074 [hep-ph].

[93] J. Braun, M. Leonhardt, M. Pospiech, "Fierz-complete NJL model study. II. Toward the fixed-point and phase structure of hot and dense two-flavor QCD", *Phys. Rev.* D97, 076010 (2018), arXiv:1801.08338 [hep-ph].

[94] R.-A. Tripolt, P. Gubler, M. Ulybyshev, L. Von Smekal, "Numerical analytic continuation of Euclidean data" (2018), arXiv:1801.10348 [hep-ph].

[95] A. J. Helmboldt, J. M. Pawlowski, N. Strodthoff, "Towards quantitative precision in the chiral crossover: masses and fluctuation scales", *Phys.Rev.* D91, 054010 (2015), arXiv:1409.8414 [hep-ph].

[96] J. R. Pelaez, "From controversy to precision on the sigma meson: a review on the status of the non-ordinary $f_0(500)$ resonance", *Phys. Rept.* 658, 1 (2016), arXiv:1510.00653 [hep-ph].

[97] A. Maas, "Gauge bosons at zero and finite temperature", *Physics Reports* 524, 203 (2013). Gauge bosons at zero and finite temperature.

[98] R.-A. Tripolt, "Spectral Functions and Transport Coefficients from the Functional Renormalization Group", Ph.D. thesis, Darmstadt, Tech. U. (2015).

[99] R.-A. Tripolt, J. Weyrich, L. von Smekal, J. Wambach, "Fermionic spectral functions with the Functional Renormalization Group", *Phys. Rev.* D98, 094002 (2018), arXiv:1807.11708 [hep-ph].

[100] J. Wambach, R.-A. Tripolt, N. Strodthoff, L. von Smekal, "Spectral functions from the functional renormalization group", *Nuclear Physics A* 928, 156 (2014). Special Issue Dedicated to the Memory of Gerald E Brown (1926-2013).

[101] J. M. Pawlowski, N. Strodthoff, N. Wink, "Finite temperature spectral functions in the O(N)-model", *Phys. Rev.* D98, 074008 (2018), arXiv:1711.07444 [hep-th].

[102] J. M. Pawlowski, N. Strodthoff, "Real time correlation functions and the functional renormalization group", *Phys. Rev.* D92, 094009 (2015), arXiv:1508.01160 [hep-ph].

[103] A. Jakovac, A. Patkos, "Bound states in Functional Renormalization Group" (2018), arXiv:1811.09418 [hep-th].

[104] J.-P. Blaizot, J. M. Pawlowski, U. Reinosa, "Exact renormalization group and Φ-derivable approximations", *Phys. Lett.* B696, 523 (2011), arXiv:1009.6048 [hep-ph].

[105] J. Braun, M. Leonhardt, J. M. Pawlowski, "Renormalization group consistency and low-energy effective theories" (2018), arXiv:1806.04432 [hep-ph].

[106] K.-I. Aoki, S.-I. Kumamoto, M. Yamada, "Phase structure of njl model with weak renormalization group", *Nuclear Physics B* 931, 105 (2018).

[107] K.-I. Aoki, K. Morikawa, J.-I. Sumi, H. Terao, M. Tomoyose, "Analysis of the Wilsonian effective potentials in dynamical chiral symmetry breaking", *Phys. Rev.* D61, 045008 (2000), arXiv:hep-th/9908043 [hep-th].

[108] V. E. Rochev, P. A. Saponov, "The four fermion interaction in D = 2, D = 3, D = 4: A Nonperturbative treatment", *Int. J. Mod. Phys.* A13, 3649 (1998), arXiv:hep-th/9710006 [hep-th].

[109] C. Boehmer, U. Fritsch, S. Kraus, M. Thies, "Phase structure of the massive chiral Gross-Neveu model from Hartree-Fock", *Phys. Rev.* D78, 065043 (2008), arXiv:0807.2571 [hep-th].

[110] D. J. Gross, A. Neveu, "Dynamical Symmetry Breaking in Asymptotically Free Field Theories", *Phys. Rev.* D10, 3235 (1974).

[111] D. Benedetti, S. Carrozza, R. Gurau, A. Sfondrini, "Tensorial Gross-Neveu models", *JHEP* 01, 003 (2018), arXiv:1710.10253 [hep-th].

[112] J. A. Gracey, T. Luthe, Y. Schroder, "Four loop renormalization of the Gross-Neveu model", *Phys. Rev.* D94, 125028 (2016), arXiv:1609.05071 [hep-th].

[113] N. Dorey, R. D. Kenway, "The Schwinger-Dyson equation and dynamical mass generation in two-dimensional field theories", *Nucl. Phys.* B333, 419 (1990).

[114] D. D. Scherer, "Low-dimensional chiral physics. gross-neveu universality and magnetic catalysis" (2012).

[115] H. Gies, S. Lippoldt, "Renormalization flow towards gravitational catalysis in the 3d Gross-Neveu model", *Phys. Rev.* D87, 104026 (2013), arXiv:1303.4253 [hep-th].

[116] B. Knorr, "Ising and Gross-Neveu model in next-to-leading order", *Phys. Rev.* B94, 245102 (2016), arXiv:1609.03824 [cond-mat.str-el].

[117] W. H. Press, S. A. Teukolsky, W. T. Vetterling, B. P. Flannery, *Numerical Recipes 3rd Edition: The Art of Scientific Computing* (Cambridge University Press, New York, NY, USA, 2007), third edn.

[118] W. Gautschi, "Quadrature formulae on half-infinite intervals", *BIT Numerical Mathematics* 31, 437 (1991).

[119] H. Takahasi, M. Mori, "Double exponential formulas for numerical integration", *Publications of the Research Institute for Mathematical Sciences* 9, 721 (1974).

[120] C. S. Fischer, D. Nickel, R. Williams, "On Gribov's supercriticality picture of quark confinement", *Eur. Phys. J.* C60, 47 (2009), arXiv:0807.3486 [hep-ph].

[121] D. F. Litim, "Optimized renormalization group flows", *Phys. Rev.* D64, 105007 (2001), arXiv:hep-th/0103195 [hep-th].

[122] W. R. Inc., "Mathematica, Version 11.3". Champaign, IL, 2018.

[123] M. Q. Huber, J. Braun, "Algorithmic derivation of functional renormalization group equations and Dyson-Schwinger equations", *Comput.Phys.Commun.* 183, 1290 (2012), arXiv:1102.5307 [hep-th].

[124] A. K. Cyrol, M. Mitter, N. Strodthoff, "Formtracer. a mathematica tracing package using form", *Computer Physics Communications* (2016).

[125] OpenMP Architecture Review Board, "OpenMP application program interface version 3.0" (2017).

[126] G. Guennebaud, B. Jacob, *et al.*, "Eigen v3", http://eigen.tuxfamily.org (2010).

Acknowledgements

First of all, I would like to express my sincere gratitude to my advisor Prof. Reinhard Alkofer for his continuous support, motivation and encouragement. His guidance helped me in all the time of research and writing of this thesis. I would also like to thank him for giving me the opportunity to work on this challenging topic and for his knowledge that helped me during these three years.

Besides my advisor, I would like to thank Dr. Hèlios Sanchis-Alepuz for all his constant help, the fruitful discussions and the priceless conversations we had since the very day I started the PhD.

During my stay abroad I worked in the institute of theoretical physics of the University of Heidelberg, Germany, under the supervision of Prof. Jan Pawlowski. My sincere gratitude goes to him and to Dr. Mario Mitter for their hospitality and for letting me work in their team. I would also like to thank them for the numerous discussions and guidance during the time I was learning FRG.

I want to thank all the members of the doctoral school for making these three years an unforgettable experience. I also want to express my gratitude for the support of Austrian Science Fund FWF doctoral school W1203-N16 (Doctoral programm "Hadrons in vacuum, nuclei and stars").

Special thanks go to my colleagues in Mozartgasse, with whom I shared remarkable moments, countless hours of fun and a strong friendship.

I am grateful to my family for their endless support, for encouraging me to do a PhD far from home and for all the delightful visits that let me felt like I never left.

Last, but most important, my deepest gratitude goes to my girlfriend Cristina for having come with me to Austria and making it our new home. I want to thank her for being by my side every day of my life, her constant support, endless patience and beautiful smile that always gives me strength when I need it the most.